# Interaction of STDP and metaplasticity in modelling heterosynaptic plasticity

Azam Shirrafiardekani

a thesis submitted for the degree of

Doctor of Philosophy

at the University of Otago, Dunedin,

New Zealand.

2015

**Abstract**

Although neuroscientists have still not found a comprehensive mechanism to underlie learning and memory, many investigations suggest that long term potentiation (LTP) and long term depression (LTD) are involved in establishment of learning and memory. As a consequence of certain neural activity, neurons need to modulate the activity of the synapse or the properties of ion channels, therefore, they use a mechanism called homeostatic plasticity to balance their activity and control their firing rate. Two forms of plasticity phenomena that are necessary for plasticity regulation are homosynaptic and heterosynaptic plasticity. In the dentate granule cell, induction of homosynaptic LTP in the activated pathway is accompanied by heterosynaptic LTD in the inactivated pathway. Because, the dentate granule cell shows changes in synaptic strengths, we used this cell to test the following hypotheses. The first hypothesis we propose is, with plasticity and metaplasticity models introduced in this thesis, and the modification of an average postsynaptic spike, we can reproduce homosynaptic LTP and concurrent heterosynaptic LTD. The second hypothesis is the metaplasticity generated after a high frequency stimulation (HFS) reduces the level of synaptic plasticity caused by a second HFS. To test these hypotheses we use computer simulation and combine the nearest-neighbour spike time dependent plasticity (STDP) and metaplasticity rules accompanied with noisy spontaneous activity and the nine compartmental model of a granule cell. For this study we use the experimental data from Abraham *et al.* (2001), Abraham *et al.* (2007) and Bowden *et al.* (2012). With the method mentioned above our model is able to reproduce homosynaptic LTP in the activated pathway and heterosynaptic LTD in the neighbouring inactivated pathway. We also show, due to the metaplasticity effects of the plasticity

generated from the first HFS, the same magnitude of LTP and LTD will not occur in both pathways during the second HFS. Our finding supports the assertion that the combination of our metaplasticity and nearest-neighbour STDP rules can be a reliable choice to reproduce synaptic plasticity in the dentate granule cell neuron. Our investigation also supports the idea that metaplasticity modulates synaptic plasticity and prevents the synapse from extreme increases, therefore, the same magnitude of synaptic plasticity will not occur during the second stimulation.

**Acknowledgements**

Firstly, I would like to express my special thanks to my supervisor Associate Professor Lubica Benuskova. It would not be possible for me to finish this PhD journey without your support and help. I would also like to give thanks to my co-supervisor, Professor Jörg Frauendiener for his valuable advice. I would like to express my most sincere appreciation to Professor Cliff Abraham for his absolutely helpful comments and suggestions, and our head of department Michael Albert for all his help and support. I would like to thank my friends in Dunedin, my colleagues in the Owheo Building, and my fellow postgraduate students, especially Maryam Bagheroskoei for her kind help and support.

I would like to express special appreciation to my amazing beloved husband Michael Wilson who supported and accompanied me patiently throughout these moments.

I also would like to thank Caroline Stockman for her kind support and help. And a special thanks to my parents for all of the sacrifices that you have made on my behalf.

Last but not least, I would like to thank the University of Otago Computer Science department as a whole for supporting my study.

# Contents

# List of Tables

# List of Figures

## Acronyms

**AHP** *after hyperpolarisation*

**AP** *action potential*

**bAP** *back-propagating action potential*

**BCM** *Bienestock, Cooper and Munro*

**DBS** *delta-burst simulation*

**DD** *distal dendrite*

**EC** *Entorhinal cortex*

**EPSP** *excitatory postsynaptic potential*

**fEPSP** *field excitatory postsynaptic potential*

**GABA** *gamma-amino butyric acid*

**GC** *granule cell*

**GCL** *granule cell layer*

**GCLD** *granule cell layer dendrite*

**het-LTD** *heterosynaptic LTD*

**HFS** *high-frequency stimulation*

**hom-LTP** *homosynaptic LTP*

**ISI** *inter-spike interval*

**LAH** *lateral frequency after HFS*

**LFS** *low-frequency stimulation*

**LPP** *lateral prefrontal pathway*

**LTD** *long-term depression*

**LTP** *long-term potentiation*

**MD** *middle dendrite*

**MPP** *medial prefrontal pathway*

**PD** *proximal dendrite*

**SAS** *Santhakumar Aradi and Soltesz*

**STDP** *spike-time-dependent plasticity*

**TBS** *theta-burst stimulation*

# Chapter 1

# Introduction

Although during the last century our understanding of how neurons work and how they process information has grown rapidly, still we have not managed to find a comprehensive cellular mechanism to explain memory and learning phenomena. Experimental studies from a variety of brain regions reveal that several mechanisms are involved in memory and learning. Neural stem cells are able to generate new neurons in a process called neurogenesis and this plays a significant role in neural development. New investigations show that neurogenesis of the dentate gyrus might be involved in the mechanism of memory encoding (Deng *et al.*, 2010). Moreover the ability of synapses to change their efficacy in an activity-depednent way is referred to as synaptic plasticity. An investigation by Snyder *et al.* (2001) supports the idea that synaptic plasticity of adult-born dentate granule cells is involved greatly in the process of learning and memory. Therefore, to learn more about the remarkable role of synaptic plasticity in learning and memory, we dedicated our work to further investigation of the mechanisms of plasticity in the dentate granule cell. Two forms of long-lasting synaptic plasticity are long-term potentiation (LTP) and long-term depression (LTD). These can occur simultaneously in neighbouring synaptic pathways onto dentate granule cells. LTP and LTD can be induced homosynaptically or heterosynaptically. Homosynaptic plasticity occurs when a synapse is activated directly by presynaptic stimulation and heterosynaptic plasticity occurs when the activity of a particular neuron leads to changes in the strength of synaptic connections from other unactivated neurons. Experimental studies show that to regulate synaptic plasticity, both homo- and hetero- synaptic plasticity are required. In dentate granule cells, homosynaptic LTP in the activated synapse is ac-

companied by heterosynaptic LTD. Thus, when the medial perforant pathway (MPP) is tetanized by specific stimulation, homosynaptic LTP occurs in this pathway and concurrently heterosynaptic LTD occurs on the neighbouring lateral perforant pathway (LPP) (Douglas and Goddard, 1975; Levy and Steward, 1979; Abraham and Goddard, 1983; Doyère *et al.*, 1997). Because of this interesting property of granule cells, our investigation of synaptic plasticity is based on this particular cell type. In this thesis we used computer simulation to test different mechanisms that may be involved in synaptic plasticity induction. One of these mechanisms is nearest-neighbour pair-based STDP ( spike timing-dependent plasticity), as experimental studies have shown that the precise timing between pre- and postsynaptic spikes can be involved in LTP and LTD induction (Markram *et al.*, 1997). Investigations by Lin *et al.* (2006) support a role for STDP in granule cell plasticity, using pre- and postsynaptic spikes paired in either pre-post or post-pre order. Furthermore, a plasticity model is more accurate if each presynaptic spike pairs only with the two most recent postsynaptic spikes; this mechanism is known as nearest-neighbour STDP (Van Rossum *et al.*, 2000). Another mechanism that is commonly assumed to be involved in synaptic plasticity induction is metaplasticity, defined as ability of previous activity of a neuron to regulate subsequent synaptic plasticity. Metaplasticity can act homeostaticically to protect synaptic weights from extreme increases. Having such a homeostatic mechanism is necessary to regulate the neural firing rate and adjust any other neural activities that may destabilize the neural networks. The neuron model we have chosen in our research is the nine compartmental model of a granule cell with seven ion channels. (Santhakumar *et al.*, 2005). In most computational models the role of this activity has been ignored, however, in this thesis we took into account the role of this type of activity.

In this work we explored our hypotheses by combining STDP and metaplasticity rules accompanied by noisy spontaneous activity in the compartmental model of a granule cell. The hypotheses we addressed were:

1. Our model can replicate homosynaptic LTP in the tetanized pathway and concurrent heterosynaptic LTD in the neighbouring non-tetanized pathway.

2. In the nine compartmental model of a GC introduced by Santhakumar *et al.* (2005) all nine compartments are necessary to produce homo- and hetero-synaptic

LTP and LTD.

3. The seven ion channels introduced by Aradi and Holmes (1999) are not necessary to produce homo- and hetero-synaptic LTP and LTD.

4. The level of noisy spontaneous activity before HFS determines the magnitude of heterosynaptic LTD.

5. The metaplasticity of the first stimulation reduces the level of synaptic plasticity caused by the second HFS.

6. Different patterns of HFS affect the level of synaptic plasticity outcomes generated experimentally.

To test these hypotheses and examine our plasticity model we simulated four different experimental studies from three different papers.

## 1.1 Outline

The thesis is organized into 13 chapters.

Physiology background. Chapter 2 gives a brief description of memory and learning mechanisms. The hippocampus, including one of its components the dentate gyrus, is also introduced, and the necessary properties of the dentate granule cell are described. These properties are important as all our computer simulations are based on this specific cell. The structure of a single neuron and cell membrane with its ion channels and ion pumps are also introduced in this chapter. The Nernst equation, resting potential, action potential, electrical and chemical synapse with their mechanisms are also briefly explained. At the end of the chapter, the synaptic plasticity and plasticity phenomena of along with two important aspects, LTP and LTD, are described.

Computational Mathematics background. In Chapter 3, computational neuroscience and computational modeling along with their applications are introduced. Some realistic and simplified models of a neuron, such as the Hodgkin-Huxley model, multi-compartmental model, Izhikevich model and the integrate-and-fire model are described. Very basic concepts of ordinary differential equations and partial differential equations are also summarized in this chapter, and the NEURON environment with

its properties is introduced. Various kinds of synaptic regulation with different forms of synaptic plasticity are introduced as well. Finally, different mechanisms involved in synaptic plasticity, such as STDP (spike timing-dependent-plasticity) and metaplasticity are explained.

Review of experimental studies. All simulations from this thesis are based on three experimental studies from Abraham *et al.* (2001), Abraham *et al.* (2007) and Bowden *et al.* (2012). Therefore, in Chapter 4, these three papers are described. Experimental studies from Abraham *et al.* (2001) which correspond to the simulations from the first protocol, are described first. In this paper the role of metaplasticity on heterosynaptic LTD of the granule cell in a freely moving rat was investigated. Next, experimental studies from Abraham *et al.* (2007) are reviewed. In this paper the role of spontaneous activity in generating heterosynaptic LTD in the dentate gyrus of anaesthetised rats was examined. This review corresponds to the simulation from the second protocol. Moreover, the metaplasticity effect of the first medial perforant path HFS on the ability to generate synaptic plasticity by the second medial perforant path HFS was also discussed in this paper. This effect corresponds to the simulation from the third protocol. The last paper discussed is the experimental study by Bowden *et al.* (2012). In this paper the effect of different patterns of HFS on homosynaptic LTP and simultaneous heterosynaptic LTD was examined. This investigation corresponds to the fourth protocol.

Methods Chapter 5 describes the nine-compartment model of a dentate granule cell (Santhakumar *et al.*, 2005) with seven ion channels, as well as the noisy presynaptic spontaneous activity that is generated randomly. For the plasticity simulations, STDP and metaplasticity rules are employed as well. Finally the type of integration method which has been used in the simulations is discussed.

Initial results. In Chapter 6, the relation between our metaplasticity rule and the sliding modification threshold from the BCM rule is discussed. In this chapter the nine compartmental model of granule cell is re-evaluated. It is also determined whether or not the nine ion channels used in Aradi and Holmes (1999) are necessary for our plasticity model.

Finding data parameters. In Chapter 7, to find the metaplasticity parameters, the experimental study from the first protocol is examined and the simulations applying

only the first HFS to the medial pathway are run and considered. Then the magnitude of LTP and LTD as a function of the changing number of parameters: $\tau_p$, $\tau_d$, initial synaptic weights and frequency of medial and lateral noisy spontaneous activity is investigated.

First protocol. Chapter 8 corresponds to section 4.1 from Chapter 4. This chapter shows how a combination of STDP and metaplasticity rules with the reduced morphology multi-compartmental model of the granule cell, accompanied with noisy spontaneous activity can reproduce homosynaptic LTP in the MPP and concurrent heterosynaptic LTD in the LPP.

Second protocol. In Chapter 9, which corresponds to section 4.2 from Chapter 4, the role of noisy spontaneous activity in generating heterosynaptic LTD in the non-tetanized pathway (LPP) is investigated.

Third protocol. Chapter 10 corresponds to section 4.3 from Chapter 4. In this chapter the metaplasticity impact of the first medial perforant path HFS on synaptic plasticity induced in the MPP and LPP resulting from the second HFS is examined.

Fourth protocol. Chapter 11 corresponds to section 4.4 from Chapter 4. In this chapter, the role of different patterns of HFS on synaptic plasticity is investigated.

Discussion In Chapter 12, a summary of the results and the main contribution of the thesis are examined and interpreted. Finally the model is compared with the other published works and studies.

Conclusion and further work. Chapter 13 concludes the thesis with final remarks about the main outcomes of the thesis. Furthermore, some limitations of the thesis are also mentioned and, finally, we provide some predictions and suggestions for the possible future research in this area.

# Chapter 2

# Neurobiology background

In this chapter we briefly summarise memory, memory processing and learning. We also summarize some basic concepts and definitions in relation to the structure of the brain, focusing on critical regions which are involved in the processing of information and memory such as the hippocampus and one of its components, the dentate gyrus. Following this, the characteristic properties of the granule cell in the dentate gyrus, the cell in which all the computational and experimental work in this thesis takes place, are introduced.

We also briefly describe the structure of a single neuron and cell membrane with the major ionic concentration in the extracellular and intracellular regions of the membrane. The ion channels and ion pumps as components of the cell membrane which allow specific ions flow into or out of the cell membrane are then introduced. Then we briefly explain the ionic diffusion and electrical drift which respectively relate to the ionic concentration and potential difference between inside and outside the membrane. In the next section we introduce the Nernst equation, resting potential and action potential. We also briefly explain electrical synapse and the chemical synapse and chemical synapse mechanism.

Finally, we introduce the phenomenon of synaptic plasticity, which supports learning and memory formation. We briefly explain the synaptic plasticity mechanism. And finally, two different aspects of synaptic plasticity: long-term potentiation (LTP) and long-term depression (LTD) with their mechanisms are introduced.

## 2.1 Learning and memory

Learning can be defined as a lasting change in the way one acts or reacts to an event as a result of previous experience (King, 2008). Memory and learning have a very strong relationship with each of them being influenced by the same factors. While a permanent changing of behaviour as a result of new experiences would be classified as learning, memory would include the process of encoding, storing and retrieving the particular experiences. When we forget an important piece of information or event, the precious character of memory is brought to mind. With memory we can update existing knowledge and compare one experience with another. One of the more fundamental abilities of the human brain is memory processing, as what you remember determines who you are. Different areas of the brain activate simultaneously or at least, within milliseconds, during encoding, recording, and remembering specific experiences, events and skills (Seel, 2012).

### 2.1.1 Short-term memory

The ability to store and recall around five to nine items for a brief period of time, is referred to as short-term memory (Miller, 1956). Some areas of the brain that are activated during short-term memory processing are the prefrontal lobe and areas within the medial temporal gyrus (Coon and Mitterer, 2008). When a person matures, her/his short-term memory improves and this short-term memory usually reaches its highest level during young adulthood, then gradually gets worse during subsequent aging (Dempster, 1981; Huttenlocher and Burke, 1976; Kail and Salthouse, 1994).

### 2.1.2 Long-term memory

Long-term memory is designed to store potentially unlimited information over a long period of time. Interestingly the more we know, the easier it becomes for us to add new information. Long-term memory storage is thought to be based on meaning and cohesion of notions and not on how the words sound. When an error occurs during the retrieval of information from long-term memory, we are usually invoking the meaning of that piece of information. For example when trying to recall the word ‘bargain’ from

long-term memory, we might mistake it with the word ‘trade’ or ‘business’ rather than ‘bagging’ or ‘begin’ (Coon and Mitterer, 2008).

## 2.2 Divisions of the brain

The average human brain weighs about 1.5 kg, which accounts for approximately 2% of adult body weight. The brain is composed of about 80% water, 10-12% fatty lipids and 8% proteins and consumes about 20–25% of the body’s oxygen, nutrients and glucose.

Three anatomical areas of the brain coinsist of: the cerebral cortex, the brain stem and the limbic system. The brain stem is responsible for the processing of intrinsic needs including eating and breathing, whereas the limbic system processes a variety of functions such as emotions, behaviour and long term memory. The amygdala and hippocampus are two parts of the limbic system. The hippocampus is associated with episodic memory and learning, while the amygdala is associated with emotional learning and fear.

The cerebral cortex is specialised for more complex mental activities such as problem solving, high level thinking and memory. The cerebral cortex is divided into four different regions: the frontal lobe, the temporal lobe, the parietal lobe and the occipital lobe. The occipital lobes are involved in visual processing and visual memory. The temporal lobes are related to the processing of sound, language and memory, whereas the parietal lobes are concerned with the sense of touch, pain, heat and cold. Finally, the frontal lobes are involved with decision making, planning and processing of emotion (Schwartz, 2010).

## 2.3 The neuron

Neurons are the basic elements of the nervous tissue. These specialised cells construct the massive networks which communicate and transmit information from one part of the brain to another (Stahl, 2013). There are different types of neurons such as sensory neurons, interneurons and motor neurons, each of them specialised to be involved in different functions. Sensory neurons transmit information from the outside world to the brain. Motor neurons convey impulses from the brain to the muscles, and interneurons

create the connections between two or more neurons. Neurons contain a large nucleus, cell membrane, cytoplasm and a number of organelles. The nucleus consists of 46 chromosomes formed from DNA and proteins, and is separated from cytoplasm by the nuclear membrane. The cell membrane is one of the most organized parts of the cell body. Most molecular reactions and cellular processes occur within the cell membrane (Acton, 2012). An intracellular electrode can be used to measure the voltage across the membrane. The electrical potential across the membrane is variable and is called the membrane potential.

As can be seen from Figure 2.1 each neuron has three major components: the soma, dendrites and an axon. The metabolic and genomic center of the neuron is the soma; major activity of the neuron occurs in this particular area. Neurons receive electrical and chemical inputs from other neurons, or sensory receptors, through their dendrites and somata. The dendritic anatomy is a tree-like structure with many branches, which increases the surface area of the cell body to receive electrical signals. Neurons can have one or many main dendrites depending on their functions.

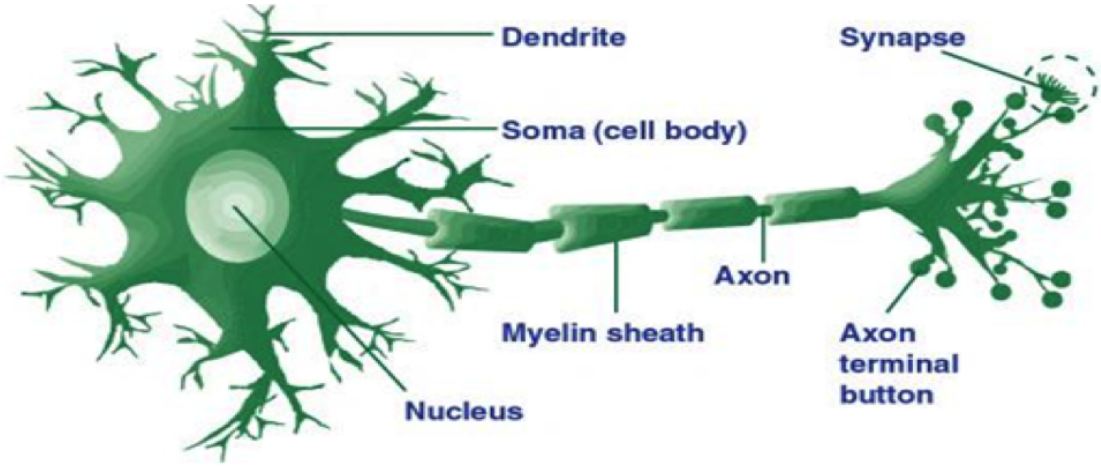


Figure 2.1: This schematic picture outlines the major structure of a single neuron (Sousa, 2011)

.

Dendrites transmit electrical signals through the neuron to the soma. Electrical signals flow from the cell body down the axon and finally transmit from one neuron to another neuron via synapses. Each neuron has only one axon, but each axon may have one or many branches to communicate with other neurons.

Many axons are covered by a myelin sheath which speeds transmission of the elec-

trical signals. Furthermore, the electrical firing usually initiates in the axon hillock which joins the axon to the soma. Unlike dendrites, transmission of information along the axons is achieved via a specific electrochemical process called an action potential (Schwartz, 2010). There are little nodules located at the end of each axon which are called terminal buttons. When electrical signals reach the end of the axon, they react with the terminal buttons to release chemicals called neurotransmitters which bind to receptors on the postsynapse to generate electrical signals in the postsynaptic neuron.

### 2.3.1 Cell membrane

The cell membrane separates the intracellular organelles from the extracellular space. The concentration of the various ions within intracellular medium (cytoplasm) and extracellular medium is different. The principal ions in the neuron such as sodium ($Na^+$), potassium ($K^+$), calcium ($Ca^{2+}$) and magnesium ($Mg^{2+}$) are positively charged (cations) while chloride ($Cl^-$) is negatively charged (anions). Usually there is a balance between anions and cations in both the intracellular and extracellular space of the cell.

As can be seen from Figure 2.2, the concentration of the extracellular sodium is higher than the intracellular sodium, however, the intracellular space has a higher concentration of potassium than the extracellular space. The major component of the membrane is the lipid bilayer. This, is made up of two layers of lipids, thereby making the membrane relatively impermeable to ions and water molecules. The relative impermeability of the membrane plus the differential ionic concentrations between the intracellular and extracellular spaces builds a net of positive ions outside the cell and negative ions inside the cell and thus an electrical field across the membrane (Sterratt *et al.*, 2011)

### 2.3.2 Ion channels

The lipid bilayer of the membrane contains pores which are called ion channels. Ion channels are made of protein and allow only certain ions to flow across the membrane. There are two types of channels, active and passive. When active channels are in open states, they allow ions to pass through the channel. However, when they are in closed states, it is not possible for ions to pass through the channel. The state of the active

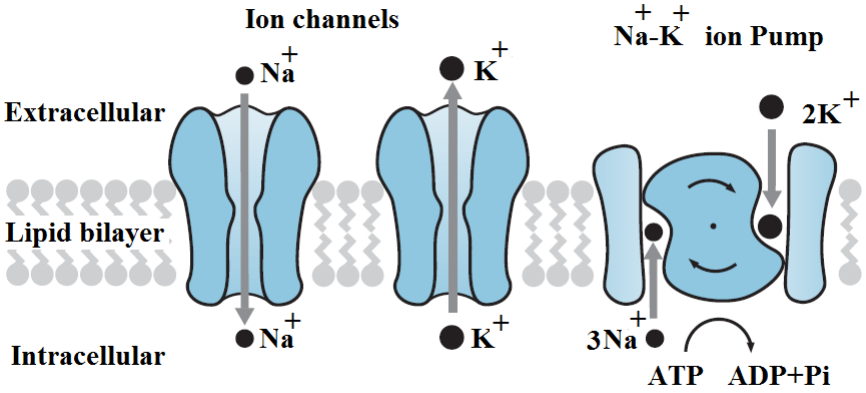


Figure 2.2: The lipid bilayer, the ion channel and ion pump from the neurons membrane are shown. The lipid bilayer is impermeable to the ions. The ion channel forms a pore through the membrane which allows specific ions pass the membrane (Sterratt *et al.*, 2011)

channels depends on the membrane potential, ionic concentration and the presence of bound ligands. Conversely, the permeability of the passive channels does not depend on the membrane potential or any other elements. Both active and passive channels at their open state are only permeable to specific types of ions.

### 2.3.3 Ionic pumps

The ionic pumps are membrane spanning proteins which pump specific types of ions and molecules. When the concentration of ions on one side of the membrane is high, ions will tend to flow to the other side of the membrane through their ion channels to diminish the concentration gradient. However, the ion pumps move the ions against their concentration gradient. Each ion pump is specific for different combinations of ions. For example, the sodium-potassium pump moves two $K^+$ ions into the cell and pumps three $Na^+$ ions out of the cell. These ionic exchanges need energy which is provided by hydrolysis of one molecule of adenosine triphosphate or ATP (Sterratt *et al.*, 2011).

Because the electrical activity of the neuron is based on the ionic movements within the cytoplasm and through ion channels, it is important to understand the phenomena that describe these ionic movements.

### 2.3.4 Diffusion

The movement of particles from the region with a high concentration to the region with a low concentration is called diffusion. [X] defines the concentration of an arbitrary molecule or ion X. When the amount of [X] is different between the two sides of the membrane, molecules diffuse from the side with the higher concentration to the side with the lower concentration. The amount of X that flows through a cross-section of the unit area per unit time is defined as the flux of diffusion with units mol $cm^{-2}s^{-1}$ and the molar flux or $J_{X,diff}$ is denoted by

$$J_{X,diff} = -D_X \frac{d[X]}{dx} \tag{2.1}$$

where $D_X$ is the diffusion coefficient of the molecule X with units $cm^{-2}s^{-1}$. The negative sign denotes that the flux is in the opposite direction.

### 2.3.5 Electrical drift

We know that ions in the cytoplasm and within the channels are moving. To understand the effect of the electrical field on the ionic movements, we consider the cytoplasm and its ion channels as a narrow cylindrical tube with the cations and anions uniformly spread within the tube (this means there is no diffusion). We connect the electrodes to a battery placed at the end of tube so that one end of tube has a higher electrical potential than the other end. Therefore, as illustrated in Figure 2.3, cations push to the negative side of the battery and anions travel to the positive side of the battery (Sterratt *et al.*, 2011). The flux of the electrical drift is denoted by:

$$J_{X,drift} = - - \frac{D_X F}{RT} z_X [X] \frac{dV}{dx} \tag{2.2}$$

where $z_X$ is the ion signed valency, $R$ is the gas constant with units J $K^{-1}mol^{-1}$, $T$ is the temperature with unit Kelvins and $F$ is Faraday's constant with units C $mol^{-1}$.

### 2.3.6 Electrodiffusion

Electrodiffusion describes both movements of ions which are related to the voltage and ionic concentration. The total flux of an ion X, $J_X$ is the sum of diffusion flux and drift

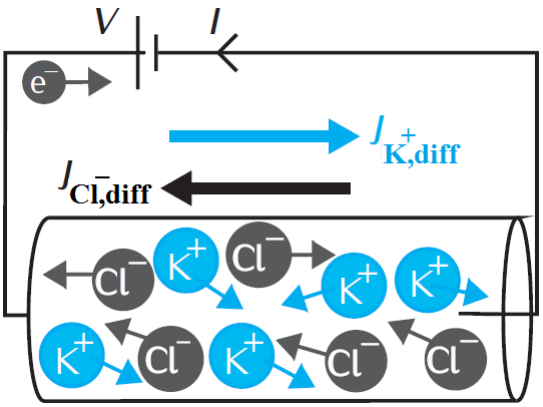


Figure 2.3: The cylindrical tube shows potassium ions with the positive charge and chloride ions with the negative charge. Because of the potential difference between the ends of tube, the potassium ions flow to the positive terminal and the chloride ions flow the negative terminal (Sterratt *et al.*, 2011)

.

flux and it is called Nernst-Planck equation which is denoted by:

$$J_{\mathrm{X}} = J_{\mathrm{X,diff}} + J_{\mathrm{X,drift}} \tag{2.3}$$

### 2.3.7 Current density

Because the neuron acts like an electrical circuit, the flow of the charge carried by molecules is more significant rather than the molecules themselves. Thus, we introduce a new component called current. Current is the amount of positive charge that flows per unit of time past a point in a conductor and ampere is a unit of a current. Current density is the amount of charge that flows per unit of time per unit of cross-sectional area. The unit of current density is $\mu$A cm$^{-2}$ and when X is a particular ion, $I_{\mathrm{X}}$ is denoted by:

$$I_X = F z_X J_X \tag{2.4}$$

where $F$ is Faraday's constant and $z_{\mathrm{X}}$ is the ion's signed valency.

## 2.4 The Nernst equation and the resting potential

The neuron membrane is at equilibrium when an equal number of positive ions flow out of the cell due to the diffusion and flow into the cell because of the electrical drift. At equilibrium, a stable potential difference across the membrane can be measured and it is called equilibrium potential (Sterratt *et al.*, 2011). The equilibrium potential is formulated by the Nernst equation:

$$E_{\mathrm{X}} = \frac{RT}{z_{\mathrm{X}}F} \ln \frac{[\mathrm{X}]_{\mathrm{out}}}{[\mathrm{X}]_{\mathrm{in}}} \tag{2.5}$$

where X is the membrane permeable ion, $[\mathrm{X}]_{\mathrm{out}}$ and $[\mathrm{X}]_{\mathrm{in}}$ are respectively the extracellular and intracellular concentration of X and $E_{\mathrm{X}}$ is the equilibrium potential or Nernst potential. Extracellular concentration, intracellular concentration and equilibrium potential of four ions from squid giant axon is shown in Table 2.1 (Sterratt *et al.*, 2011).

Table 2.1: The concentrations of four ions inside and outside the axon is shown. Equilibrium potentials are derived from these values using the Nernst equation.

| ion | $K^+$ | $Na^+$ | $Cl^-$ | $Ca^{2+}$ |
|---|---|---|---|---|
| Concentration inside (mM) | 400 | 50 | 40 | $10^{-4}$ |
| Concentration outside (mM) | 20 | 440 | 560 | 10 |
| Equilibrium potential (mV) | −72 | 57 | −64 | 139 |

If there is a balance between the concentration of the ions and permeability of the ions at both inside and outside of the cell, then the cell is at resting potential. The resting potential of the squid giant axon is around −65 mV. At the resting potential $Na^+$ and $Cl^-$ ions flow into the cell and $K^+$ ions flow out of the cell. As can be seen from Table 2.1 according to the Nernst equations, the equilibrium potential of $Cl^-$ and $K^+$ are very close to the resting potential in the squid giant axon. Therefore, we can characterize the resting membrane potential with the $Cl^-$ and $K^+$ Nernst equation (Ermentrout and Terman, 2010).

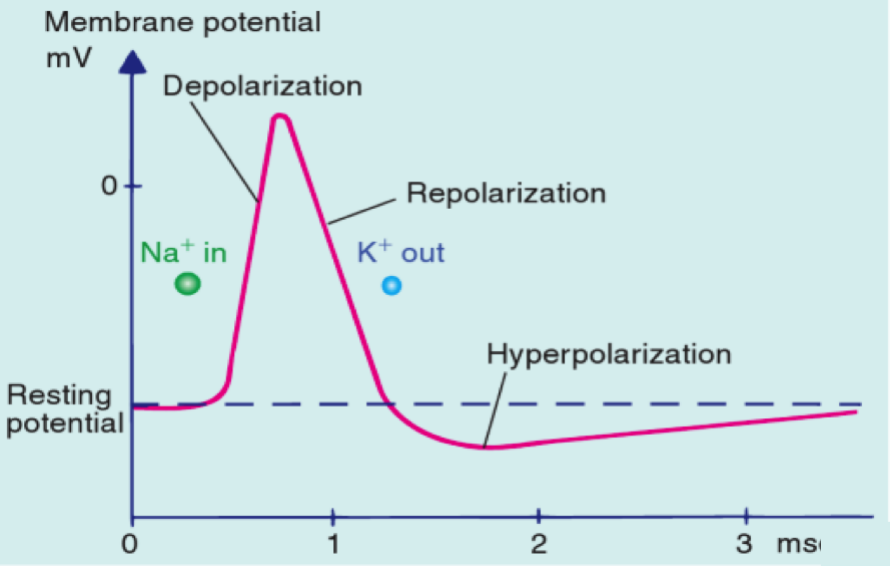


Figure 2.4: Opening $Na^+$ channels increases the membrane potential and causes depolarisation. When membrane potential reaches the peak sodium channels close and potassium channels open which decrease the membrane potential and causes repolarisation. During the hyperpolarisation phase, membrane potential continues to decrease and becomes more negative (Brodal, 2004).

## 2.5 Action potential

One form of dynamic change in membrane voltage is the action potential (AP). This phenomenon is essential for sensing, processing and communication in the nervous system. An AP is generated when the membrane voltage of a cell passes a membrane threshold and causes a neuronal spike. Once an AP is generated it propagates away from that point throughout the cell. The propagation of an AP is facilitated by both the active and passive transmission of the electrical signal. Figure 2.4 illustrates the AP of a point along the squid giant axon. When the membrane exceeds the voltage threshold, sodium channels open and allow sodium ions to diffuse into the axon and increase the membrane potential rapidly. This status is called depolarisation.

A few milliseconds after diffusion of sodium ions into the cell, the sodium channels begin to close and potassium channels open to diffuse potassium out of the cell, which returns the membrane potential to the resting state (Figure 2.4). This phase is called repolarization. During repolarization, when potassium channels are still open, the membrane potential allows potassium ions to diffuse out of the cell and make the membrane potential even more negative than the resting state. This stage is called

hyperpolarization or after hyperpolarization potential (AHP) (Hall, 2010). The AHP is generated by multiple $Ca^{2+}$-dependent and $K^{+}$-dependent ion channels and acts to limit cell firing.

In the processing of electrical signals it is very important to know when the next action potential occurs and which factors are involved in the occurrence of that action potential. The new action potential cannot happen as long as the membrane potential is still in a depolarisation or hyperpolarization status. This is because shortly after the action potential starts the sodium channels close and they cannot open until the membrane potential returns to a resting state.

The time duration that will be taken for a neuron to return to the resting potential is determined by the duration of AHP. AHP reduces the cell firing rate; however, reduction of AHP duration increases the excitability of the neuron and postsynaptic depolarisation. Reduction of AHP duration increases synaptic plasticity. This idea is well supported by experimental studies of Sah and Bekkers (1996) when blockage of AHP currents increased long-term synaptic plasticity in the hippocampus (Saar *et al.*, 1998)

Once the membrane potential returns to a resting state, or it is close to a resting state, a new action potential can be generated. The time period during which the next action potential cannot occur, even with a very strong stimulation, is called the absolute refractory period (Hall, 2010).

### 2.5.1 Propagation of the action potential

Once the action potential is generated it is conducted down the axon. This phenomenon is referred to as the propagation of an action potential and is what allows information to be transferred from one part of the nervous system to another. After enough depolarization, the axon will reach the threshold level at which voltage-gated sodium channels open. At this stage the action potential is initiated. Then the positive charge flows into the cell which depolarizes a segment of membrane until it reaches threshold level and generates its own action potential. In this way the action potential travels down the axon until it reaches the axon terminal to initiate synaptic transmission.

When an action potential is initiated at one end of an axon, it propagates in one

direction only and does not backtrack. This is because of the sodium channels being inactivated as a result of the membrane refractory period. An action potential, however, can be generated by depolarization at either end of the axon and therefore can propagate in either direction. The phenomenon that action potentials conduct in one direction is called orthodromic conduction. Backward propagation of the action potential can be evoked experimentally and is called antidromic conduction. Moreover, the axonal membrane is excitable along its entire length which helps impulses to propagate throughout the membrane (Bear *et al.*, 2007).

### 2.5.2 Backpropagation of the action potential

Once the action potential is initiated, some potential can propagate backward into the dendritic tree. This propagation can be passive, in which case it decays relatively rapidly. However, in some cells the action potential can actively backpropagate into the dendritic tree. Although the backpropagation of action potential depends upon voltage gated $Na^+$ channels, it can also depend upon voltage gated $Ca^{2+}$ channels and can be blocked by $K^+$ channels (Bear *et al.*, 2007).

## 2.6 Hippocampus

The hippocampus is a small structure of the brain which is located under the cerebral cortex (Figure 2.5). This seahorse-shaped area of the brain is essential for consolidation of information from short-term memory to long-term memory. Very basically it is thought that the hippocampus temporarily stores pieces of information as a short-term memory before transmitting them to the cortex for long-term storage. The hippocampus is also one of the few areas of the brain with the capability to grow new neurons. Moreover numerous experimental studies *in vivo* indicate the critical role of the hippocampus in sensory processing, spatial navigation and controlling spatial memory.

The structure of the hippocampus consists of the dentate gyrus, cornu ammonis (CA) fields including CA1, CA2, CA3 and CA4 and the subiculum. The input region of the hippocampus that receives signals from the entorhinal cortex is called the dentate gyrus. The hippocampus receives its major input from the entorhinal cortex via the perforant pathway (Wible, 2013). Transferring of major outputs from the hippocampus

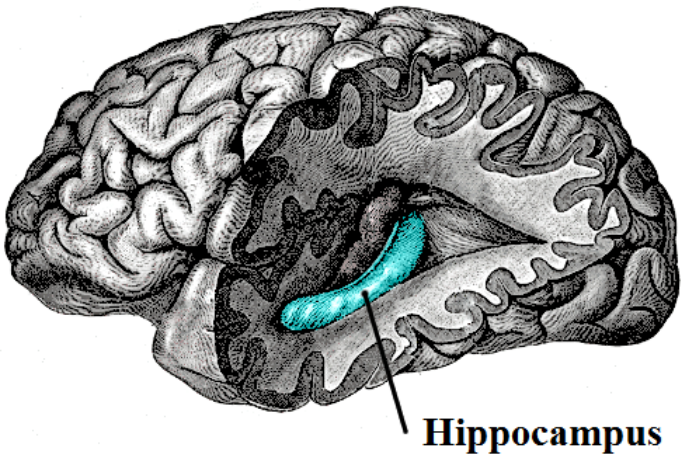


Figure 2.5: The hippocampus is located in the medial temporal lobe of the human brain. Source: https://en.wikipedia.org/wiki/Hippocampus

occurs via the fornix. These bidirectional connections of the hippocampus with many areas of the neocortex indicate the hippocampus has a critical role in the processing of long term memory. Damage to the hippocampus region has also been shown to lead to very serious memory disorders (Noback *et al.*, 2005).

### 2.6.1 Dentate gyrus

The dentate gyrus is a simple cortical region of the hippocampus formation and has a U shaped structure (Figure 2.6). It consists of three layers; a molecular layer, a granule cell layer and a polymorphic cell layer. There are three major cell types in the dentate gyrus, the granule cells, mossy cells and basket cells. Although the dentate gyrus is the major terminal region for projecting inputs from the entorhinal cortex, the dentate gyrus does not project any signals to the entorhinal cortex. Due to these characteristics, it is thought the dentate gyrus can be considered as a first step toward the processing of memory information. After transferring information from the entorhinal cortex to the dentate gyrus, dentate gyrus processes the information as a specific task and transmits them as signals to the CA3 and CA1 regions of the hippocampus (Scharfman, 2011).

In the following section we explain why our work is limited to this particular network of the hippocampus.

The phenomenon by which neurons can be generated by the neural stem cells is

called neurogenesis (birth of neurons). This process plays a central role in neural development. There are only two regions of the mammalian's brain with the capacity of generating adult neurogenesis, namely the olfactory bulb and dentate gyrus (Barker *et al.*, 2011). New evidence shows that neurogenesis in the dentate gyrus might be required for different aspects of memory encoding such as pattern separation. Pattern separation is known as the specific feature of the dentate gyrus which is related to information processing (Deng *et al.*, 2010). Data from Nakashiba *et al.* (2012) illustrate that dentate granule cell neurogenesis is involved in the evoking of old memories and the formation of new memories and it can be concluded that probably adult-born granule cells support the pattern separation behavior. Furthermore, it has been suggested that dentate gyrus neurogenesis is involved in encoding of spatial and contextual information by the hippocampus. The temporal integration theory reveals another important feature of the adult neurogenesis of dentate gyrus. This theory concentrates on a specific aspect of memory encoding, and suggests that adult neurogenesis helps evoke when events occur and the temporal proximity of events (Drew *et al.*, 2013). Moreover, Drew and his colleagues determined the dynamic character of the dentate gyrus in relation to function of memory. They also described how the process of detection, storage and encoding of memory interact with each other. Added to this, investigations from Snyder *et al.* (2001) show that adult dentate granule cell neurogenesis is involved in the process of synaptic plasticity. They also concluded that because the dentate gyrus is a major terminal for projecting inputs into the hippocampus, synaptic plasticity in adult dentate granule cells is undeniable for the hippocampal functions of learning and memory.

### 2.6.2 The dentate granule cell

Here we concentrate on the dentate granule cell as all the experimental and computational studies that were undertaken were based on this cell and its workings. Granule cells are the principal nerve cells in the dentate gyrus (Figure 2.7). Granule cell all extend into the molecular layer and terminate near the hippocampus fissure. The size of the granule cell depends on the location of the cells in the dentate gyrus. Those dendrites on cells that are located in the suprapyramidal blade are larger than those

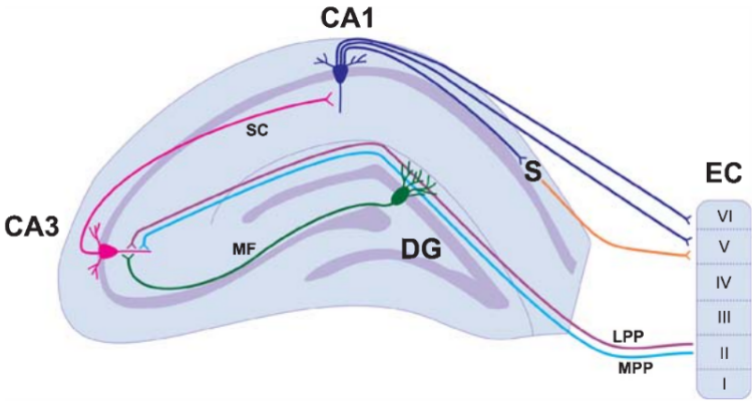


Figure 2.6: A simplified hippocampal circuitry illustrating trisynaptic and monosynaptic circuits. The basic circuitry of the hippocampus is commonly termed the trisynaptic circuit. Layer II of the entorhinal cortex provides input to the granule cells of the dentate gyrus via the medial (light blue) and lateral (purple) perforant paths. The dentate granule cells project to pyramidal cells of the CA3 via the mossy fibre pathway (green). CA3 pyramidal neurons project to the CA1 via schaffer collaterals (pink). The CA1 pyramidal cells project to both the subiculum and to layers V and VI of the entorhinal cortex. Abbreviations: Cornu Ammonis (CA); Dentate Gyrus (DG); Entorhinal Cortex (EC); Lateral Perforant Path (LPP); Medial Perforant Path (LPP); Mossy Fibres (MF); Schaffer Collaterals (SC); Subiculum (S). Source: (Patten *et al.*, 2015).

that are located in the infrapyramidal blade (Scharfman, 2011). Furthermore, granule cell dendrites receive their excitatory synaptic inputs from various sources that make synapses on precisely defined parts of their dendritic trees. The dendritic tree is divided into four parts; The granule cell layer dendrites (GCLD), the proximal (PD), middle (MD) and distal (DD) dendrites. The proximal part of the granule cell dendritic tree receives signals from commissural and associational fibres arising mostly from cells in the polymorphic cell layer. The MD receives signals from the medial entorhinal cortex, and the DD receives inputs from the lateral entorhinal cortex (Andersen *et al.*, 2006). As explained in the last section, most excitatory inputs of the dentate gyrus come from the entorhinal cortex through the perforant pathway. The perforant pathway is composed of the medial perforant pathway (MPP) and lateral perforant pathway (LPP). The MPP transmits inputs to the MD of the dentate granule cell and the LPP transmits inputs to the DD of the dentate granule cell. The MPP processes the spatial information via activation of NMDA receptors whereas, the LPP processes non-spatial information via activation of opioid receptors (Scharfman, 2011). Furthermore, those neurons that project from the MEC (medial entorhinal cortex ) via the MPP generate

subthreshold oscillations in synchrony which pace the firing of the MEC neurons. In contrast, those neurons that project from the LEC (lateral entorhinal cortex) via the LPP do not have membrane properties to generate subthreshold oscillations. Therefore, the spatial information processed by the MPP does not correlate with the non-spatial information processed by the LPP (Hayashi and Nonaka, 2011).

The reason that we have chosen the dentate granule cell in our study is because firstly, we are aware of the firing properties of the dentate granule cell due to many studies that have been done in this cell. For example, one feature of the spiking behavior of the dentate granule cell is having a large depolarizing after-potential which follows the action potential. Secondly, this cell can express three types of voltage-gated calcium channels and two types of calcium activated potassium channels. This is crucial for our compartmental model of granule cell that is explained in the next chapter (Aradi and Holmes, 1999).

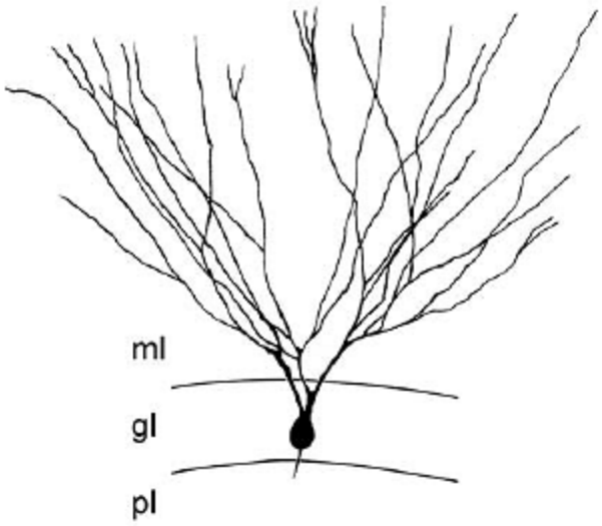


Figure 2.7: The dentate granule cell https:www.researchgate.net/figure/6074169

.

## 2.7 The synapse

A synapse is a specialized junction that allows neurons to contact and communicate with the other neurons or cell types (such as a muscle or glandular cell). The first

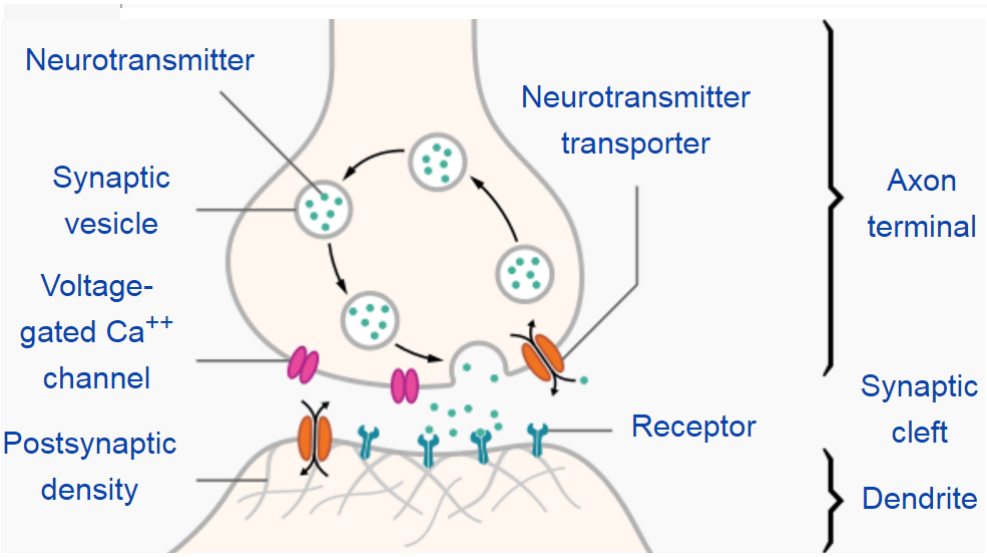


Figure 2.8: Chemical synapse. Source: https://commons.wikimedia.org/wiki)

neuron that conducts the information to the target cell (dendrite) is called the presynaptic cell and the target cell is called the postsynaptic cell. When an action potential transfers from a presynaptic neuron to the synapse, the electrical response occurs in the postsynaptic cell. There are two types of synapse, electrical synapses and chemical synapses. With electrical synapses, the ionic current can transfer directly from one cell to the other cells. This is because in the electrical synapses the membranes of the two cells are separated by the actual protein called gap junction or connexinns, therefore allowing the speedy transfer of signals between the pre- and postsynaptic cells. Most gap junctions allow the ionic current to flow in both direction; therefore electrical synapses are bidirectional (Bear *et al.*, 2007).

Chemical synapses are more common in mammals and humans. The structure of the chemical synapse is illustrated in Figure 2.8. The end of the axon in the presynaptic terminal is referred to as the terminal button. The narrow cleft (about 10 to 50 nm) between the presynaptic terminal and postsynaptic side of the chemical synapse is referred to as the synaptic cleft. Because the synaptic cleft in the chemical synapses is much wider than the gap junction in the electrical synapses, the presynaptic action potential cannot actually pass the synapse. This explains why the postsynaptic potential of the chemical synapse is independent of the action potential's magnitude.

The presynaptic terminal carries the synaptic vesicles that have submicroscopic

spherical structure. Synaptic vesicles contain neurotransmitters which flow into the synaptic cleft. When neurotransmitters pass the synaptic cleft, they interact with the receptors of the post synaptic membrane (Schmidt et al., 2013).

### 2.7.1 Neurotransmitters

As illustrated in Table 2.2 (Bear *et al.*, 2007) neurotransmitters can be divided into three chemical categories: amino acids, amines and peptides. The amino acid and amine neurotransmitters are all small molecules stored in and released from synaptic vesicles. However, peptide neurotransmitters are large molecules stored in and released from secretory granules.

Table 2.2: The Major Neurotransmitters.

| Amino Acids | Amines | Peptides |
|---|---|---|
| $\gamma$ -aminobutyric acid (GABA) | Acetylcholine (ACh) | Cholecystokinin |
| Glutamate (Glu) | Dopamine (DA) | Dynorphin |
| Glycine (Gly) | Epinephrine | Enkephalins (Enk) |
| | Histamine | N-acetylaspartylglutamate |
| | Norepinephrine | (NE) Neuropeptide Y |
| | Serotonin (5-HT) | Somatostatin |
| | | Substance P |
| | | Thyrotropin-releasing hormone |
| | | Vasoactive intestinal polypeptide |

Different neurons release different neurotransmitters and each neurotransmitter will be released for different purposes. All three categories of neurotransmitters mediate fast synaptic and slow synaptic transmission at the CNS. The amine acetylcholine (ACh) mediates fast synaptic transmission at all neuromuscular junctions and the amino acids such as glutamate (Glu), gamma-aminobutyric acid (GABA) and glycine (Gly) mediates fast synaptic transmission at most CNS synapses.

Once the action potential arrives at the axonal terminal, how can it trigger the neurotransmitters to be released? Depolarizing of the terminal membrane opens voltage-gated calcium channels. These are permeable to $Ca^{2+}$ and they are similar to the sodium channels. As long as the calcium channels are open large amounts of $Ca^{2+}$ flow

into the terminal, forcing neurotransmitters to be released from synaptic vesicles.

After neurotransmitters are released into the synaptic cleft, they bind to the specific kind of receptor proteins that are embedded in the postsynaptic density. Binding of neurotransmitters to the receptors cause changes in their functions. There are two classes of receptors: transmitter-gated ion channels and G-protein-coupled receptors (Bear *et al.*, 2007).

Transmitter-gated channels are not as selective as voltage-gated channels. However, when the open channels are permeable to $Na^+$, it causes the postsynaptic cell to be depolarized. The phenomenon in which the postsynaptic membrane is depolarized by the presynaptic release of neurotransmitter is called an excitatory postsynaptic potential (EPSP). Synaptic activation of ACh-gated and glutamate-gated ion channels causes EPSPs. When the transmitter-gated channels are permeable to $Cl^-$, it causes the postsynaptic cell to be hyperpolarized (because the chloride equilibrium potential is negative). Therefore, the phenomenon whereby the postsynaptic membrane is hyperpolarized by the presynaptic release of neurotransmitter is referred to as an inhibitory postsynaptic potential (IPSP). Synaptic activation of glycine-gated or GABA-gated ion channels cause an IPSP.

All types of neurotransmitters could bind on G-protein-coupled receptors and cause slower, long-lasting and diverse postsynaptic action potentials. After the neurotransmitter molecules attach to the receptor proteins that are embedded in the postsynaptic membrane, small proteins will be activated by the receptor proteins. These small proteins freely move on the intracellular surface of the postsynaptic membrane. Activation of G-proteins activates effector proteins, that can activate additional enzymes in the cytosol to regulate ion channel function and alter cellular metabolism. Because G-protein receptors trigger extensive metabolic effects, they are referred as metabotropic receptors (Bear *et al.*, 2007).

## 2.8 Synaptic plasticity

We are interested to know which mechanisms at the molecular and cellular level of the brain are involved in the establishment of new memories and how these new experiences transit from the short-term memory to the long-term memory. The experience-

dependent changes in the efficacy of synaptic activity have a remarkable role in translation of experiences to new memories (Davis *et al.*, 2002) and are referred to as synaptic plasticity.

Synaptic plasticity is the ability of neural activity to modify the behavior of neural circuits. This theoretical idea was proposed for the first time by Hebb (1949) and Konorski (1948). According to this idea, those neurons that are activated simultaneously increase the strength of mutual communication. However, this theory did not suggest the conditions that lead to synaptic weakening, which may also contribute to memory formation. L$\phi$mo in 1966 was the first to observe these activity-dependent synaptic changes in the mammalian brain, during his experimental studies. A few years later, he and his colleague Bliss published this first evidence of long-lasting potentiation. These breakthroughs were a great motivation for scientists to further investigate synaptic plasticity in the mammalian brain, including the investigation of synaptic plasticity at the Schaffer-collateral pathway in the hippocampus (Bliss and Cooke, 2011; Blundon and Zakharenko, 2008).

Synaptic plasticity can be classified as being either homosynaptic or heterosynaptic. During homosynaptic plasticity synapses need to be activated directly by presynaptic stimulation. However, for heterosynaptic plasticity to occur, synapses do not need to be activated by presynaptic stimulation for its induction. Therefore, all synapses from a nerve cell can manifest heterosynaptic plasticity after a strong stimulation. Both homosynaptic and heterosynaptic plasticity are characteristic for learning and memory formation (Chistiakova *et al.*, 2014).

Three mechanisms can be involved in the modification of neural circuits: modification in the efficacy and strength of synaptic transmission at pre-existing synapses, creating new synaptic connections, and regulation of the excitatory properties of individual neurons. The amplitude of the excitatory postsynaptic potential (EPSP) reflects synaptic efficacy (synaptic weight) and depends on presynaptic and postsynaptic factors. Presynaptic factors include the amount of neurotransmitters which are released, and postsynaptic factors include the altered number or properties of postsynaptic receptors (Jedlicka, 2002). Alteration of these synaptic properties can last for a few milliseconds to a few days or weeks. Short-term synaptic plasticity and long-term synaptic plasticity are two distinct forms of synaptic plasticity (Davis *et al.*, 2002).

### 2.8.1 Synaptic plasticity mechanisms

Two main receptors involved in synaptic plasticity are $\alpha$-amino-3-hydroxy-5-methyl-4-isoxazolepropionic acid (AMPA) and N-methyl-D-aspartate (NMDA) receptors (Dingledine *et al.*, 1999). During the most common excitatory transmission process the excitatory neurotransmitter glutamate binds to the AMPA and NMDA receptors. AMPA and NMDA receptors are both permeable to $Na^+$ and $K^+$ ions (Figure 2.9). During the activation of these receptors, large amounts of $Na^+$ flow into the postsynaptic membrane while only small amount of $K^+$ flows out of the postsynaptic membrane. These intracellular and extracellular ionic behaviors depolarize the membrane potential.

Between AMPA and NMDA receptors, the AMPA receptor is the one that carries the large amount of synaptic signaling. This channel has a high permeability for $Na^+$ ions and can also be permeable to $Ca^{2+}$ ions. AMPA receptors carry inward currents at negative potentials and outward currents at positive potentials, with a zero mV reversal potential. Inward and outward ionic currents in the NMDA receptor are a bit different from AMPA receptor. When membrane potential is at the resting potential, the $Mg^{+2}$ ion blocks the NMDA receptor and does not allow other ions to pass the membrane. However, during depolarization of the membrane the magnesium ion emits from the pore and allows sodium, potassium and also calcium ions to pass the channel. When membrane potential is positive relative to rest, the permeability of the NMDA receptor is at the highest level.

The kinetics of the NMDA receptor is much slower than for the AMPA receptor, as is the activation of the NMDA receptor. NMDA receptors can stay open for hundreds of milliseconds after presynaptic release of glutamate while the AMPA receptors stay open for only a few milliseconds. Only when the glutamate neurotransmitter is bound the NMDA receptor and postsynaptic membrane is depolarized does the NMDA receptor open and allow the ionic current to pass. Through this mechanism NMDA receptor plays the role of a molecular coincidence detector, which is essential for several forms of synaptic plasticity (Lüscher and Malenka, 2012)

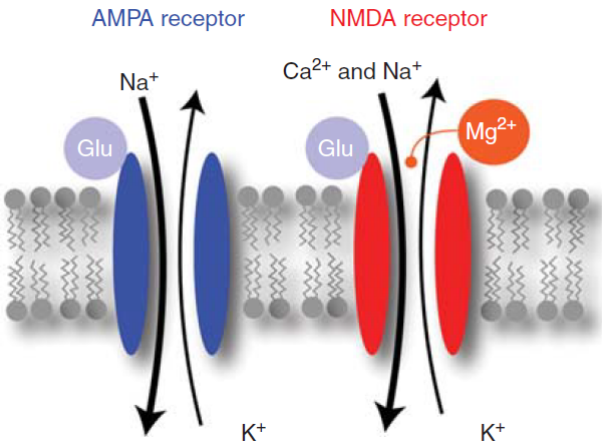


Figure 2.9: AMPA and AMPA are two significant receptors that are involved in the LTD and LTP process. Binding glutamate to the AMPA receptors, causes diffusion of sodium ions into the membrane and potassium ions out of the membrane which depolarize the membrane. However NMDA receptors are permeable to the calcium when the magnesium is removed from the NMDA pore causing the membrane to depolarize (Lüscher and Malenka, 2012).

### 2.8.2 Short-term plasticity

Short-term plasticity is a form of activity-dependent plasticity which alters synaptic efficacy and can last for tens of milliseconds to several minutes. It is believed that short-term plasticity is also related to memory and information processing. If, during short-term synaptic plasticity, synaptic strength is reduced for hundreds of milliseconds to seconds, short-term depression occurs. In contrast, when synaptic strength is enhanced for hundreds of milliseconds to seconds, short-term potentiation occurs (Fioravante and Regehr, 2011).

### 2.8.3 Long-term plasticity

Long-lasting modification in synaptic efficacy is referred to as long-term plasticity. There are two kinds of long-term synaptic plasticity, long-term potentiation and long-term depression. Mechanisms that support activity-dependent long-lasting modifications in synaptic strength have become a well-studied area in neuroscience. Enhancements or weakenings of synaptic efficacy are believed to be involved in the physical and chemical formation of learning and memory (Menon, 2012).

### 2.8.4 Long-term potentiation (LTP)

Long-term potentiation (LTP) is the long-lasting enhancement of synaptic efficacy that can last for hours or even months (Abraham *et al.*, 1994, 2002).The first published observation of long-term potentiation was in 1973 by L ∅mo and Bliss. They observed the enhancement in the excitatory postsynaptic potential in the dentate gyrus in anaesthetised rabbits following electrical stimulation applied to the perforant path. During in vivo experiments, long-term potentiation (LTP) lasted up to 60 min. Although scientists used to apply 15 Hz stimulation to induce LTP, Douglas and Goddard discovered that high-frequency stimulation produces much stronger and longer LTP than 15 Hz stimulation at the perforant path synapses. Many experimental studies from other regions of the brain indicate that the LTP can be induced by a high-frequency simulation (Bliss and Lømo, 1973). In addition, numerous experimental studies indicate that not only in the frequency of the presynaptic activity critical for inducing LTP, but so is the precise timing of pre-and postsynaptic spikes (Levy and Steward, 1983). It is widely believed that long-term potentiation can be considered as a cellular mechanism for storage of information and memory formation (Blundon and Zakharenko, 2008).

Experimental studies show that the hippocampus is not the only area that shows long-term potentiation; many other regions of the brain can also manifest LTP, i.e, all major brain areas such as the cortex, cerebellum, midbrain, brainstem and ganglia. Moreover, not only excitatory synapses show LTP, as evidence reveals that inhibitory synapses can also manifest LTP (Kullmann and Lamsa, 2007).

### 2.8.5 Long-term depression (LTD)

Long-term depression is the long-lasting reduction of synaptic efficacy that generally lasts for hours or months. LTD is a decrease in the level of the synaptic neural response of the neurons to stimuli from afferents (Collingridge *et al.*, 2010). In the hippocampus, long-term depression happens when depolarisation of postsynaptic cells is relatively weak; this is in contrast to LTP induction, which requires a strong depolarisation. One of the more robust theories used to explain LTD and LTP and their rules is the Bienenstock, Cooper and Munro (BCM) theory of synaptic plasticity (Bienenstock *et al.*, 1982; Cooper *et al.*, 2004). The BCM theory stipulates that because

of the LTD mechanism, as long as postsynaptic neurons are depolarised weakly, active synapses become depressed. Furthermore, when postsynaptic action potentials precede excitatory presynaptic activities, LTD occurs (Markram *et al.*, 1997). LTD can be considered as an initial step in synaptic elimination (Bastrikova *et al.*, 2008). This means those synapses that lose their strength may eventually be eliminated. According to the real experimental studies in vivo, homosynaptic LTP can be induced by applying HFS to the medial perforant pathway. However, simultaneously heterosynaptic LTD can occur in the neighbouring lateral pathway (Abraham *et al.*, 2001). Synaptic plasticity manifested as LTP and LTD can occur simultaneously in many regions of the brain. In the granule cell of the dentate gyrus both LTP and LTD can occur simultaneously in neighbouring synaptic pathways (Douglas and Goddard, 1975; Levy and Steward, 1979; Abraham and Goddard, 1983; Doyère *et al.*, 1997).

### 2.8.6 Induction of LTP and LTD

To induce LTP and LTD, specific patterns of activity are needed (Malenka, 1994). When glutamate is released from the presynaptic membrane and the postsynaptic membrane is depolarized, the $Mg^{2+}$ ion will be removed from the NMDA receptor which causes LTP to be induced. Therefore, both pre- and postsynaptic membranes need to be activated simultaneously during LTP induction. As a result of simultaneous depolarization and glutamate binding, a large amount of $Ca^{2+}$ ions flow into the membrane through the NMDA receptor which activates intracellular signaling and finally causes modification of synaptic efficacy (Lüscher and Malenka, 2012).

By contrast, only repeated activation of presynaptic activity at low frequency will be enough to induce the LTD. Because even at the resting potential, the AMDA receptor is not blocked properly by $Mg^{2+}$ ions and also driving force of the $Ca^{2+}$ ions into the membrane is quite high which causes the $Ca^{2+}$ ions to flow into the cell during low-frequency synaptic stimulation. Flowing $Ca^{2+}$ into the cell through the NMDA receptor can cause either LTP and LTD induction; therefore there needs to be a way for the cell to decide whether to potentiate or depress synaptic connections. Experimental studies show that moderate activation of NMDA receptor causes generation of a moderate calcium level intracellularly which favors LTD induction. Conversely, strong

activation of the NMDA receptor causes a release of a high level of calcium which favors LTP induction (Malenka, 1994). Moreover, other experimental studies indicate that specific timing between pre- and postsynaptic action potentials affects LTP and LTD induction. Concurrent timing of pre- and postsynaptic membrane causes back-propagation of both synaptic potential and action potential into the dendrites which makes additional depolarization to activate the NMDA receptor and flow calcium into the postsynaptic membrane. When a presynaptic spike is repetitively evoked slightly before firing the postsynaptic membrane, the EPSP precedes the backpropagation of action potential and repetitive firing of pre-post action potential evokes LTP (Lüscher and Malenka, 2012). By contrast, if repetitive backpropagation of action potential is followed slightly before the presynaptic spike, repetitive post-pre firing leads to LTD induction. A high concentration of calcium ions in the dendritic spine (postsynaptic membrane) leads to activation of calcium/calmodulin-dependent kinase II (CaMKII) which is required for triggering LTP (Lisman *et al.*, 2002). A moderate concentration of calcium ions into the dendritic spine (postsynaptic membrane) leads to activation of protein phosphatases which triggers LTD (Lüscher and Malenka, 2012).

## 2.9 Summary

The aim of this chapter was to introduce some structures of the brain that are involved in learning and memory processing. Introducing different aspects of a single neuron was necessary for the next chapter as we want to introduce the multi-compartmental model of neuron to model the granule cell dendrites and soma. We briefly explained about diffusion, electrical drift and electrodiffusion to better understand ionic behavior inside and outside the membrane. We also briefly described the mechanism of chemical synapses and neurotransmitters, which is necessary to perceive how the action potential conducts from presynaptic axonal terminal to the postsynaptic dendrites. The main purpose of this thesis is to test different experimental studies supported by different mechanisms such as multi-compartmental model of neuron, synaptic plasticity and metaplasticity models to see which mechanisms are sufficient for producing synaptic plasticity in the dentate granule cell. Therefore, we provided a brief description of different types of synaptic plasticity, with the main focus on LTP and LTD and their

mechanisms.

# Chapter 3

# Mathematical and computational modeling

In this chapter we examine the meaning of computational neuroscience and the goal of computational modeling in neuroscience. In the next section we introduce two realistic models of a neuron, the Hodgkin-Huxley model which describes the generation and propagation of action potential, and the multi-compartmental model which is used to simulate signal processing within the dendritic tree of a single neuron. We then introduce some simplified models of a neuron with their properties. In the next section we summarize some basic concepts of the ordinary differential equations and partial differential equations. We also briefly describe the NEURON environment and its properties as all our simulations are in this environment. In the next section we examine some synaptic mechanisms for regulating the output of the neuron and its firing rate to stabilize the neuron. Then we describe two complementary forms of synaptic plasticity, the homosynaptic and heterosynaptic plasticities. Then we introduce different models of plasticity with their properties. We focus on STDP (spike timing dependent plasticity), the mechanism of plasticity that we have selected for our simulations. At the end we introduce the metaplasticity phenomenon with some metaplasticity models.

## 3.1 Computational neuroscience

Computational neuroscience is the computational implementation of theoretical concepts of brain functions which uses specific techniques, models and methods to advance

our understanding of processing, retrieving and organising information in the nervous system. Thus, the aim of computational neuroscience is to implement and test various hypotheses of the mechanisms of functions of the brain and nervous system. Analysis and evaluation of these models is an essential component for continual development in this area. The importance of comparing real experimental studies with computational models is evident through the ability to generate hypotheses and improve theoretical models. Within computational modeling, it is possible to employ different numerical and analytical techniques to control different aspects of the models. On the one hand, an appropriate computational model should be comprehensive enough to be comparable with real experimental studies. On the other hand, it should also be simple enough to explain certain specific aspects of brain function, because keeping too many details might be irrelevant and unnecessary to investigate the specific aspect of the brain (Ulinski, 1999).

## 3.2 Ordinary differential equations

There are a variety of phenomena in technology and science that can be described by differential equations (DEs), therefore, solving (DEs) accurately and efficiently is an important issue.

The first order ordinary differential equation (ODE) is indicated by:

$$\frac{dy}{dt} = f(t, y), \tag{3.1}$$

where $f$ is a given function of $t$ and $y$ and $y$ contained in $R^m$ is a vector. Here $t$ is called the independent variable and $y = y(t)$ is the dependent variable. Because the order of derivative is one, the order of the equation will be one as well and is called an ordinary differential equation as $y$ depends on one independent variable only.

### 3.2.1 Analytic solutions

A differentiable function $y(t)$ is a solution of equation 3.1, if for all $t$

$$\frac{dy}{dt} = f(t, y(t)). \tag{3.2}$$

If we suppose that $y(t_0)$ is known and the solution of equation 3.2 is valid in the interval $[t_0, t_1]$, with integrating of both side of the equation 3.1 with respect to $t$, we have:

$$y(t) - y(t_0) = \int_{t_0}^{t} f(s, y(s))ds \quad s \in [t_0, t_1]. \tag{3.3}$$

Equation 3.3 has an analytic solution if there is an exact solution for the integration for $y$.

If the order of derivative in equation 3.1 is higher than one, the order of ordinary differential equation will be higher than one. For example the second order equations of the form:

$$\frac{d^2y}{dt^2} = f(t, y, \frac{dy}{dt}). \tag{3.4}$$

arise in many practical applications.

### 3.2.2 Initial values

A solution of equation 3.1 will be the solution of the integration 3.3. If we are looking for a unique solution, we should add one extra condition that is called initial value.

The general form of a first order initial value problem (IVP) is:

$$\begin{aligned} \frac{dy}{dt} &= f(t, y) \\ y(t_0) &= y_0, \end{aligned} \tag{3.5}$$

where $y$ can be a vector.

For the second order equations such as equation 3.4, it is necessary to introduce two conditions to define $y$ uniquely. In an initial value problem, both these conditions are prescribed at the initial point ($t_0$).

For example:

$$\begin{aligned} \frac{d^2y}{dt^2} &= f(t, y, \frac{dy}{dt}) \\ y(t_0) &= y_0 \\ \frac{dy}{dt}(t_0) &= \frac{dy_0}{dt}, \end{aligned} \tag{3.6}$$

### 3.2.3 Numerical methods

Most systems in real life consist of complicated system of equations that need an approximate solution therefore, the numerical solution will be the best option for them rather than the analytic solution. In the numerical method the domain of the independent variable $t$ is subdivided into a number of discrete points, $t_0$, $t_1 = t_0 + \Delta t$,..., and then the approximate values of the dependent variable $y$ and the derivatives of $y$ with respect to $t$ will be calculated only in these points.

Thus, a sequence of values $y_0$, $y_1$, ..., $y_n$, such that

$$y_n \approx y(t_n) \quad n \geq 0 \tag{3.7}$$

The approximate solution calculates at point $t_n$ while, $t_n = t_0 + n\Delta t$ and $y(t_n)$ is the analytic solution at $t_n$ and $y_n$ is the numerical solution obtained at $t_n$.

### 3.2.4 Explicit and implicit method

Explicit methods calculate the state of the system at a later time from the state of the system at the current time without the need to solve algebraic equations. Implicit methods find a solution by solving an equation involving both the current state of the system and the later one. For example, if $y(t)$ is the current system state and $y(t+\Delta t)$ is the state at the later time ($\Delta t$ is a small time step) therefore, for an explicit method $y(t + \Delta t) = f(y(t))$.

However, in the implicit method to find the solution for $y(t + \Delta t)$, at first

$$G(y(t), y(t + \Delta t)) = 0. \tag{3.8}$$

should be solved. As can be seen, implicit methods require an extra computation (solving the above equation).

### 3.2.5 The Euler Method

One of the oldest numerical methods for solving the initial value problem is the Euler method.

$$\begin{aligned} y' &= f(t, y) \\ y(t_0) &= y_0, \end{aligned} \tag{3.9}$$

Suppose that $f(t, y)$ is analytic in the neighborhood of the initial value $t_0$, $y_0$

Choose a value $\Delta t$ for the size of every step and set $t_n = t_0 + n\Delta t$. Now, one step of the (forward) Euler method from $t_n$ to $t_{n+1} = t_n + \Delta t$ is

$$y_{n+1} = y_n + \Delta t f(t_n, y_n). \tag{3.10}$$

The value of $y_n$ is an approximation of the solution to the ODE at time $t_n$: $y_n \approx y(t_n)$. The Euler method is explicit, i.e. the solution $y_{n+1}$ is an explicit function of $y_i$ for $i \leq n$.

However, the backward Euler method can be calculated by:

$$y_{n+1} = y_n + \Delta t f(t_{n+1}, y_{n+1}). \tag{3.11}$$

In contrast with the forward Euler method, the backward Euler method is an implicit method in which the new approximation $y_{n+1}$ appears on both sides of the equation, and thus the method needs to solve an algebraic equation for the unknown $y_{n+1}$.

### 3.2.6 Integration method of Crank-Nicholson

The Crank-Nicholson method or the central difference is a finite difference method with the accuracy of the second order in time, which was developed by Crank and Nicholson. The error oscillation of this method decays with time, therefore the solution is stable and safe for most solutions. The Crank-Nicholson method is a combination of the backward and forward Euler methods. It is equivalent to advancing by one half step using backward Euler and then advancing by one half step using forward Euler. The global error for this method is proportional to the square of the step size (Hines and Carnevale, 1997).

By considering the forward Euler method as:

$$\frac{y_{n+1} - y_n}{\Delta t} = f(t_n, y_n) \tag{3.12}$$

and the backward Euler method as:

$$\frac{y_{n+1} - y_n}{\Delta t} = f(t_{n+1}, y_{n+1}) \tag{3.13}$$

the Crank-Nicholson method can be calculated as:

$$\frac{y_{n+1} - y_n}{\Delta t} = \frac{f(t_n, y_n) + f(t_{n+1}, y_{n+1})}{2}. \tag{3.14}$$

## 3.3 Partial differential equations

The dependent variable like $y$ in the ordinary differential equations is a function of only one variable like $(x)$. However in the partial differential equations (PDEs) the function of dependent variable might be dependent on more than one independent variable. A general representation of a second order PDE with two independent variables, $x_1$, $x_2$ is:

$$F(x_1, x_2, y, \frac{\partial y}{\partial x_1}, \frac{\partial y}{\partial x_2}, \frac{\partial^2 y}{\partial x_1^2}, \frac{\partial^2 y}{\partial x_2^2}, \frac{\partial^2 y}{\partial x_1 x_2}) = 0. \tag{3.15}$$

For a partial differential equation to be uniquely specified extra conditions are needed. In each of the independent variables, one needs as many extra conditions as the highest order of the derivatives in this variable.

There are two classes of neuron models: realistic neuron models and simplifying neuron models. In this section we compare each of these models and explain different aspects of them.

## 3.4 Realistic neuron models

Realistic models of the neuron are based on the cellular mechanisms of neural function. These models describe the internal properties of a real neuron. The Hodgkin-Huxley model, otherwise known as the active conductance-based model of the neuron is a realistic model with high biological accuracy. This model is based on the different concentration of various ions internal and external to the membrane (D?Angelo *et al.*, 2013). One of the benefits of this model is having parameters relevant and measurable with biological tools. The multi-compartmental model of the neuron is another realistic

model of the neuron that models the dendritic tree of a single neuron. Synaptic integration, interaction between ion channels and dendritic morphology and other behaviours involved in the single neuron can also be described with this model (Izhikevich, 2004).

### 3.4.1 Hodgkin-Huxley model

The Hodgkin-Huxley model of a neuron was developed by Hodgkin and Huxley (1952). This active conductance based model contains the detailed mathematical equations to describe the generation and propagation of action potential of a neuron. The Hodgkin-Huxley model is a realistic model of neuronal spike generation based on cellular mechanisms of the neural membrane which is able to describe the intrinsic properties of a real neuron. These different ion concentrations are responsible a potential difference between the inside and the outside of the membrane. The Hodgkin and Huxley model describes the changes in membrane potential by ordinary differential equations. In this model, depending on real experimental data, new ion channels can be implemented to make the firing patterns the same as in a real neuron (D?Angelo *et al.*, 2013). The Hodgkin-Huxley model is also capable of reproducing significant features of the membrane potential such as the absolute refractory period and the relative refractory period, which were discussed in the last chapter (Paugam-Moisy and Bohte, 2012).

The Hodgkin-Huxley model is formulated by a set of ordinary equations and non-linear differential equations. The membrane potential $V$ is calculated as

$$C\frac{dV}{dt} = -i_{\mathrm{Na}} - i_{\mathrm{K}} - i_l + I, \tag{3.16}$$

where $C$ is referred as membrane capacitance, $I$ is the external current, $i_{\mathrm{Na}}$, $i_{\mathrm{K}}$ and $i_l$ are ion currents of sodium, potassium and leakage respectively:

$$i_{\mathrm{Na}} = g_{Na} m^3 h (V - E_{\mathrm{Na}}), \tag{3.17}$$

$$i_{\mathrm{K}} = g_K n^4 h (V - E_{\mathrm{K}}), \tag{3.18}$$

$$i_l = g_l (V - E_l), \tag{3.19}$$

where $g_{\mathrm{Na}}$, $g_{\mathrm{K}}$ and $g_l$ are the maximum conductance of the sodium channel, potassium and leakage channel. $E_{\mathrm{Na}}$ , $E_{\mathrm{K}}$ and $E_l$ are sodium, potassium and leakage reversal

potentials, respectively. Variables $m$ and $n$ are dimensionless sodium and potassium activation gates respectively, and $h$ is a dimensionless inactivation gate:

$$\frac{dm}{dt} = \alpha_m(V)(1-m) - \beta_m(V)m, \tag{3.20}$$

$$\frac{dn}{dt} = \alpha_n(V)(1-n) - \beta_n(V)n, \tag{3.21}$$

$$\frac{dh}{dt} = \alpha_h(V)(1-h) - \beta_h(V)h, \tag{3.22}$$

where $\alpha_m$, $\beta_m$ and $\alpha_n$, $\beta_n$ and $\alpha_h$, $\beta_h$ are the rate functions, which determine the transition between open and closed states of ion channels (Moujahid *et al.*, 2011). Rate functions for the gating variables obey these equations:

$$\alpha_m(V) = (2.5 - 0.1V)/[\exp(2.5 - 0.1V) - 1], \tag{3.23}$$

$$\beta_m(V) = 4\exp(-V/18), \tag{3.24}$$

$$\alpha_n(V) = (0.1 - 0.01V)/[\exp(1 - 0.1V) - 1], \tag{3.25}$$

$$\beta_n(V) = 0.125\exp(-V/80), \tag{3.26}$$

$$\alpha_h(V) = 0.07\exp(-V/20), \tag{3.27}$$

$$\beta_h(V) = 1/[\exp(3 - 0.1V) + 1], \tag{3.28}$$

The Hodgkin-Huxley model of the neuron can describe the firing behaviour of the neuron well only when the membrane potential is isopotential (the membrane potential is constant in all area of the membrane). However, dendrites cannot be considered as isopotential because different parts of the dendrites are at different potentials (Sterratt *et al.*, 2011). Therefore, if we want to model the complete behavior of a neuron with a large dendritic tree, a compartmental model should be used.

### 3.4.2 Models of dendritic tree of neurons

According to real experimental studies, when the dendritic tree is extensive, the effects of synaptic inputs onto different locations of the dendrites are not the same. Therefore, for taking into account the morphological details of the dendritic tree, it may be necessary to use a large number of compartments. In the compartmental models, each

dendrite (or axon) can be divided into some small segments or compartments. According to the shape of dendrites (and axon) each compartment has a different radius, length and voltage that can be formulated by ordinary differential equations (Sterratt *et al.*, 2011).

#### 3.4.2.1 Ohm's law

In the fixed temperature of the wire when the current $I$ is proportional to the potential difference $V$, then the wire obeys the ohmic law.

$$I = GV \tag{3.29}$$

where $G$ is constant and called conductance with the unit siemens. The inverse of conductance is called resistance $R$ with unit ohms. Therefore the above equation can also be denoted as:

$$I = \frac{V}{R} \tag{3.30}$$

#### 3.4.2.2 Kirchhoff's current law

Kirchhoffs current law or KCL, states that the total current or charge entering a junction or node is exactly equal to the current leaving the node, as no charge is lost within the node. In other words the algebraic sum of all the currents entering and leaving a node must be equal to zero, $I_{\text{exiting}} + I_{\text{entering}} = 0$. This is a consequence of the principle of conservation of charge.

#### 3.4.2.3 The capacitive current

The rate of the change of the membrane potential is proportional to the net flow of the current through the membrane and is inversely proportional to the capacitance and it is described by the following equation:

$$\frac{dV}{dt} = \frac{I}{C} \tag{3.31}$$

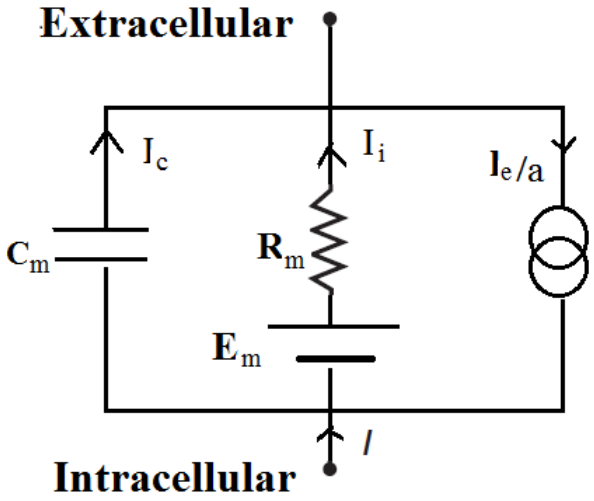


Figure 3.1: The electrical circuit representing a passive patch of membrane.

#### 3.4.2.4 The RC circuit

Figure 3.1 shows the RC circuit. To find out how the membrane potential changes as the current is injected into the circuit, we need to monitor the variation of current with voltage. According to Kirchhoff's current law, the sum of the current $Ia$ flowing through the membrane and the injected current $I_e$ is equal to the sum of the capacitance current $I_c a$ and the ionic current $I_i a$ when $a$ is the curved surface area of the cylinder (Sterratt *et al.*, 2011):

$$Ia + I_e = I_c a + I_i a \tag{3.32}$$

When the ionic current flows though the resistor and battery, the following equation is denoted:

$$I_i a = \frac{V - E_m}{\frac{R_m}{a}} \tag{3.33}$$

where $R_m/a$ is the resistance of the membrane and $E_m$ is the equilibrium potential of the membrane. And finally the capacitive current is proportional to the rate of change of the voltage and it is denoted by the following equation:

$$I_c a = C_m a \frac{dV}{dt} \tag{3.34}$$

The membrane capacitance is $C_m a$. If we suppose that the circuit is isolated then $Ia$ is zero. If we substitute the $I_i$ and $I_c$ in equation (3.32), therefore:

$$C_m \frac{dV}{dt} = \frac{E_m - V}{R_m} + \frac{I_e}{a} \tag{3.35}$$

This is the first-order ordinary differential equation (ODE) for the membrane potential $V$ with units from Table 3.1 (Source : (Sterratt *et al.*, 2011)).

Table 3.1: Passive quantities

| Quantity | Description | Typical units | Relationships |
|---|---|---|---|
| $d$ | Diameter of neurite | $\mu$m | |
| $l$ | Length of compartment | $\mu$m | |
| $R_m$ | Specific membrane resistance | $\Omega$ cm$^2$ | |
| $C_m$ | Specific membrane capacitance | $\mu$F cm$^{-2}$ | |
| $R_a$ | Specific axial resistance (resistivity) | $\Omega$ cm | |
| $r_m$ | Membrane resistance per inverse unit length | $\Omega$ cm | $r_m$=$R_m/\pi d$ |
| $c_m$ | Membrane capacitance per unit length | $\mu$F cm$^{-1}$ | $c_m$=$C_m$ $\pi d$ |
| $r_a$ | Axial resistance per unit length | $\Omega$/cm$^{-1}$ | $r_a$= $4R_a/\pi d^2$ |
| $V$ | Membrane potential | mV | |
| $E_m$ | Leakage reversal potential due to different ions | mV | |
| $I$ | Membrane current density | $\mu$A cm$^{-2}$ | |
| $I_e$ | Injected current | nA | |
| $I_c$ | Capacitive current density | nA/$cm^2$ | |
| $I_i$ | Ionic current density | mA/$cm^2$ | |

### 3.4.3 Multi-compartmental models

A multi-compartmental approach is a useful way to model the complicated structure of the dendrites. Basically the dendritic tree splits up into the small segments or compartments. Therefore, each compartment can be considered isopotential (Ermentrout and Terman 2010). According to Figure 3.2, if we consider each compartment as a cylinder with a length $l$ and a diameter $d$, the curved surface area of the cylinder $a = \pi dl$.

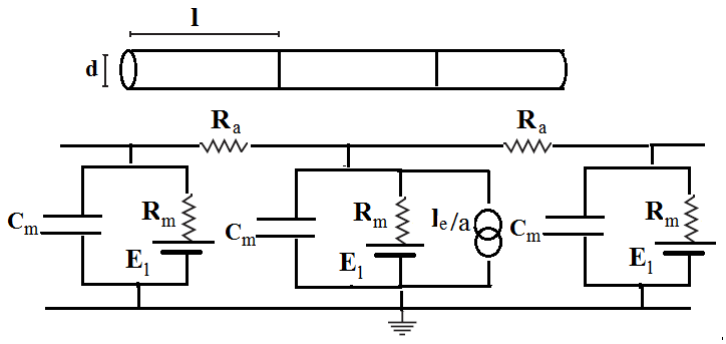


Figure 3.2: Passive membrane is described by a compartmental model.

Although the current flows through each compartment into the membrane capacitance and the membrane resistance, it also flows intracellularly and extracellularly of the membrane and can be modeled by axial resistances. The extracellular resistance can be considered zero.

According to Figure 3.2, $R_a$ is the specific axial resistance with units $\Omega$ cm and the axial resistance of the cylindrical compartment is $4R_a l/\pi d^2$ which $\pi d^2/4$ is a cross-sectional area. $j$ is the number of compartment and $V_j$ is the membrane potential in the $j$ the compartment and $I_{e,j}$ is the injected current into the compartment $j$. Now as we noted in the RC circuit we can use Kirchhoff's current law. The only difference is the current density $I_j$ is equal to the sum of the leftwards and rightwards axial currents. Therefore according to Ohm's law:

$$I_j a \quad = \frac{V_{j+1} - V_j}{4R_a l/\pi d^2} + \frac{V_{j-1} - V_j}{4R_a l/\pi d^2}. \tag{3.36}$$

where $I_j a$ is a current and according Kirchhoff's current law and equation (3.32) we have:

$$\begin{aligned} I_{c,j}a + I_{i,j}a &= I_j a + I_{e,j} \\ I_{c,j}a + I_{i,j}a &= \frac{V_{j+1} - V_j}{4R_a l/\pi d^2} + \frac{V_{j-1} - V_j}{4R_a l/\pi d^2} + I_{e,j}. \end{aligned} \tag{3.37}$$

The following equations are similar to equation (3.37) for a patch of membrane with two extra equations which describe the flowing current through two compartments $j-1$ and $j+1$:

$$\pi dl C_m \frac{dV_j}{dt} = \frac{E_m - V_j}{R_m/\pi dl} + \frac{V_{j+1} - V_j}{4R_a l/\pi d^2} + \frac{V_{j-1} - V_j}{4R_a l/\pi d^2} + I_{e,j} \tag{3.38}$$

where $a$ is the surface area of the cylinder.

$$C_m \frac{dV_j}{dt} = \frac{E_m - V_j}{R_m} + \frac{d}{4R_a}\left(\frac{V_{j+1} - V_j}{l^2} + \frac{V_{j-1} - V_j}{l^2}\right) + \frac{I_{e,j}}{\pi dl}. \tag{3.39}$$

This equation is the fundamental equation for the compartmental model. Numerically, we can solve equation (3.39) with the very high resolution by using many compartments. To understand the behavior of the system it is good to examine the analytical solutions for the equation (3.39) which leads to the cable equations (Sterratt *et al.*, 2011).

### 3.4.4 The cable equation

To find the analytical solution for equation (3.39) we divide the neuron into an infinite number of small compartments with the small quantity $\delta x$, therefore a compartment with the index $j$ will be at position $x = j\delta x$ along the cable. Here $V_j = V(x,t)$, $V_{j-1} = V(x - \delta x, t)$, $V_{j+1} = V(x + \delta x, t)$ and $I_e(x,t) = I_{e,j} l \delta x$ are respectively the membrane potentials at compartments $j$, $j-1$, $j+1$ and the current injected at compartment $j$. Therefore, equation (3.39) can be rewritten as:

$$\begin{aligned} C_m \frac{\partial V(x,t)}{\partial t} &= \frac{E_m - V(x,t)}{R_m} \\ &+ \frac{d}{4R_a}\left[\frac{1}{\delta x}\left(\frac{V(x+\delta x,t) - V(x,t)}{\delta x} + \frac{V(x-\delta x,t) - V(x,t)}{\delta x}\right)\right] + \frac{I_e \pi dl}{\pi d}. \end{aligned} \tag{3.40}$$

when $\delta x$ becomes very small and goes to 0, the second term from the left side of the equality is known as second derivation and it is written as:

$$\frac{\partial^2 V(x,t)}{\partial t^2} = \lim_{\delta x \to 0} \frac{1}{\delta x}\left(\frac{V(x+\delta x,t) - V(x,t)}{\delta x} + \frac{V(x-\delta x,t) - V(x,t)}{\delta x}\right). \tag{3.41}$$

Equation (3.41) which is derived from the compartmental equation is called cable equation and it is denoted by (Sterratt *et al.*, 2011):

$$C_m \frac{\partial V}{\partial t} = \frac{E_m - V}{R_m} + \frac{d}{4R_a}\frac{\partial^2 V}{\partial x^2} + \frac{I_e}{l}\pi d. \tag{3.42}$$

## 3.5 Simplified neural models

Because of the complexity of biological models, especially for investigating the specific properties of neural dynamics, simplified models are helpful. However, not all the

intrinsic properties of a neuron can be described by the simplified neuron model as many details of the physiological properties of the neuron will be missed. For example, their firing patterns do not explain the full range of real experimental data, such as the case of the leaky 'integrate-and-fire' model. However, these simplified models can capture the essential properties of the physical systems. 'Integrate-and-fire' model of neuron and the Izhikevich model of a neuron are known as simple models of spiking neurons.

### 3.5.1 Leaky integrate-and-fire neuron

The leaky integrate-and-fire model of neuron is one of the simplest spiking neuron models, which is very easy to simulate and analyze. The overall membrane current is

$$C\frac{dV}{dt} = I - \frac{V}{R} \tag{3.43}$$

where $V$ represents the membrane potential, $C$ is capacitance, $R$ is resistance and $I$ is an input current. When the membrane potential $V$ reaches a certain threshold $V_{\text{threshold}}$ (spiking threshold), the neuron makes a spike and the membrane potential is reset to $V_{\text{reset}}$. This model is able to reproduce some important features of biological neurons including the ability to fire over a wide frequency range and to fire tonic spikes. However, because this model has only one variable it is not able to produce burst spiking (Izhikevich, 2004).

### 3.5.2 Izhikevich model of neuron

The Izhikevich model is an example of a simple model of neuron with two dimensions, that are shown in the following equations:

$$\begin{aligned} \frac{dv}{dt} &= 0.04v^2 + 5v + 140 - u + I \\ \frac{du}{dt} &= a(bv - u) \end{aligned} \tag{3.44}$$

$$\text{if } v > +30 \text{ mV}, \quad \text{then} \quad v \leftarrow c \quad \textit{and} \quad u \leftarrow d + u \tag{3.45}$$

where $v$ is the membrane potential $u$ is a recovery variable and $I$ is a current input to the model. Parameters $a$, $b$, $c$, $d$ control the type and spiking behavior of the simulated

neuron. By choosing appropriate values for these four parameters, the model can exhibit varieties of spiking behaviors, such as bursting or chattering spiking activity, in addition to regular or fast-spiking activity. This model is also efficient for modeling large-scale networks (Izhikevich, 2004).

## 3.6 The NEURON environment

The NEURON environment is capable of simulating both biological and artificial neurons, and can efficiently simulate networks of neuron. Application of the NEURON environment is not limited only to the simulation of continuous systems, but discrete event and hybrid systems with combinations of artificial and biological neurons can be simulated also. In addition, some characteristic properties of the individual and networks of neurons such as multiple channel types, complex branching morphology, inhomogeneous channel distribution and synaptic plasticity can be described in the NEURON environment.

Furthermore, the variety of subjects that can be investigated in NEURON include the role of pre- and post-synaptic activity in the mechanism of synaptic transmission, and the function of dendritic tree and active membrane properties in synaptic integration. Apart from these applications, implementing networks of neurons with this environment helps to investigate issues such as the role of gap junctions in neuronal synchrony, information encoding in biological networks, and visual orientation selectivity (Hines and Carnevale, 2001). Applications of NEURON also include the estimation of inaccessible parameters and supporting data. The NEURON environment can be run using MacOS, Microsoft Windows, and UNIX/Linux. An interpreter programming language used by the NEURON simulator is called the hoc language. With C-like syntax, the hoc language is used to set up the basic topology of the neuron models. The hoc code was first introduced by Kernighan and Pike (1984). It is easy to write short programs with the hoc language and then execute these simulations. New types of ion channels can be described by the high-level language NMODL and can be incorporated into the NEURON environment. Thus, NEURON can simulate differential and algebraic equations of the model. To maintain effectiveness, the user-defined mechanisms in the NMODL language translate into the C language, and after compiling, they link

into NEURON (Hines and Carnevale, 1997).

### 3.6.1 Section variables

Three parameters, cytoplasmic resistivity $R_a$ ($\Omega$ cm), the section length $l$ and compartmentalization parameter "nseg" apply to the section, while the first two parameters do not affect the structure of the equations of the model.

### 3.6.2 Range variables

NEURON uses a special tool called range variable to define the variety of cellular properties such as the membrane potential and ionic conductance. With defining this variable, users are able to separate property specification from segment number.

### 3.6.3 Graphical interface

The default graphical interface is suitable for exploratory simulations involving the setting of parameters, control of voltage and current stimuli, and graphing variables as a function of time and position. The NEURON environment introduces some functions that implement graphical images of the neuron model to show what is built up by the computer. These graphical views give a reasonable image to the users for supervision and controlling a simulation (Hines and Carnevale, 1997).

### 3.6.4 Object-oriented interpreter

A useful tool in the NEURON environment is the object-oriented interpreter which facilitates simulations with a large body of content. This interpreter not only defines the membrane potential and ion channel properties of the neurons but also it controls the simulation of the program and establishes the appearance of a graphic interface.The default graphical interface is suitable for exploratory simulations involving the setting of parameters, control of voltage and current stimuli, and graphing variables as a function of time and position.

### 3.6.5 Recording and saving data

In this step, at first some vectors are created within the NEURON code for recording presynaptic activities, postsynaptic activities, synaptic weights, voltage, potentiation and depression. After that a procedure called "record()" is created to record these data. At the end two procedures such as "plasticity()" and "save()" are created. The procedures of "plasticity()" are created for calculating potentiation and depression and the procedure of "save()" is created for saving the mean of synaptic weights into the file. In the next stage we will introduce some methods to solve the differential equations from Hodgkin-Huxley and passive cable models and then how to manage a time step to execute a simulation.

### 3.6.6 The integration methods used in NEURON

The NEURON applies two stable implicit integration methods such as backward Euler (see section 2.5), and a variant of Crank-Nicholson (see section 2.6). Backward Euler is the default integration method in NEURON. This method is numerically stable and produces good results even with large time steps. NEURON can also use the Crank-Nicholson method. As a general statement one can say that both the Euler methods are first order methods while the Crank-Nicolson method is second order. This means that the error in the computed solution of the equation goes down by a factor of 2 when the time step is halved in the case of the Euler methods, while the error decreases by a factor 4 for the Crank-Nicholson method. This means that for the same accuracy one needs smaller time steps in the Euler case and therefore the running time is longer (Cohen and Hindmarsh, 1994).

## 3.7 Homeostatic plasticity

Neurons are able to modulate their excitability relative to network activity. This phenomenon is called homeostatic plasticity. Homeostatic plasticity controls the synaptic strength of the neuron. This mechanism regulates the output of the neuron and its firing rate to keep the neuron in the stable condition. There are variety of mechanisms in the brain that dramatically change the neuron's input and put the neuron's output

into the very unstable state, therefore having such a mechanism stabilizes the neuron's activity and protects their output. Three specific forms of homeostatic plasticity are synaptic scaling, homeostatic intrinsic plasticity and metaplasticity (Watt and Desai, 2010).

The synaptic scaling mechanism modulates the strength of synapses and has been reported in many neurons. Those synapses that have experienced synaptic plasticity can generate, a more unstable firing rate. Therefore, synaptic scaling keeps the synapses in the desirable size ranges. Experimental study shows that synaptic scaling occurs in different part of the brain such as cortical and spinal neurons. Burrone and colleagues in 2002, found that when the firing rate of the neuron was reduced, the synaptic input onto the neuron was scaled up. Therefore having a mechanism like synaptic scaling helps the firing rate return to the normal range. This outcome shows that the homeostatic synaptic scaling occurs at the scale of individual neurons. This study shows how synaptic scaling makes a balance between changes in presynaptic and postsynaptic activity. The intrinsic electrical property of neurons can be interpreted by voltage and calcium gated ion channels. Changes to the intrinsic properties of the neurons occur via the transition of cellular excitability. These changes help neurons and circuits to maintain electrical activity at a suitable level. Various hypotheses can explain the relation between synaptic scaling and homeostatic intrinsic plasticity. The first idea says that these two homeostatic mechanisms act in parallel to regulate synaptic plasticity. The second interesting idea says that they might be active at different stages and might be involved in a definite temporal order. And the last idea is that synaptic scaling and homeostatic intrinsic plasticity cooperate together (Watt and Desai, 2010).

## 3.8 Homosynaptic and heterosynaptic plasticity

Heterosynaptic plasticity can be induced by episodes of strong postsynaptic activity that can target any synapse. Both homosynaptic and heterosynaptic plasticity have their own computational properties and play important roles in the learning and memory systems. Moreover, these two forms of plasticity are complementary to each other and both are necessary for plasticity regulation.

Homosynaptic LTD and LTP are two forms of homosynaptic plasticity. homosy-

naptic LTD occurs when repeated activation of a synapse reduces synaptic weights. In contrast, homosynaptic LTP occurs when activity increases synaptic weights. Specific patterns of presynaptic activity such as high-frequency stimulation are needed for homosynaptic LTP induction, and a long low-frequency stimulation is typically needed for homosynaptic LTD induction. Although homosynaptic plasticity mediates associative learning and can be considered as a mechanism for short-term memory, it has the potential to increase synaptic weights to extreme values which would make a system unbalanced. As explained previously, heterosynaptic plasticity occurs on those synapses that are not activated therefore, it can target these synapses for modification. Because synaptic weights depend on the direction of heterosynaptic plasticity, it keeps the synaptic weights away from the extremes toward an equilibrium within the operation range. Therefore, to keep the synaptic weights balanced, there is a need for both homosynaptic and heterosynaptic plasticity to be induced (Chistiakova *et al.*, 2014).

LTP and LTD also can be induced heterosynaptically. Heterosynaptic LTD was detected for the first time in the dentate gyrus in vivo in 1979. In the hippocampus, homosynaptic LTP can be induced without causing any heterosynaptic plasticity but if LTP induction is to last longer, for example, more than a few hours, then a heterosynaptic mechanism is needed. Therefore these observations show that memory mechanism needs both forms of plasticity and in most experimental studies, the induction of homosynaptic plasticity in the activated synapse is accompanied by heterosynaptic LTD in the inactivated pathway, this mechanism especially occurs on the dentate GC synapses (Foy, 2001).

## 3.9 Models for synaptic plasticity

Despite a variety of experimental evidence with respect to different forms of synaptic plasticity in human and other animals, the exact mechanisms of synaptic plasticity are still unknown. In the following sections we review some of synaptic plasticity rules and mechanisms.

### 3.9.1 Hebb rule

The first models of synaptic plasticity were introduced by Donald Hebb. He predicted that correlation in the activity between postsynaptic and presynaptic cells strengthens the connections between neurons: those neurons that fire together, wire together. Hebbian plasticity is a kind of plasticity that is induced homosynaptically. According to Hebb rules, increasing the synaptic weights increases the postsynaptic firing rate which causes a positive feedback loop. Although the Hebbian learning rule explains varieties of problems such as feature selectivity and cortical map development, this form of homosynaptic plasticity is very unstable and cannot explain synaptic depression (Bush *et al.*, 2010).

$$\frac{dw_{ij}}{dt} = \alpha v_i u_j \tag{3.46}$$

where $w_{ij}$ is the synaptic weight between presynaptic $j$ with $u_j$ activity and postsynaptic $i$ with $v_i$ and $\alpha$ as a learning rule. This model of plasticity has no boundary to stop synapses from strengthening which makes the post-synaptic activity increase dramatically (Yger and Gilson, 2015). As can be seen from equation (3.46), there is no mechanism to describe synaptic depression which causes a problem for any implementation.

### 3.9.2 BCM rule

The Bienenstock, Cooper and Munro (BCM) rule was one of the primary theories of synaptic plasticity resulting from experimental studies in the visual cortex. This theory was the first plasticity rule that took into account the role of spontaneous activity. The BCM plasticity rule specifies two principal properties. Firstly, the synaptic modification threshold, or $\theta_m$, determines the direction of synaptic plasticity, whether it will be potentiation or depression. Secondly, it specifies that $\theta_m$ is a non-linear function of the time-average of postsynaptic activity; this property is called the sliding modification threshold (Bienenstock *et al.*, 1982; Cooper *et al.*, 2004). This modification threshold can change over time corresponding to the average of postsynaptic activity of the neuron. Such a cellular modification of synaptic plasticity is referred as metaplasticity (Abraham, 2008). BCM rules can be explained according to the following equations:

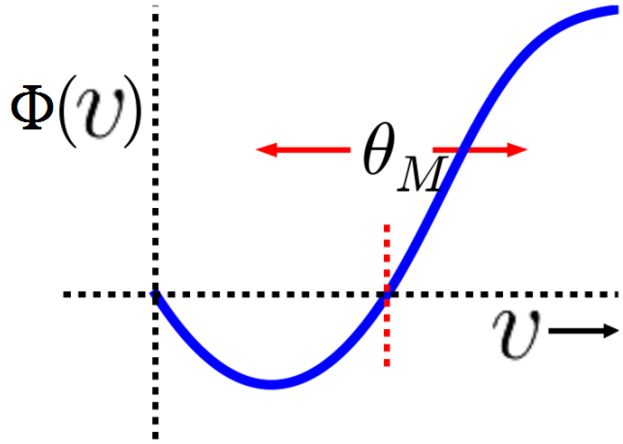


Figure 3.3: BCM response curve, $v$ is postsynaptic activity, $\theta_m$ is the modification threshold and variation of this function depends on variation of presynaptic activity. BCM function $\Phi(v)$ is the magnitude of weight change. Source: http://www.scholarpedia.org/article/BCM/

$$\Phi(v(t), \theta_m(t)) = v(t)(v(t) - \theta_m(t)); \tag{3.47}$$

$$v(t) = \sum u(t)w(t); \tag{3.48}$$

$$\frac{dw}{dt} = \eta \Phi u; \tag{3.49}$$

where $v(t)$ is the average of postsynaptic activity over time, $u(t)$ is the presynaptic activity over time, $w(t)$ is the synaptic weight over time, $\Phi$ is the synaptic modification function and $\eta$ is the modification rate (Figure 3.3). When postsynaptic activity is less than $\theta_m$ ($v < \theta_m$) but above the baseline, $\Phi(v)$ is negative and synaptic weight is weakened. However, when postsynaptic activity is bigger than $\theta_m$ ($v > \theta_m$) but below the baseline $\Phi(v)$ is positive and synaptic weight is increased. In the BCM rule, as for Hebb's rule, correlation between pre and postsynaptic activities change synaptic weight and cause plasticity (Jedlicka, 2002).

### 3.9.3 STDP rule

One of the principal mechanisms proposed to be involved in producing LTP and LTD is the STDP rule (Markram *et al.*, 1997). STDP rule can be classified as a Hebbian

learning rule and one of the characteristic property of the Hebbian rule which determines the direction of synaptic modification can be indicated by this rule. STDP rule has been observed at excitatory synapses in different neural circuits. The variety of experimental studies indicates that in addition to frequency of presynaptic activity, the relative timing of the presynaptic and postsynaptic spikes also plays a significant role in induction of LTP and LTD. Repeated presynaptic spikes that precede postsynaptic spikes within a certain time window produce LTP; however, if repeated presynaptic spikes follow postsynaptic spikes within a certain time window, LTD occurs (Sjöström and Gerstner, 2011). There are different ways that pre and postsynaptic spikes interact together and one of the famous ones is the classical spike-pair-based model of STDP (Markram *et al.*, 1997; Sjöström *et al.*, 2008). The idea of spike-pair interactions in the dentate is based on the experimental study of Lin *et al.* (2006). In their experiments, they delivered presynaptic and postsynaptic spikes to dentate granule cells in different orders (pre-post and post-pre) and observed that STDP occurred with two exponential windows. When a presynaptic spike was paired with the following postsynaptic spike with some time delay, LTP occurred. While, when the postsynaptic spike was paired with the following presynaptic spike with some time delay, LTD occurred (Lin *et al.*, 2006). This is called standard STDP and can be formulated as follows:

$$\Delta w_+ = P \exp(-\frac{\Delta t}{\tau_p}), \quad \text{if } \Delta t > 0 \tag{3.50}$$

$$\Delta w_- = D \exp(-\frac{\Delta t}{\tau_d}), \quad \text{if } \Delta t < 0 \tag{3.51}$$

Here $\Delta t$= $t_{\text{post}}$ - $t_{\text{pre}}$ is the time difference between the time of postsynaptic spikes and the time of presynaptic spike arrival. $\tau_p$ is the decay constant of windows for LTP and $\tau_d$ is the decay constant of windows for LTD. $P$ is the amplitude of potentiation, $D$ is the amplitude of depression, which according to Izhikevich and Desai (2003) are constant values.

There are several options for implementing the pre- and postsynaptic spike interactions for the spike-pair-based STDP rule. One is the the all-to-all interaction (Gerstner *et al.*, 1996) and another is the nearest-neighbour interaction (Izhikevich and Desai, 2003). In the all-to-all interaction, each presynaptic spike pairs with all postsynaptic

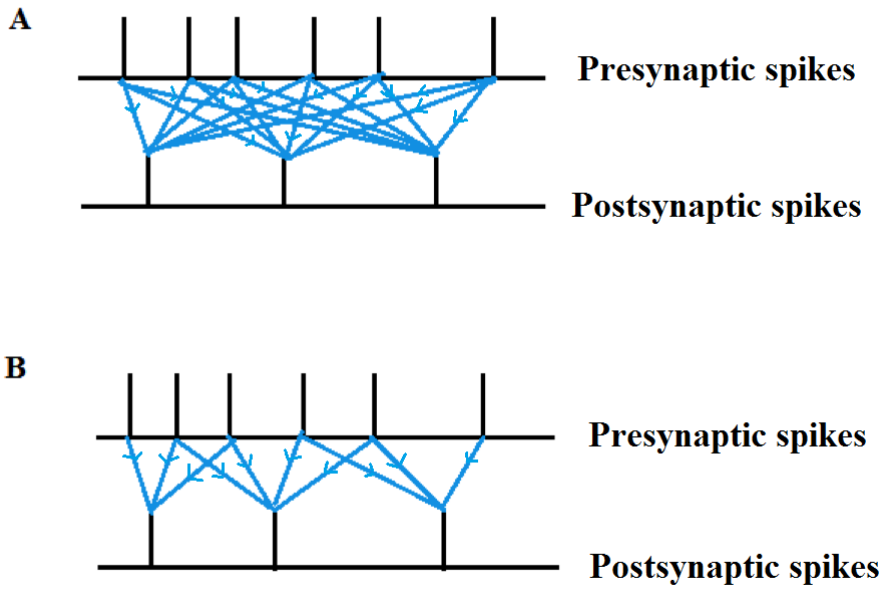


Figure 3.4: (A) Shows the all-to-all interaction of pre- and postsynaptic spikes. Each presynaptic spike pairs with all postsynaptic spikes and vice versa. (B) Shows the nearest-neighbour interaction scheme. Each presynaptic spike pairs with only two postsynaptic spikes, the one before and the one after the presynaptic spike.

spikes and vice versa (Figure 3.4A). On the other hand, in the nearest-neighbour interaction each presynaptic spike pairs only with two postsynaptic spikes: the postsynaptic spike that precedes the given presynaptic spike and the postsynaptic spike that follows the given presynaptic spike (Van Rossum *et al.*, 2000), see Figure 3.4B.

In the following section we examine the cellular mechanisms involved in determining the STDP window.

### 3.9.4 The mechanism of STDP

As we examined in the last chapter, induction of LTP and LTD needs activation of NMDA receptors and a rise in postsynaptic $Ca^{2+}$ level. In this section we show how the induction of spike timing dependent LTP (tLTP) and LTD (tLTD) also depend on the same mechanism as LTP and LTD induction.

When the activation of presynaptic input occurs a few milliseconds before the back-propagating action potential (BAP) in the postsynaptic dendrite, tLTP occurs. The reason for this is that the BAP facilitates the removal of $Mg^{+2}$ ions from the NMDA

receptors and therefore lets $Ca^{2+}$ to flux into the postsynaptic cell and cause the induction of tLTP. Apart from the $Mg^{+2}$ unblock of NMDA receptors, pairing the EPSP and BAP in the positive interval causes the diffusion of the large amount of $Ca^{2+}$ and leads to induction of tLTP window.

To explain the tLTD window we can also use the $Ca^{2+}$ hypothesis by considering that the afterdepolarization of the BAP lasts for milliseconds and all $Ca^{2+}$ ions enter the postsynaptic cell through NMDA receptors. Therefore, pairing the EPSP and the afterdepolarization causes diffusion of a moderate amount of $Ca^{2+}$ which leads to tLTD. Another model of tLTD induction is based on the supposition that a BAP preceding the EPSP causes diffusion of $Ca^{2+}$ through VDCCs. This process inactivates the NMDA receptors which reduce the amount of $Ca^{2+}$ through NMDA receptors and leads to tLTD. According to this model, activation of VDCCs is necessary for the induction of tLTD. However, the interaction of EPSPs and BAPs at negative intervals leads to sublinear summation of $Ca^{2+}$ influx (Caporale and Dan, 2008).

### 3.9.5 Dependence of STDP on the dendritic location

The interaction of dendritic factors such as the geometry of dendrites, ion channels and receptor distributions determine the magnitude of the long-term synaptic modifications.

The behavior of the backpropagating action potential and EPSPs in the dendrites of the cortical neurons suggests that the sign and magnitude of STDP may depend on the dendritic location of the synaptic input. Indeed, experimental studies from neocortical pyramidal neurons have shown that STDP phenomena depend on the location of synapses on the dendrites. Synapses proximal to the soma coupled with the large and narrow backpropagating action potentials exhibit conventional STDP. Therefore, when presynaptic activity proceeds postsynaptic activity with a short interspike interval ($\approx$ 25 ), LTP is induced. And when presynaptic activity follows postsynaptic activity with a certain interspike interval ($\approx$ 50 ), LTD is induced. However, these studies showed that in the distal synapses, the sign and magnitude of synaptic modification during STDP is profoundly different from the proximal synapses. The magnitude of STDP at distal synapses ($>$ 100 $\mu$m from the soma) at the lateral connections within layer

2/3 of developing visual cortex was about half of that for the proximal synapses ($< 50$ $\mu$m from the soma). Also LTD induction window in the distal layer 2/3 synapses was much wider than that of proximal synapses. When pairing post- and presynaptic spikes (between 50 and 100 ms), LTD at the distal synapses was less than in proximal ones (Froemke *et al.*, 2010).

### 3.9.6 Wei and Koulakov model

New investigations from Wei and Koulakov show that the STDP rule (with both LTP and LTD windows) combined with neural noise will extend the life-time of long-term memory. However, a STDP rule with only LTP windows combined with neural noise cannot make stable memory. Wei and Koulakov calculated synaptic wights according to the following equations (Wei and Koulakov, 2014).

$$\tau \frac{\delta u(t)}{dt} = -\delta u(t) + gW\delta u(t) + \xi(t) \tag{3.52}$$

$$f(t) \approx f + g\delta u(t) \tag{3.53}$$

$$\begin{aligned} \tau_0 \frac{dW_{ij}}{dt} = -W_{ij} &+ \gamma \int_{-\infty}^{t} dt_1 \langle f_i(t_1) K(t_1 - t) f_j(t) \rangle \\ &+ \gamma \int_{-\infty}^{t} dt_1 \langle f_i(t) K(t - t_2) f_j(t_2) \rangle \end{aligned} \tag{3.54}$$

To simulate noise at each step, the fluctuating changes of input current ($\delta u(t)$) due to noise will be calculated with equation (3.52), where, $\tau$ is a time constant, $u(t)$ is the input current, $g = F^{'}(u)$ with activation function $F$, $\xi(t)$ is the noise and $W$ is the synaptic weight. Then firing rate $f$ will be updated according to equation (3.53). Therefore, synaptic weights can be calculated with equation (3.54), where $W_{ij}$ is the synaptic weight from neurons $i$ and $j$, $\tau_0$ is the time constant for calculating synaptic weights, $\gamma$ is the learning rule, $f_i$ and $f_j$ are firing rate from neurons $i$ and $j$ and $K$ is the STDP rule.

## 3.10 Metaplasticity and metaplasticity rules

Synaptic plasticity is a plastic phenomenon itself. Therefore, plasticity of synaptic plasticity has been described as a different phenomenon termed metaplasticity, in which the meta term represents the higher-order nature of the plasticity. This phenomenon can serve a homeostatic function when previous activity modulates further synaptic plasticity. Metaplasticity plays a main role in regulating synaptic plasticity rules by considering the history of activity. This regulation can happen minutes, hours, or days after the previous episode of activity. For example, if LTP is induced in a synapse by delivering a particular sort of stimulation, delivering the same stimulation to the same synapse only minutes later does not achieve the same level of LTP (Morrison, 2012). Furthermore metaplasticity can help keep neuronal activity at a stable level and so protects the neuron from extreme changes (Yger and Gilson, 2015). The same as synaptic plasticity, metaplasticity also has two classes: homosynaptic metaplasticity and heterosynaptic metaplasticity. Homosynaptic metaplasticity occurs when synaptic plasticity is regulated by the previous activity at the same synapse, whereas, heterosynaptic metaplasticity occurs when synaptic plasticity is regulated by previous activity from other synapses. Experimental studies in the dentate gyrus show that previous stimulation of the medial perforant path increases the threshold for LTP in the neighbouring lateral perforant pathway heterosynaptically for up to several weeks (Abraham *et al.*, 2001).

### 3.10.1 Induction of metaplasticity

Experimental studies show the NMDA receptors play important roles in the induction of LTP. Decreasing the permeability of the NMDA receptors to the $Ca^{2+}$ ions inhibits the level of LTP. In addition, prior activation of these receptors can facilitate the induction of LTD. For example, delivering low-frequency stimulation activates the NMDA receptors which facilitates subsequent induction of LTD; this form of metaplasticity can last for 60 to 90 minutes in vitro (Abraham, 2008).

In the following section we introduce some metaplasticity rules.

### 3.10.2 Benuskova and Abraham rule

Izhikevich and Desai in 2003 found the link between nearest-neighbor implementation of STDP rule and the BCM rule. According to their idea the value of $\theta_m$ from the BCM rule is fixed and it is equal to:

$$\theta_m = \frac{\frac{P}{\tau_d} + \frac{D}{\tau_p}}{P + D} \tag{3.55}$$

where $P$ and $D$ are amplitudes for potentiation and depression, $\tau_p$ and $\tau_d$ are decay constants of windows for LTP and LTD from equations (3.50) and (3.51) (STDP rule).

Benuskova and Abraham employed the nearest-neighbor additive implementation of STDP rule to incorporate with $\theta_m$ the sliding modification threshold from the BCM rule. However, according to their idea the value of $\theta_m$ is not fixed but depends on the average postsynaptic activity $\langle c(t) \rangle$ which can be calculated numerically as the following equation:

$$\langle c(t) \rangle = \frac{c_0}{\tau_m} \int_{-\infty}^{t} c(t^{'}) \exp(-\frac{(t - t^{'})}{\tau_m}) dt^{'} \tag{3.56}$$

Here, $c_0$ is a scaling constant, $\tau_m$ is the time constant for calculating $\theta_m$ and $c$ is the postsynaptic spike count: $c(t) = 1$ if there is a postsynaptic spike at time t, otherwise $c(t) = 0$.

In their implementation of STDP and the metaplasticity rule, the amplitudes of $P$ and $D$ are not constant but depend on the previous history of postsynaptic activity which is the sliding threshold $\theta_m$. $P$ and $D$ can be calculated according to the following equations:

$$P = \frac{P(0)}{\langle c(t) \rangle} \quad and \quad D = D(0) \langle c(t) \rangle \tag{3.57}$$

Here, $\langle c(t) \rangle$ is an average of postsynaptic activity in the recent past, $P(0)$and $D(0)$ are the initial amplitudes for $P$ and $D$. Therefore, when activity is high there is less chance for LTP induction but more chance for LTD induction and vice versa (Benuskova and Abraham, 2007).

### 3.10.3 Froemke rule

The suppression model of STDP is a form of metaplasticity introduced by Froemke and his colleagues. In their model, pairing of pre- and postsynaptic spikes depends on the time interval between incoming presynaptic spike and outgoing postsynaptic spike. It also depends on the efficacy of each spike. The value of spike efficacy is between zero and one. That means, when the spike is coming the value is one and it goes to zero immediately after spike, while, as an exponential function, it recovers again to one and it can be depicted as the following equations (Froemke *et al.*, 2010).

$$\epsilon_i = 1 - \exp(-\frac{(t_i - t_{i-1})}{\tau_s}) \tag{3.58}$$

where $\epsilon_i$ is the efficacy of the $ith$ spike, $t_i$ and $t_{i-1}$ are the timing of the $i$th and $(i-1)$th spike, and $\tau_s$, is the decay constant for the suppression effect.

According to Froemke's rule, the changes of synaptic weights are calculated as follows:

$$\Delta w_{ij} = \epsilon_i^{\text{pre}} \epsilon_j^{\text{post}} F(\Delta t_{ij}) \tag{3.59}$$

where $\Delta w_{ij}$ is synaptic modification of the $i$th presynaptic spike and the $j$th postsynaptic spike. $\epsilon_i^{\text{pre}}$ and $\epsilon_j^{\text{post}}$ are the efficacy of the two spikes. $\Delta t_{ij}$ is the interval between the two spikes, $t_j^{\text{post}} - t_i^{\text{pre}}$. $F(\Delta t_{ij})$ is a dynamic scaling factor to the original STDP rule which is depicted as:

$$F(\Delta t) = \begin{cases} A_+ \exp(\frac{-|\Delta t|}{\tau_+}) & \text{if } \Delta t > 0 \\ A_- \exp(\frac{-|\Delta t|}{\tau_-}) & \text{if } \Delta t < 0 \end{cases} \tag{3.60}$$

where, $A_+$ and $A_-$ are potentiation and depression factors with constant values, $\tau_+$ is the time constant for potentiation and $\tau_-$ is time the constant for depression. The suppression effect on the model does not allow the synaptic weights to grow extremely, and therefore, this model does not need any hard bound.

### 3.10.4 Pfister rule

Pfister and Gerstner extended the pair-based classical model of STDP rule to the triplet-based model. As introduced in the last section, in the classic model of STDP

rule, only two pre- and postsynaptic spikes effects change on synaptic weights. However, in the triplet-based model of STDP, the effect of a third spike is also considered on the overall weight change. The Pfister rule can be depicted according to the following equations:

$$\frac{dr_1(t)}{dt} = -\frac{r_1(t)}{\tau_+}; \quad if \quad t = t_{pre} \quad then \quad r_1 \longrightarrow r_1 + 1 \tag{3.61}$$

$$\frac{dr_2(t)}{dt} = -\frac{r_2(t)}{\tau_x}; \quad if \quad t = t_{pre} \quad then \quad r_2 \longrightarrow r_2 + 1 \tag{3.62}$$

$$\frac{do_1(t)}{dt} = -\frac{o_1(t)}{\tau_-}; \quad if \quad t = t_{post} \quad then \quad o_1 \longrightarrow o_1 + 1 \tag{3.63}$$

$$\frac{do_2(t)}{dt} = -\frac{o_2(t)}{\tau_y}; \quad if \quad t = t_{post} \quad then \quad o_2 \longrightarrow o_2 + 1 \tag{3.64}$$

Here $r_1$ and $r_2$ are the first and second detectors for presynaptic events, $t_{pre}$ is any time when a presynaptic spike occurs and $\tau_+$ and $\tau_x$ are time constants. $o_1$ and $o_2$ are the first and second detectors for postsynaptic events, $t_{post}$ is any time when a postsynaptic spike occurs and $\tau_-$ and $\tau_y$ are time constants.

Synaptic weights are updated according to the following equations.

$$w(t+1) = w(t) - o_1(t)[A_2^- + A_3^- r_2(t-\epsilon)] \quad if \quad t = t_{pre} \tag{3.65}$$

$$w(t+1) = w(t) + r_1(t)[A_2^+ + A_3^+ o_2(t-\epsilon)] \quad if \quad t = t_{post} \tag{3.66}$$

Here $w$ is synaptic weight. $A_2^+$ and $A_2^-$ are the amplitudes of the weight change when pre and post synaptic spikes are paired. $A_3^+$ and $A_3^-$ are the amplitudes of the triplet of the potentiation and depression factors (Pfister and Gerstner, 2006).

### 3.10.5 Clopath rule

In the metaplasticity model introduced by Clopath, the potentiation factor defined as $A_{\mathrm{LTP}}$ had a fixed value but the depression factor defined as $A_{\mathrm{LTD}}(\bar{\bar{u}})$ was a function of a homeostatic variable. Therefore, the way they have introduced LTD and LTP is different (Clopath *et al.*, 2010):

$$A_{LTD}(\bar{\bar{u}}) = A_{LTD}\frac{\bar{\bar{u}}^2}{u_{ref}^2} \tag{3.67}$$

where $u_{ref}^2$ is a reference value that is a constant value. $\bar{u}_-$ is a low pass filter of the average of postsynaptic potential and $\bar{\bar{u}}^2$ (the average of the postsynaptic potential) is a homeostatic variable that depends on a low pass filter. In this model of metaplasticity, spikes are considered as continuous events and at each time step the way that synaptic weight changes is based on the average of membrane potential. While, in the other metaplasticity rules introduced in this thesis spikes are considered as discrete events.

$$\tau_x \frac{dx}{dt} = -x(t) + X(t) \tag{3.68}$$

where $X(t)$ is a variable that sets to 1 if there is a presynaptic spike and 0 when there is not, $\tau_x$ is the decay time constant. In their model $\bar{u}_-$ is calculated by:

$$\tau_- \frac{d\bar{u}_-}{dt} = -\bar{u}_-(t) + u(t) \tag{3.69}$$

where $u(t)$ is the postsynaptic membrane potential and $\tau_-$ is the time decay constant. Therefore, synaptic weights are calculated as follows:

$$\frac{dw^-}{dt} = -A_-(\bar{u})X(t)(u_-(t) - \theta_-) \quad if \quad w > w_{min} \tag{3.70}$$

$$\frac{dw^+}{dt} = -A_+x(t)(u - \theta_+) \quad if \quad w < w_{max} \tag{3.71}$$

where $u$ is the membrane potential, $\theta_-$ and $\theta_+$ are adjustable parameters, $A_+$ and $A_-$ are potentiation and depression factors.

### 3.10.6 Zhenq and Schwabe model

Zhenq and Schwabe investigated the effects of action potential (AP) duration on synaptic plasticity. For that purpose for the neuron model they employed a simple one compartment model, for the plasticity model they employed the voltage-dependent STDP model proposed by Clopath *et al.* (2010) and extended that model to the AP-dependent STDP and they referred it as dSTDP. Their model has two inputs: synchronous spikes as the signal and Poisson spike as noise.

$$\Delta w^i_{exc} = \begin{cases} w_{\max} A_+ \exp(\frac{-\Delta t}{\tau_+}) & \text{if } \Delta t > 0 \\ w_{\max} A_+ & \text{if } -d_{AP} < \Delta t < 0 \\ \Delta w_{\mathrm{LTD}} A_+ \exp(\frac{\Delta t + d_{AP}}{\tau_-}) & \text{if } \Delta t < -d_{AP} \end{cases} \tag{3.72}$$

where $w^i_{\mathrm{exc}}$ is the synaptic weight in the $i$-th excitatory synapse, $w_{max}$ is an upper bound synaptic weight, $A_+$ is the potentiation factor, $\tau_+$ and $\tau_-$ are both the time constant (Zheng *et al.*, 2014).

## 3.11 Summary

In this chapter we introduced two different models of neuron, realistic and simplified models. We then briefly examined two realistic models of neuron Hodgkin-Huxley model and multi-compartmental model. We also introduced a cable theory which is a mathematical interpretation of the multi-compartmental model. It was necessary to describe this model because, as we will explain in the method Chapter, our simulation is based on a single granule cell, and therefore the intrinsic neuron properties such as morphological details and channel distributions of the dendritic tree is necessary for our experiments. In our simulations we used a numerical integration method called Crank-Nicholson method. Therefore, we briefly described some integration methods. Introducing the NEURON environment with its properties was necessary as our all simulations are based in this environment. In the next section we described homeostatic plasticity mechanism that regulates synaptic plasticity and keeps the neuron activity at a stable level. We also introduced homosynaptic and heterosynaptic forms of plasticity. As we will explain later, in the medial pathway of the dentate granule cell, homosynaptic LTP occurs in the activated synapses and heterosynaptic LTD occurs in the lateral pathway. Finally we described different types of plasticity and metaplasticity models. The aim of introducing these models was firstly to show how they are employed for different experimental studies and different environments, and secondly to show the similarities and contrasts between these models and our plasticity model.

# Chapter 4

# Review of experimental studies

In this chapter we will describe experimental protocols and main findings of three papers describing in vivo experimental studies of plasticity in dentate granule cells, namely Abraham *et al.* (2001), Abraham *et al.* (2007) and Bowden *et al.* (2012). In this thesis, we have used the experimental data from these papers to validate the results of our computational simulations and investigations of synaptic plasticity and metaplasticity rules. The first paper that we will discuss is the experimental study of Abraham *et al.* (2001), which corresponds to the first protocol of our simulations. In this paper they examined homosynaptic LTP and heterosynaptic LTD and their metaplastic modifications according to the BCM theory in awake rats. The next paper we will review is Abraham *et al.* (2007). In this paper they found that spontaneous activity is required for heterosynaptic LTD to occur in the DG of an anaesthetised rat. They also examined the metaplasticity effect of the first medial HFS plus spontaneous activity on the synaptic plasticity induced by the second HFS. The last paper that we will describe is the experimental study of Bowden *et al.* (2012). In this paper the effect of HFS pattern on the magnitude of homosynaptic LTP and simultaneous heterosynaptic LTD was examined and this corresponds to our fourth protocol.

## 4.1 Experimental studies for the first simulation protocol

The main aim of the Abraham *et al.* (2001) experiments was to test heterosynaptic metaplasticity in the hippocampus and to examine the modification of LTP threshold

by BCM rules in awake rats. In this paper they did various experiments but we focus on the main one. For the purpose of this study, awake Sprague-Dawley rats were prepared for stimulation in the recording chamber to record the field excitatory postsynaptic potentials (fEPSP) before and after the experimental stimulation. The percentage of synaptic plasticity was calculated from the fEPSP slope of the medial and lateral pathways. To establish the baseline, at first test stimulation was applied to the medial and lateral pathways. Then, according to Figure 4.1, the first HFS protocol was 400 Hz delta burst stimulation (DBS) with 30-s interburst intervals repeated 10 times (Figure 4.2) was applied to the medial pathway. Delta burst stimulation as trains within one burst are delivered at the delta frequency of 1 Hz. Following this, after about 270 minutes, the same protocol was applied to the lateral pathway.

As can be seen from Figure 4.1, when the first HFS was applied to the medial pathway, synaptic weights increased ($37 \pm 5\%$) homosynaptically in the medial pathway and decreased heterosynaptically in the lateral pathway ($30 \pm 5\%$). When the second HFS was applied to the lateral pathway 4 hours later, although the synaptic weights increased in the lateral pathway, they did not pass above the baseline and LTP could not be observed in the lateral pathway and instead and ongoing small ($-7 \pm 5\%$) LTD was observed. However, in the neighbouring medial pathway, synaptic pathway was depressed, but this depression was not enough to pass below the baseline and LTD was not observed in the medial pathway and ongoing ($20 \pm 3\%$) LTP was observed.

## 4.2 Experimental studies for the second simulation protocol

In this section we review one part of the study reported in Abraham *et al.* (2007). Various experimental studies from dentate gyrus indicate that heterosynaptic LTD is hard to induce in vitro compared to induction of homosynaptic LTD. The difference between dentate gyrus *in vivo* and dentate gyrus in slice (i.e. *in vitro*) is the degree of spontaneous activity. The level of spontaneous activity of dentate gyrus in the slice is virtually zero, whereas in the anesthetized or awake preparations it is about 2–8 Hz. The question is whether spontaneous activity is involved in induction of heterosynaptic

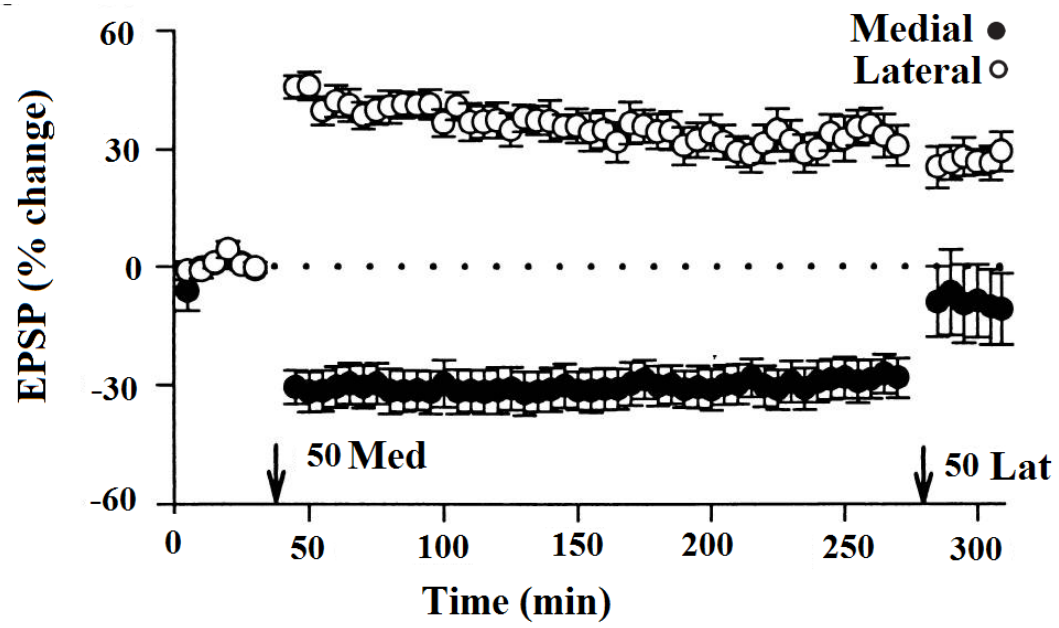


Figure 4.1: Plot of change of the slope of fEPSP that reacts to changes of synaptic weights in the medial and lateral pathways. 50 Med is the first HFS (400 Hz delta burst stimulation (DBS) with 30-s interburst intervals repeated 10 times) applied to the medial pathway. '50 Lat' is the second HFS applied to the lateral pathway (with the same pattern as the medial one). White circles show in percentage the average change of synaptic weights in the medial pathway. The black circles show in percentage the average change of synaptic weights in the lateral pathway. When the first medial HFS is applied to the medial pathway, we can see LTP of (37 ± 5%) above the baseline in the medial pathway and LTD of (30 ± 5%) below the baseline. When the second HFS is applied to the lateral pathway, synaptic weights depress in the medial pathway, but remain above the baseline. And synaptic weights potentiate in the lateral pathway but this is not enough to pass the baseline. Source: (Abraham *et al.*, 2001)


Figure 4.2: Schematic illustration of the 400 Hz delta burst stimulation (DBS) form of HFS, which consists of 5 trains at 1 Hz, while each train contains 10 spikes at 400 Hz. Bursts are repeated 10 times at every 30-s.


Figure 4.3: 400 Hz delta burst stimulation (DBS) form of HFS, which consists of 5 trains at 1 Hz and each train contains 10 spikes at 400 Hz. Bursts are repeated 10 times at every 60-s.

LTD in the dentate gyrus or not. The aim of the experimental studies by Abraham *et al.* (2007) was to examine the requirement of spontaneous activity for inducing the heterosynaptic LTD in anaesthetized rats. For that purpose, adult male Sprague-Dawley rats (2–4 mo) were anaesthetised by urethane and prepared for implanting the stimulation electrodes to the medial and lateral pathways and recording fEPSPs in the dentate hilus. In this paper, two different groups of rats named procaine and control were tested. In the control group (white circles in Figure 4.4) when the first HFS (as can be seen from Figure 4.3, 400 Hz-DBS with 60-s interburst intervals repeated 10 times) was applied to the medial pathway, synaptic weights increased by about 37 $\pm$ 5% ($n = 7$) in the medial pathway and thus homosynaptic LTP occurred. At the same time in the lateral pathway, synaptic weight decreased by about –24 $\pm$ 3% ($n = 7$) and thus heterosynaptic LTD happened (white circles in Figure 4.5).

In the procaine group (black circles in Figure 4.5), when the first HFS was applied to the medial pathway, procaine was applied to the lateral pathway to block its spontaneous activity. However, procaine also blocked the response evoked by the test pulses, therefore we can see a large "depression" in the procaine group, which is considered to be an artefact. Then, the procaine was washed out. As can be seen in Figure 4.5, after procaine washed out in the lateral pathway, the degree of LTD was reduced to –5 $\pm$ 8% ($n = 6$), although potentiation happened in the medial pathway with the same magnitude as the control group.

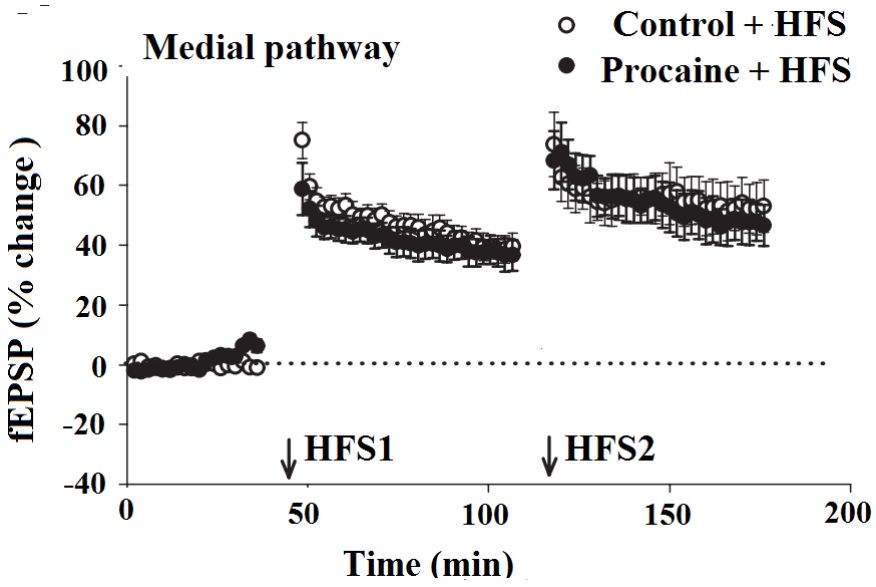


Figure 4.4: Comparing the average change in the slope of fEPSP in the medial pathway between the control group (white circles) and procaine group (black circles). Procaine was injected only to the lateral pathway to stop its spontaneous activity when the first medial HFS was applied. Before application of the second medial HFS, the procaine was washed out. The first medial HFS produces LTP in both groups (37±5%, n = 7) whereas, the second HFS following the first one causes no larger LTP in both groups. Source: (Abraham *et al.*, 2007)

## 4.3 Experimental studies for the third simulation protocol

In this section we review the second part of the study reported in Abraham *et al.* (2007), which is a continuation of the first part. The aim of this study was to investigate the metaplasticity effect of the first medial HFS on synaptic plasticity when the second HFS was applied to the medial pathway. Following the first HFS, a second HFS with the same pattern as the first one was applied to the medial pathway a few minutes later. As can be seen from Figure 4.4, in both control and procaine group, LTP was induced by the first HFS but no further LTP occurred in response to the second. With the application of the second medial HFS, no LTD occurred in the procaine group (Figure 4.5). In the control group when the second medial HFS was applied, no further LTD occurred (white circles).

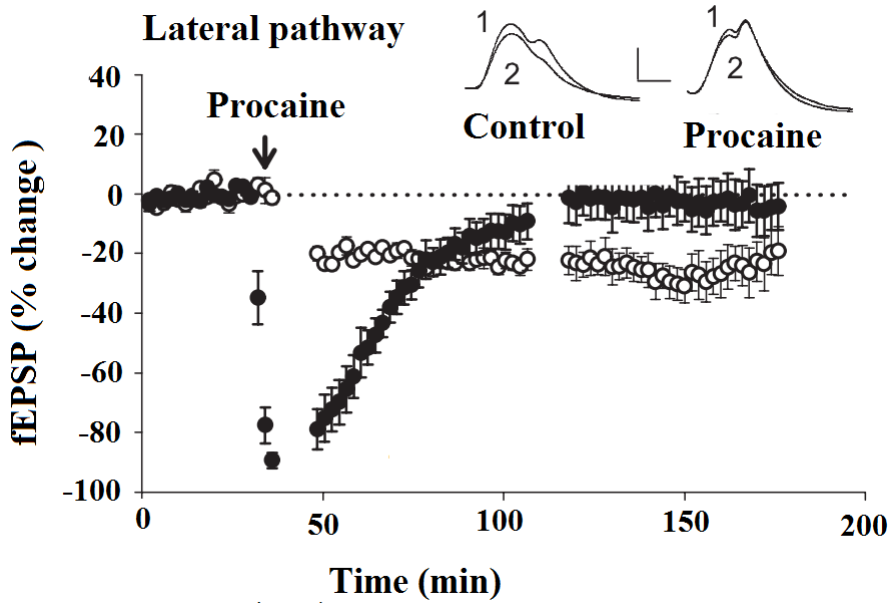


Figure 4.5: Comparing the average change in the slope of fEPSP in the lateral pathway between the control group (white circles) and procaine group (black circles). Procaine was injected only to the lateral pathway when the first medial HFS was applied. Procaine blocked the lateral spontaneous activity and inhibited LTD in the procaine group. The reason why we see depression (black circles) is that procaine also inhibits the response evoked by the test pulses. However, after applying HFS to the control group, heterosynaptic LTD occurred in the lateral pathway (white circles). Source: (Abraham *et al.*, 2007)

## 4.4 Experimental studies for the fourth simulation protocol

In this section we review the experimental data reported in Bowden *et al.* (2012). These researchers investigated the effect for several patterns of HFS on LTP and simultaneous LTD in the DG of freely moving (awake) rats. They examined a group of Long-Evans rats during the dark phase of the diurnal cycle with three patterns of HFS applied to the medial pathway of DG. These were: 400 Hz DBS, 400 Hz theta-burst stimulation (TBS) and 100 Hz TBS (Christie and Abraham, 1994). TBS refers to trains within one burst that are delivered at the theta frequency of 5 Hz. The percentage of LTP and simultaneous LTD was calculated from the fEPSP slope. As can be seen in Figure 4.8 A and B, activation of the medial pathway with the 400 Hz DBS pattern (Figure 4.3) induced vigorous LTP in the medial pathway and strong simultaneous LTD in the lateral pathway (Bowden *et al.*, 2012) but see also (Douglas and Goddard, 1975;

Winson and Dahl, 1986). The second-most efficient pattern was 400 Hz TBS burst (Figure 4.6) and least effective pattern was 100 Hz TBS (Figure 4.7).

Thus, 400 Hz DBS induced the most robust LTP in the medial pathway (42.5 ± 5.4%). As the number of pulses decreased from 10 in 400 Hz DBS to 4 pulses in 400 Hz TBS (Figure 4.6), amount of LTP decreased as well (35 ± 4.5%), although still comparable with 400 Hz DBS, whereas as the frequency decreased from 400 Hz to 100 Hz, the amount of LTP dramatically decreased to (9.8 ± 4.9%) in the medial pathway. The same scenario was similar for heterosynaptic LTD in the lateral pathway. When 400 Hz DBS was applied to the medial pathway, the most robust heterosynaptic LTD occurred in the lateral pathway (about 25%) compared with 20% LTD with the 400 Hz TBS pattern and almost no LTD when the frequency decreased from 400 Hz to 100 Hz in the TBS pattern. Comparing two patterns of theta burst stimulation, i.e., 100 Hz, and 400 Hz with the same pulse number and train spacing but different frequency of pulses within the train shows that increasing frequency from 100 Hz to 400 Hz is critical for inducing observable synaptic plasticity. However, when the frequency of pulses is the same, i.e., 400 Hz, but the number of pulses in the trains and spacing of trains were different, synaptic plasticity does not change very much. These findings in vivo in the DG are quite surprising, because in the CA1 region when 100 Hz TBS was applied to the Schaffer collaterals either in vitro or in vivo, vigorous LTP was induced (Larson *et al.*, 1986; Staubli and Lynch, 1987; Abraham and Huggett, 1997; Raymond and Redman, 2006). Moreover, induction of LTP and concurrent LTD by 100 Hz TBS in the DG of anaesthetized pentobarbital rat was also reported. These experiments were simulated in our fourth protocol to propose an explanation for why different patterns of HFS cause different magnitudes of LTP and LTD.

## 4.5 Summary

In the first section, we introduced the experimental paper by Abraham *et al.* (2001). Here the effect of a single medial HFS on synaptic plasticity (LTP and LTD) of the medial and lateral pathways, respectively, was examined. They also examined whether the second HFS applied to the lateral pathway depresses the medial pathway and potentiates the lateral pathway or not. The main focus of the second section was


Figure 4.6: 400 Hz theta burst stimulation (TBS) of HFS consists of 10 trains at 5 Hz, while each train contains 4 spikes at 400 Hz, are repeated 8 times every 10-s. Source: Shirrafiardekani

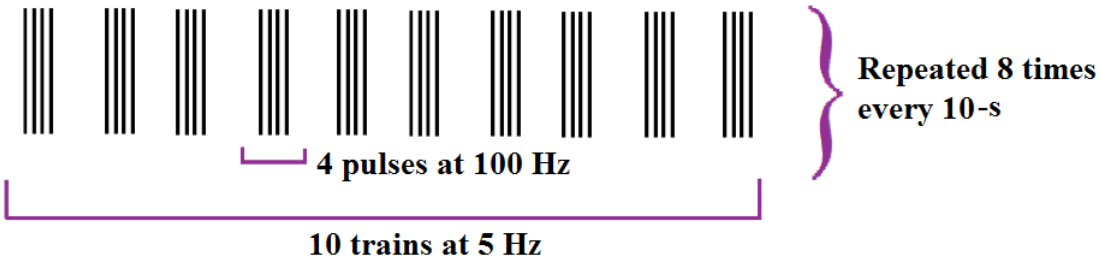


Figure 4.7: 100 Hz theta burst stimulation (TBS) of HFS consists of 10 trains at 5 Hz while each train contains 4 spikes at 100 Hz, which are repeated 8 times every 10-s. Source: Shirrafiardekani

on experiments in Abraham *et al.* (2007). In this section we described the effects of procaine on the synaptic plasticity induced by a medial HFS. In the third section we reviewed the second part of Abraham *et al.* (2007). In that experiment metaplasticity effects of the first medial HFS on synaptic plasticity induced by second medial HFS in the procaine and control groups was investigated. The experimental studies of Bowden *et al.* (2012) were described in the last section. The aim of this section was comparing LTP and LTD in the medial and lateral pathways that were evoked by different patterns of medial HFS. In the next chapter we will briefly describe different mechanisms that have been used to simulate synaptic plasticity and metaplasticity in the granule cell model.

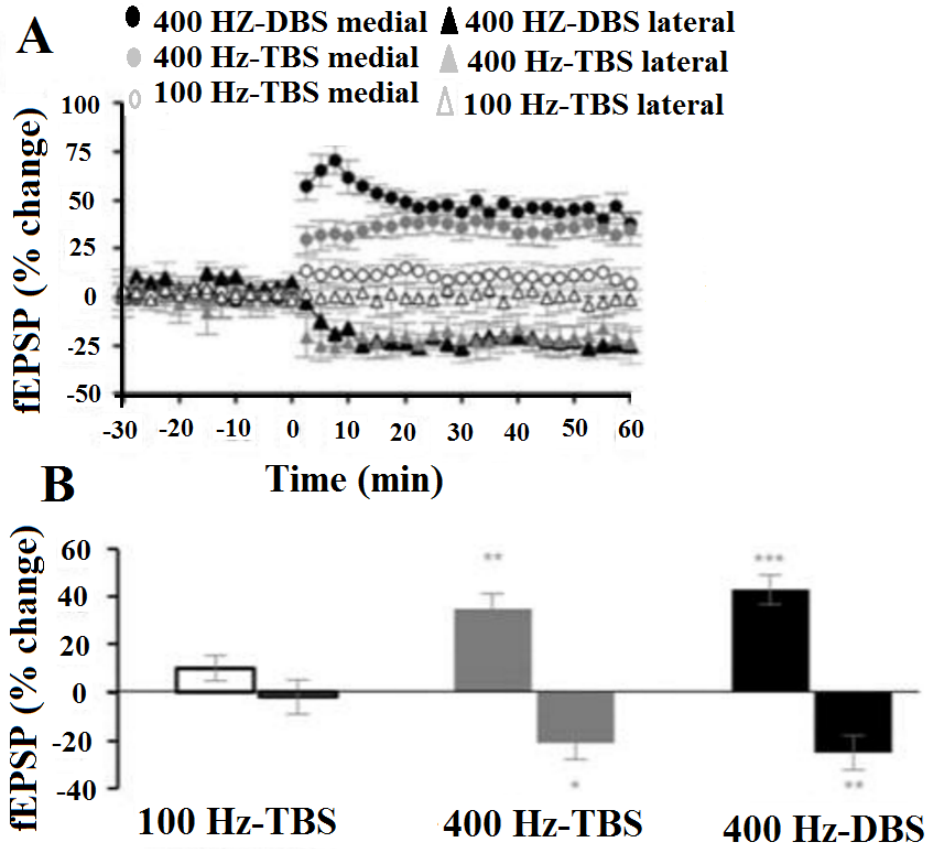


Figure 4.8: (A) The graph shows the magnitude and time course of homosynaptic LTP and heterosysnaptic LTD (het-LTD) resulting from three different patterns of HFS applied to the medial pathway. (B) Summary of magnitude of hom-LTP and het-LTD for three patterns of HFS after 60 min: 400 Hz delta burst stimulation (DBS) at the medial pathway causes homosynaptic LTP 42.5 ± 5.4% and lateral het-LTD about 25%, 400 Hz theta burst stimulation (TBS) applied to the medial pathway causes homosynaptic LTP 35 ± 4.5% and het-LTD about 20%, and 100 Hz TBS, the percentage of average medial homosynaptic LTP reduces to 9.8 ± 4.9%, while there is almost no heterosynaptic LTD in the lateral pathway. Source:(Bowden *et al.*, 2012)

# Chapter 5

# Methods

To model the dendritic tree of the a granule cell we employed the multi-compartmental model introduced by Aradi and Holmes (1999) and implemented in NEURON by Santhakumar *et al.* (2005). To generate random noisy presynaptic spontaneous activity we used a homogeneous Poisson distribution. We also produced different patterns of HFS along the medial and lateral pathways. STDP and metaplasticity equations are employed so that all 300 perforant path synapses onto the granule cell are affected by these two rules. Finally we explain the integration method that we have used in our simulations.

## 5.1 Modeling the dentate granule cell

The dendritic tree of the granule cell (GC) plays a significant role in transferring synaptic inputs from the entorhinal cortex to the granule cell soma (Moujahid *et al.*, 2011). To account for morphological details of the dendritic tree of the granule cell (GC), different compartmental models with various degree of accuracy have been introduced. The full passive morphological model was constructed by Desmond and Levy in 1982 and 1984 (Desmond and Levy, 1984). Yuen and Durand were the first to create a reduced compartmental model of GC with four types of ion channels (Yuen and Durand, 1991). Although this model could reproduce some electrophysiological behaviors of GCs, it was not able to reproduce one of the important properties of GC, which is the hyperpolarisation after an action potential (AHP). However, in 1999, Aradi and Holmes enhanced the Yuen and Durant model by creating a reduced 60-compartmental

model with 9 types of ion channels. The first aim of this model was to replicate the specific behavior of the granule cell in response to the injection current and the second aim was to investigate the effect of the blocking channels on the granule cell (Aradi and Holmes, 1999). A reduced morphology model (with a reduced complexity and number of compartments) was introduced to investigate the mechanisms that are fundamental for the depolarizing after-potential (DAP) and coactivation of calcium related channels (Aradi and Holmes, 1999). This model could reproduce the firing patterns of GC with high accuracy, which is in accordance with the variety of real experimental studies (Tejada and Roque, 2014). The 60-compartmental model of Aradi and Holmes has two dendrites, one soma and an axon, with one compartment for soma, 14 compartments for each dendrite and 31 compartments for an axon. Aradi and Holmes recognized four sections in the dendritic tree; granule cell layer dendrites (GCLD), proximal (PD), middle (MD), and distal dendrites (DD). They also included four sections for the axon, called axon-1, axon-2, axon-3 and axon-4 and one section for soma. Each of these sections has different number of segments (summation of all segments is 60) with different distributions of voltage-activated channels.

To model the dentate GC in this work, we employed a reduced morphology model introduced by Aradi and Holmes and implemented in NEURON by Santhakumar *et al.* (2005). Our simulation files were downloaded from the ModelDB database at (http://senselab.med.yale.edu/modeldb/, accession No. 51781). As we were interested only in generation of action potentials and not their propagation, we did not need to include the axon in our GC model. Also, we used 9 compartments in order to reduce the time of simulation. We also did our simulations with 29 compartments (14 compartments for dendrites and one compartment for soma) and did not see any significant change in our results. Seven ion channels that are implemented in this model are: fast sodium (Na), fast delayed rectifier potassium ($fK_{DR}$), slow delayed rectifier potassium ($sK_{DR}$), A-type potassium ($K_A$), large conductance and T-type (TCa), N-type (NCa), and L-type (LCa) calcium channels. These channel types are described by Hodgkin-Huxley-like equations (Aradi and Holmes, 1999). We also did our simulations with nine ion channels which included calcium-voltage-dependent potassium (BK) and small conductance calcium-dependent potassium (SK) channels, but the results were very close to when only seven ion channels were implemented.

The membrane current density at each compartment with unit $\mathrm{mA/cm^2}$ is described by the following sets of equations taken from Aradi and Holmes (1999) and all the parameter values presented in Table 7.1 are taken from Santhakumar *et al.* (2005):

### 5.1.1 Fast Sodium Current

The equations for $I_{\mathrm{Na},i}$ current at compartment $i$ are:

$$\begin{aligned} I_{\mathrm{Na},i} &= G_{\mathrm{Na},i}(V_i - E_{\mathrm{Na}}) \\ G_{\mathrm{Na},i} &= g_{\mathrm{Na},i} m_i^3 h_i \end{aligned} \tag{5.1}$$

where $V_i$ is the membrane potential, $i$ represents the compartment numbers, $g_{\mathrm{Na},i}$ is the maximum conductance of the sodium channel, $E_{\mathrm{Na}}$ is the $Na$ reversal potential. Variable $m_i$ is the dimensionless sodium activation gate and $h_i$ is the dimensionless inactivation gate (see equations A.1, A.2 and A.3 from Appendix A (rate function)).

### 5.1.2 Fast and slow delayed rectifier potassium currents

The equations for $f\mathrm{K}_{DR}$ current at compartment $i$ are:

$$\begin{aligned} I_{f\mathrm{K}_{DR},i} &= G_{f\mathrm{K}_{DR},i}(V_i - E_K) \\ G_{f\mathrm{K}_{DR},i} &= g_{f\mathrm{K}_{DR},i} n_{f,i}^4 \end{aligned} \tag{5.2}$$

where, $g_{f\mathrm{K}_{DR},i}$ is the maximum conductance of the fast delayed rectifier potassium channel, $E_K$ is the $K$ reversal potential, and $n_{f,i}$ is the dimensionless fast potassium activation gate (see equations A.1, A.6 and A.7 from appendix A (rate functions)).

The equations for $\mathrm{sK_{DR}}$ current at compartment $i$ are:

$$\begin{aligned} I_{s\mathrm{K_{DR}},i} &= G_{s\mathrm{K_{DR}},i}(V_i - E_K) \\ G_{s\mathrm{K_{DR},}i} &= g_{s\mathrm{K_{DR}},i} n_{s,i}^4 \end{aligned} \tag{5.3}$$

where, $g_{s\mathrm{K_{DR}},i}$ is the maximum conductance of the slow delayed rectifier potassium channel and $n_{s,i}$ is the dimensionless slow potassium activation gate.

### 5.1.3 A-type potassium current

The equations for the A-type potassium current at compartment $i$ are:

$$
\begin{aligned}
I_{\mathrm{K}_A,i} &= G_{\mathrm{K}_A,i}(V_i - E_{\mathrm{K}}) \\
G_{\mathrm{K}_A,i} &= g_{\mathrm{K}_A,i} k_i l_i
\end{aligned}
\tag{5.4}
$$

where, $g_{\mathrm{K}_A,i}$ is the maximum conductance of the A-type potassium channel, $k_i$ is the dimensionless A-type potassium activation gate and $l_i$ is the dimensionless A-type potassium inactivation gate.(see equations A.1, A.10, A.11, A.12 and A.13, from appendix A (rate functions)).

### 5.1.4 Calcium channels

Three voltage-gated calcium channels called T-, N-, and L-type channels have been described for the dentate GC. The rate of change of the intracellular calcium concentration at compartment $i$ is given by:

$$
\frac{d[\mathrm{Ca}^{2+}]_i}{dt} = B_i(I_{\mathrm{TCa},i} + I_{\mathrm{NCa},i} + I_{LCa,i}) - \frac{[\mathrm{Ca}^{2+}]_i - [\mathrm{Ca}^{2+}]_0}{\tau}, \tag{5.5}
$$

where $B_i = \frac{5.2\times10^{-6}}{Ad}$ in units of mol/(C. m$^3$) for a shell of surface area $A$ and thickness $d$ (0.2 $\mu$m), $\tau = 10$ ms was the calcium removal rate. $[\mathrm{Ca}^{2+}]_0 = 70$ nM was the resting calcium concentration (Aradi and Holmes, 1999).

The equations for calcium channels at the compartment $i$ are:

$$
\begin{aligned}
I_{\mathrm{TCa},i} &= G_{\mathrm{TCa},i}(V_i - E_{Ca}) \\
G_{\mathrm{TCa},i} &= g_{\mathrm{TCa},i} a_i^2 b_i
\end{aligned}
\tag{5.6}
$$

$$
\begin{aligned}
I_{\mathrm{NCa},i} &= G_{\mathrm{NCa},i}(V_i - E_{Ca}) \\
G_{\mathrm{NCa},i} &= g_{textNCa,i} c_i^2 d_i
\end{aligned}
\tag{5.7}
$$

$$
\begin{aligned}
I_{\mathrm{LCa},i} &= G_{\mathrm{LCa},i}(V_i - E_{Ca}) \\
G_{\mathrm{LCa},i} &= g_{\mathrm{LCa},i} e_i^2
\end{aligned}
\tag{5.8}
$$

where, $g_{\mathrm{TCa},i}$, $g_{\mathrm{NCa},i}$, $g_{\mathrm{LCa},i}$ are the maximum conductance of T-, N-, and L-type calcium channels respectively. $E_{\mathrm{Ca}}$ is the $Ca$ reversal potential. Variables $a_i$ and $b_i$ are the dimensionless T-type calcium activation and inactivation gates respectively. Variables $c_i$ and $d_i$ are the dimensionless N-type calcium activation and inactivation gates respectively. Variables $e_i$ is the dimensionless L-type calcium activation gates.(see equation

A.1, A.14, A.15, A.16, A.17, A.18, A.19, A.20, A.21, A.22 and A.23 from appendix A (rate functions))

### 5.1.5 Leak current

Leak current at the compartment $i$ is represented as:

$$\begin{aligned} I_{L,i} &= G_{L,i}(V_i - E_L) \\ G_{L,i} &= g_{L,i} \end{aligned} \tag{5.9}$$

where, $V_i$ is the membrane potential, $g_{L,i}$ is the maximum conductance of leakage channel and $E_L$ is the leak reversal potential.

Table 5.1: Parameter values of all compartments of GC model, where compartments are; Distal dendrites (DD), Middle dendrites (MD), Proximal dendrites (PD), granule cell layer dendrites (GCLD) and soma.Source: (Santhakumar *et al.*, 2005)

| Parameters | DD | MD | PD | GCLD | Soma |
|---|---|---|---|---|---|
| $C_m$ ($\mu$F/cm$^2$) | 1.6 | 1.6 | 1.6 | 1 | 1 |
| $g_{\mathrm{Na}}$ (S/cm$^2$) | 0 | 0.008 | 0.013 | 0.018 | 0.12 |
| $g_{f\mathrm{K}_{DR}}$ (S/cm$^2$) | 0.001 | 0.001 | 0.004 | 0.004 | 0.16 |
| $g_{s\mathrm{K}_{DR}}$ (S/cm$^2$) | 0.008 | 0.006 | 0.006 | 0.006 | 0.006 |
| $g_{\mathrm{K}_A}$ (S/cm$^2$) | 0 | 0 | 0 | 0 | 0.012 |
| $g_{\mathrm{TCa}}$ (S/cm$^2$) | 0.001 | 0.005 | $2.5\times\ 10^{-4}$ | $7.5\times10^{-5}$ | $3.7\times10^{-5}$ |
| $g_{\mathrm{NCa}}$ (S/cm$^2$) | 0.001 | 0.001 | 0.001 | 0.003 | 0.002 |
| $g_{\mathrm{LCa}}$ (S/cm$^2$) | 0 | 0.0005 | 0.0075 | 0.0075 | 0.005 |
| $g_{\mathrm{L}}$ (S/cm$^2$) | $6.3\times10^{-5}$ | $6.3\times\ 10^{-5}$ | $6.3\times10^{-5}$ | $4.0\times10^{-5}$ | $4.0\times10^{-5}$ |
| $E_{\mathrm{Na}}$ (mV) | 45 | 45 | 45 | 45 | 45 |
| $E_{\mathrm{K}}$ (mV) | $-90$ | $-90$ | $-90$ | $-90$ | $-90$ |
| $E_{\mathrm{L}}$ (mV) | $-75$ | $-75$ | $-75$ | $-75$ | $-75$ |
| $E_{\mathrm{Ca}}$ (mV) | 130 | 130 | 130 | 130 | 130 |
| $\tau_{\mathrm{rise}}$ (ms) | 0.2 | 0.2 | 0.2 | 0.2 | 0.2 |
| $\tau_{\mathrm{decay}}$ (ms) | 2.5 | 2.5 | 2.5 | 2.5 | 2.5 |

Figure 5.2 shows a schematic picture of the cylindrical 9-compartmental model of the dentate granule cell. The granule cell layer (GCLD) is the closest dendritic compartment to the soma. This represents that part of the dendrite before it emerges from

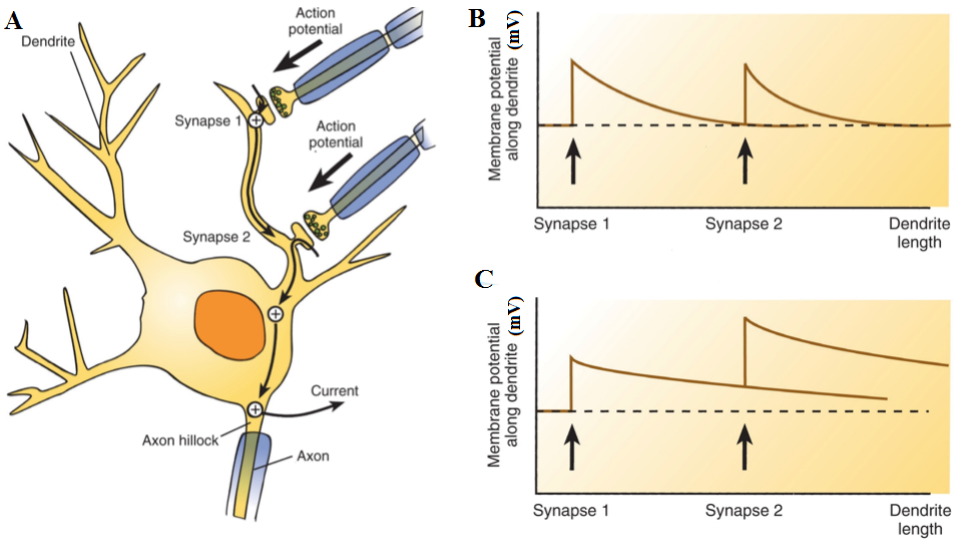


Figure 5.1: A) Granule cell receives presynaptic activity from LPP and MPP axons which causes postsynaptic potentials at the synaptic connections 1 and 2. Dendrites propagate postsynaptic activity to the soma and backpropagation of action potential flows from soma to dendrites. Adapted from: https://www.studyblue.com/.

the cell body layer. Proximal, middle and distal dendrites are the second, third and farthest dendritic compartments to the soma, respectively. Each compartment has a length $l$ with diameter $\varphi$ (Table 5.2) and curved surface area $a = \pi\varphi l$. According to the cable equations and compartmental model of neuron from the previous chapter, each compartment acts like a circuit with its membrane capacitance $C_m$ and compartments connect with each other through axial resistance ($R_a$.). The granule cell receives two main excitatory inputs (there are no inhibitory synapses in our model) on the middle and distal compartments of the dendrites and learning occurs on all excitatory synapses. Presynaptic spikes at MPP and LPP axons cause postsynaptic potentials in the GC dendrites, which propagate in all directions, while action potentials generated in the soma backpropagate into dendrites.

The MPP and LPP had 150 synapses each; half of the MPP synapses (75) are evenly distributed along the MD of dendrite 1 and the other half (75) on the MD of dendrite 2. Half of LPP synapses (75) are evenly distributed along the DD of dendrite 1 and the other half (75) on the DD of dendrite 2. As it can be seen in Figure 2.7 and Figure 5.1, granule cell has two main dendritic trunks (main stems) of the dendritic tree, therefore in our reduced-morphology model we simulate only two dendrites.

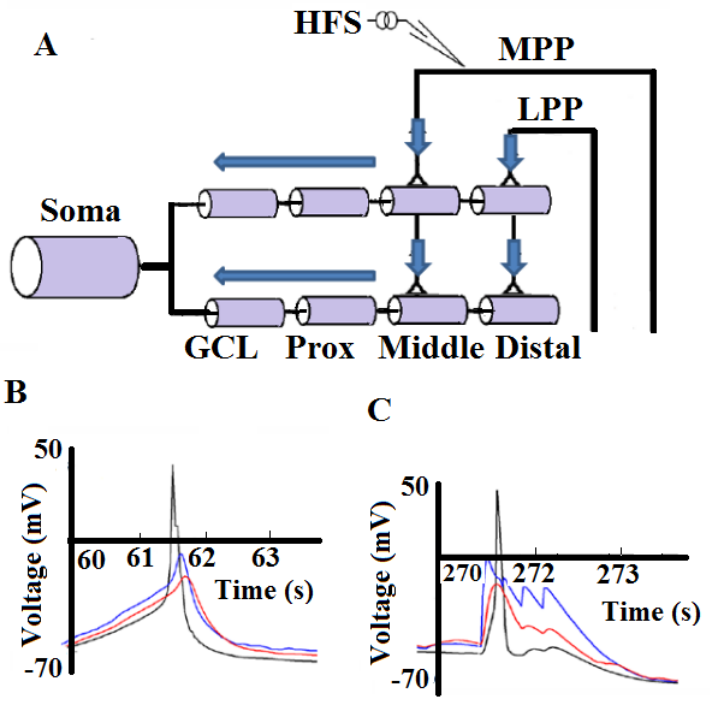


Figure 5.2: (A) A cylindrical 9-compartmental model of the dentate GC has two dendrites with 300 excitatory synapses (each dendrite has 150 synapses). Each dendrite consists of four compartments and soma has one compartment. This model does not have an axon. The lateral perforant pathway (LPP) relays presynaptic inputs from the entorhinal cortex to the distal dendrites (DD), and medial perforant pathway (MPP) relays presynaptic inputs from the entorhinal cortex to the middle dendrites (MD). Lines showing LPP and MPP pathways are only for illustration, because input spikes are delivered directly to synapses in our model. Filled arrows show the flow of input activities and empty arrows the direction of backpropagating action potential. Currents flow through the axial resistance $R_a$ between compartments. (B) Somatic action potential (black) and backpropagation of action potential plus EPSPs from MPP (red) and LPP (blue) before HFS. (C) Somatic membrane potential (black) and backpropagation of action potential plus EPSPs from MPP (red) and LPP (blue) during HFS.

Table 5.2: Parameter values for individual compartments. Source: (Santhakumar *et al.*, 2005)

| Parameters | DD | MD | PD | GCLD | Soma |
|---|---|---|---|---|---|
| $R_a$ ($\Omega$ cm) | 210 | 210 | 210 | 210 | 210 |
| l ($\mu$m) | 150 | 150 | 150 | 150 | 16.8 |
| $\varphi$ ($\mu$m) | 3 | 3 | 3 | 3 | 16.8 |

## 5.2 Simulation of spontaneous presynaptic activity and HFS

Our model granule cell receives presynaptic noisy spontaneous activities via the medial and lateral pathways from entorhinal cortex. In our model, spontaneous activity was generated randomly as Poisson spike trains along the MPP and LPP. The Poisson process is a simple yet accurate model of a neuron's spontaneous firing (Fellous *et al.*, 2003). In the real brain, spontaneous activity is the result of interactions within neural networks and electrophysiological properties of single neurons. This activity is related to the functional state of the brain with the key elements of the level of activation of neuromodulatory systems (Herz *et al.*, 2006). In this thesis, the frequency of presynaptic spontaneous activity has been chosen to be <10 Hz (Gloveli *et al.*, 1997). In our compartmental model of the neuron, presynaptic spontaneous activity are simulated by using independent spike generators (NEURON's built-in point process NetStim). In the NEURON code, the interspike interval (ISI) of spiking activity is generated according to the following equation:

$$\text{ISI} \quad = (1-n)\text{ISI}_0 + \text{neg}\exp(-n\text{ISI}_0) \tag{5.10}$$

where, $n$ is noise function with $0 < n < 1$, negexp(-x) is the negative exponential distribution, which is equal to homogeneous Poisson distribution with probability of the next spike occurring after time ISI. When $n$ is zero, the ISI is equal to $\text{ISI}_0$ (initial value of ISI) and spiking activity is periodic. When $n$ is between zero and one, spiking activity is quasi-periodic. When $n = 1$, then the spike series obeys the homogeneous Poisson distribution. For all the simulations we have chosen 0.02 for the value of $n$. In our NEURON code, each synapse gets an independent series of spikes with $\text{ISI}_0 =$

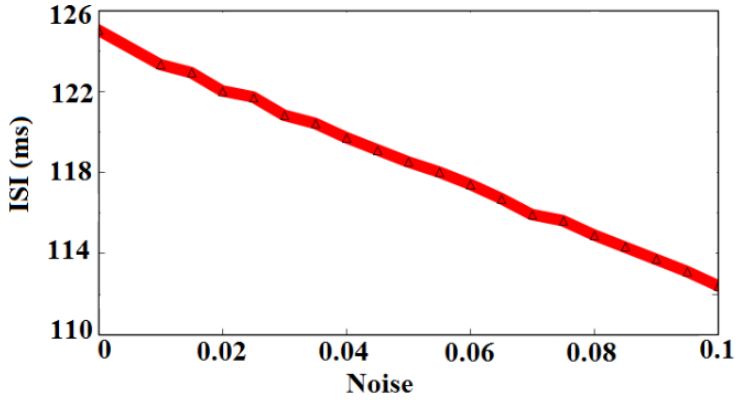


Figure 5.3: ISI is a decreasing function of noise.

125 ms. As it can be seen from Figure 5.3, ISI is a decreasing function of noise which means, as amount of noise increases the value of ISI decreases as well.

In addition to the natural random input from the entorhinal cortex, we also must simulate the artificial sources of HFS that were present in the experiment.

## 5.3 Applying HFS for LTP induction

Another source of input activity that was represented in experiments was HFS. Benuskova and Abraham showed in their previous work that presynaptic spontaneous activity is necessary for induction of heterosynaptic plasticity (Hananeia and Benuskova, 2016). Therefore, for all protocols, HFS was applied along with noisy spontaneous preysynaptic activity (except those times that we switch spontaneous activity off).

In the first simulation protocol, the pattern of HFS was the same as the review of the first experimental studies from Chapter four. After 4 min of starting simulation, HFS with 400 Hz DBS was applied to the MPP and lasted for about 4.58 min. Sixteen min after the first HFS, a second HFS with the same time and pattern as the first one was applied to the LPP. Lateral HFS also lasted for about 4.58 min.

In the second simulation protocol, a pattern of HFS was the same as the review of the second experimental studies from the Chapter four. 400 DBS of HFS was applied to the medial pathway 4 min after starting simulation. 400 Hz DBS consists of 5 trains at 1 Hz and each train contains 10 spikes at 400 Hz. Bursts are repeated 10 times at every 60-s (Figure 4.3). The whole HFS protocol lasted for about 9.58 min. In

this protocol, to simulate inhibition effect of the procaine on lateral pathway, irregular presynaptic spontaneous activity was switched off only during the medial HFS.

The third protocol contains two parts. At the first part, two HFS following each other are simulated. Firstly, 4 min after starting simulation, 400 DBS of HFS was applied to the medial pathway. 400 Hz DBS consists of 5 trains at 1 Hz and each train contains 10 spikes at 400 Hz. Bursts are repeated 10 times at every 60-s (Figure 4.3). 9.25 min after applying the first HFS, the second HFS with the same pattern as the first one was applied to the medial pathway. In this simulation we examined the plasticity impact of the first medial HFS on the synaptic plasticity caused by the second medial HFS. In the second part, the number of HFS and the patterns of HFS are exactly the same as the first part. Except, irregular spontaneous activity was switched off in the LPP during the first medial HFS. The aim of this simulation was to examine the effect of procaine inhibition of lateral spontaneous activity and metaplasticity upon the outcome of the second HFS.

In the last protocol, patterns of HFS were the same as the review of the fourth experimental studies from Chapter four. Three different patterns of single HFS were applied to the medial pathway. The goal of this simulation was to compare the effect of different patterns of HFS on the synaptic plasticity of the dentate granule cell. The first pattern is 400 DBS of HFS, one burst of HFS consisted of five trains of 10 pulses at 1 Hz. Pulses in the train were delivered at 400 Hz. Bursts were repeated 10 times at 60-s intervals (Figure 4.3) and lasted for about 9.58 min. The second pattern of HFS, 400 TBS (theta-burst stimulation), consisted of ten trains of four 400 Hz pulses at 5 Hz (duration 250 ms) that were repeated 8 times at 10-s intervals (Figure 4.6). The third pattern was 100 TBS (theta burst stimulation) consisting of ten trains of four 100 Hz pulses at 5 Hz (duration 10 ms) that were repeated 8 times at 10-s intervals (Figure 4.7).

## 5.4 Modelling STDP rule

To model the synaptic plasticity of the dentate granule cell we employed standard STDP (see equations 3.51 and 3.52) based on classical spike-pair model (Markram *et al.*, 1997; Sjöström *et al.*, 2008) which was explained briefly in the third chapter.

To implement the pre- and postsynaptic spike, we used the nearest-neighbour interaction. As we briefly explained before, in the nearest-neighbour interaction each presynaptic spike pairs only with two postsynaptic spikes: the postsynaptic spike that most closely precedes the given presynaptic spike and the postsynaptic spike that most closely follows the given presynaptic spike (Van Rossum *et al.*, 2000) (see Figure 3.4B). The first reason we used the nearest neighbour rules is because the back-propagation of postsynaptic spikes to the medial and lateral synapses resets the membrane voltage in the dendritic spines. Therefore, the most recent postsynaptic spikes suppress the effect of previous postsynaptic spikes, which results in the membrane voltage being affected mostly by the recent postsynaptic spike. The second reason is that the nearest-neighbour pairing makes a link between the STDP rule and BCM rule (Izhikevich and Desai, 2003), and because our synaptic plasticity model is based on the STDP and BCM rules, we prefer a nearest-neighbor STDP rule.

The nearest-neighbour nature of the STDP rule is expressed by the following equation:

$$\Delta\omega(t+\Delta t) \quad = \omega(t)(1+\Delta\omega_{+}-\Delta\omega-) \tag{5.11}$$

Synaptic weight updates when the second postsynaptic spike in the nearest neighbours scenario is detected. In our compartmental model, $t_{\text{post}}$ is the time when the postsynaptic voltage crosses a dendritic voltage threshold of $-37$ mV (Jedlicka *et al.*, 2015). Therefore, postsynaptic spikes are actually postsynaptic membrane events (Jedlicka *et al.*, 2015). As we mentioned in the last section, spontaneous activity is on all the time during all protocols except those where it is deliberately blocked. In addition to STDP, according to Benuskova and Abraham (2007), metaplasticity should be combined with the STDP rule.

## 5.5 Metaplasticity

In the third chapter, we discussed different models of metaplasticity rules such as Benuskova and Abraham rule, Clopath et al rule, Froemke rule, etc. In the metaplasticity rule by Clopath et al, only the depression amplitude $D$ depends on the average of postsynaptic activity ($\langle c(t)\rangle_{\tau}$) while the potentiation amplitude is a constant value.

Therefore, we were motivated by their idea and to add metaplasticity to the STDP model, only depression is dependent. To test their idea with our plasticity model we tried to find out, when only one of the potentiation or depression factors is subject to the metaplastic change, whether we can observe the same synaptic plasticity result. Therefore for our metaplasticity, we hid the simulations with setting the $D$ factor as a constant value and the $P$ factor as a function of average of postsynaptic activity ($\langle c(t)\rangle_\tau$) with considering a constant value equal to 0.75.

$$P(t) \quad = \frac{0.75P(0)}{\langle c(t)\rangle_\tau} \quad \text{and} \quad D(t) = D(0) \tag{5.12}$$

where, $P(0)$ and $D(0)$ are initial amplitude values for synaptic potentiation and depression, and $\langle c(t)\rangle_\tau$ is the average of postsynaptic activity.

We also ran all our simulations with setting the $P$ factor as a constant value and $D$ as a function of average of postsynaptic activity ($\langle c(t)\rangle_\tau$) with considering a constant value equal to 1.5,

$$P(t) \quad = P(0) \quad \text{and} \quad D(t) = 1.5D(0)\langle c(t)\rangle_\tau \tag{5.13}$$

where, $P(0)$ and $D(0)$ are initial amplitude values for synaptic potentiation and depression. Running the simulations with both metaplasticity rules did not show a significant change in our result. Therefore, we concluded either potentiation and/or depression being dependent on $\langle c(t)\rangle_\tau$ is enough to lead to homosynaptic LTP and heterosynaptic LTD phenomena.

As can be seen in Benuskova and Abraham rule from Chapter three, the running average of postsynaptic spikes is calculated by counting the number of postsynaptic spikes with exponential decay (equation 3.57).

However, in this thesis, instead of treating spikes as all-or-nothing events, we introduce a modification in which the running average of postsynaptic spikes is calculated based on the difference between the postsynaptic voltage and resting potential at the soma, because we believe that the average of postsynaptic spikes is dependent on the average of voltage of the granule cell rather than a postsynaptic spike count. Therefore, according to our modification, the average of postsynaptic activity is calculated by the following integral:

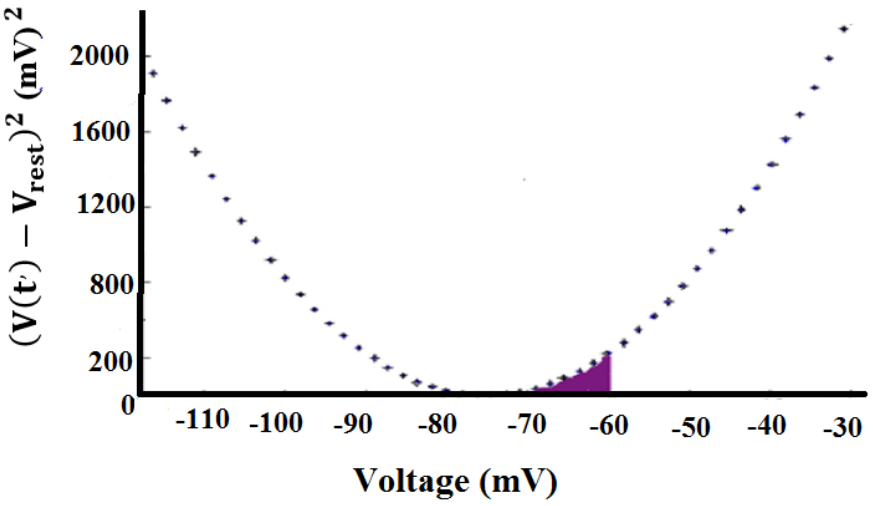


Figure 5.4: Parabola function $(V(t^{'}) - V_{\text{rest}})^2$ as a function of voltage.

$$\langle c(t)\rangle_\tau = \frac{c_0}{\tau}\int_{-\infty}^{t}(V(t^{'}) - V_{rest})^2 \exp(-\frac{(t-t^{'})}{\tau})\, dt^{'} \tag{5.14}$$

where $\langle c(t)\rangle_\tau$ is unitless and is calculated numerically in our metaplasticity codes (see appendix codes). The scaling constant $c_0$ is equal to 0.0025 $1/\text{mV}^2$. $(V(t^{'}) - V_{\text{rest}})$ is the difference between the postsynaptic voltage and resting potential at the soma, $V_{\text{rest}}$ is the initial resting potential and equal to $-75$ mV. By taking the second power of this difference we ensure that $\langle c(t)\rangle_\tau \geq 0$.

Now we explain when the voltage of membrane potential is between the initial values and after hyperpolarization values, the average of postsynaptic activity is in the lowest point. The term $(V(t^{'}) - V_{\text{rest}})^2$ is a parabola function. When granule cell receives spontaneous activity, a new steady-state potential of around $-55$ mV establishes. Therefore all voltage values will be above the initial resting potential ($-75$ mV) and the minimum values of equation $(V(t^{'}) - V_{rest})$ occur between the initial resting potential and the after hyperpolarisation potential (Figure 5.4). That means between these values the average postsynaptic activity is at the lowest value.

## 5.6 The integration method used in this thesis

As we pointed in the third chapter, backward Euler and Crank-Nicholson are two implicit numerical integration methods offered by NEURON. In this thesis we have

solved our equations with the Crank-Nicholson method. We use this method because it is more accurate for small time steps and it can be achieved by setting the global parameter secondorder to 2. As we have some nonlinear equations (for example rate functions), they need to be solved by iteration. However, the backward Euler method does not resort to iteration to deal with nonlinear equations as the error in this method is proportion to $dt$. However, the error in Crank-Nicholson method is proportional to $dt^2$ and it uses a staggered time step algorithm to avoid iteration of nonlinear equations (Hines and Carnevale, 1997). The time step that we have chosen for the numerical integration is 0.2 ms, we also tested our model with different values of time steps $dt =$ 0.1 ms, 0.07 ms, 0.05 ms, 0.027 ms, 0.026 ms and 0.02 ms and observed the same results.

## 5.7 Summary

In this chapter we explained the reduced multi-compartmental model for modelling the dendritic tree of the GC. In this model, seven ion channels are implemented for each compartment. We also introduced two main types of inputs to the GC: HFS and noisy spontaneous activity. To model synaptic plasticity of GC we employed STDP rule. To implement the pre- and postsynaptic spikes for the spike-pair-based STDP rule, we have chosen the nearest- neighbour interaction. We also introduced different metaplasticity rules and compared these rules. And at the end we explained why we used Crank-Nicholson method in our integration method. As synaptic plasticity is a complex mechanism, using computational modeling helps to better understand the different aspects of this complicated mechanism. It also helps to test the different hypotheses which would be difficult to examine in the experimental studies.

# Chapter 6

# Initial results

## 6.1 The relation between metaplasticity rule and sliding modification threshold

The aim of this section is to see if any of the metaplasticity rules considered in Chapter Three are related to our metaplasticity rule. As Izhikevich and Desai (2003) found a relation between the STDP and BCM rules, we are motivated to find the equations that describe the relation between our metaplasticity rule and the sliding modification threshold or $\theta_m$ from the BCM rule. With the following derivation we show how the relation between BCM theory and metaplasticity rules will make sense. The $\theta_m$ sliding modification threshold that determines the direction of synaptic plasticity is not fixed, but it can itself be regulated in proportion to the average of postsynaptic activity according to the equation below (Benuskova and Abraham, 2007),

$$\theta_m \quad = \alpha \langle c(t) \rangle_\tau \tag{6.1}$$

where $\alpha$ is a scaling constant and $\langle c(t) \rangle$ is the average of postsynaptic activity. Therefore, the previous postsynaptic activity not only controls the amplitude of $P(t)$ and $D(t)$ from the STDP rule but it also controls the sliding modification threshold from the BCM rule. We found that the ratio of $D(t)$ and $P(t)$ with metaplasticity rule from equation (5.13) is equal to the sliding modification threshold times some constant,

$$\frac{D(t)}{P(t)} \quad = \frac{1.5D(0)\langle c(t) \rangle}{P(0)} = \frac{1.5D(0)}{P(0)} \langle c(t) \rangle \tag{6.2}$$

We also found that with the metaplasticity rule from equation (5.12), the ratio of $D(t)$ and $P(t)$ is equal to the sliding modification threshold times some constant.

$$\frac{D(t)}{P(t)} = \frac{D(0)}{\frac{0.75P(0)}{\langle c(t)\rangle}} = \frac{D(0)}{0.75P(0)}\langle c(t)\rangle \tag{6.3}$$

According to the above equations, because $1.5D(0)/P(0)$ and $D(0)/0.75P(0)$ are constant values, the ratio of depression and potentiation is only a function of $\langle c(t)\rangle$ or average of postsynaptic activity, which is equal to the modification threshold or $\theta_m$.

We are also interested to see whether the relation between metaplasticity from equation (3.58) (Benuskova and Abraham, 2007) and sliding modification threshold for LTP/LTD from BCM rule will make sense:

$$\frac{D(t)}{P(t)} = \frac{D(0)\langle c(t)\rangle}{\frac{P(0)}{\langle c(t)\rangle}} = \frac{D(0)}{P(0)}\langle c(t)\rangle^2 \tag{6.4}$$

since $D(0)/P(0)$ is a constant value, therefore the ratio of depression and potentiation is a function of squared average of postsynaptic activity. Therefore, the square root of $D(t)/P(t)$ will be a function of the average of postsynaptic plasticity or $\theta_m$. Thus, we showed mathematically that the metaplasticity effect from the previous postsynaptic activity controls the synaptic plasticity of these modified STDP rules.

## 6.2 Reevaluation of the granule cell model

### 6.2.1 The role of nine compartments on synaptic plasticity

Our granule cell model is based on nine compartments, four compartments for each dendrite and one for the soma. In this section, we assess the role of these compartments on the synaptic plasticity of our model. For simulations, we used the first part of the experimental studies described in section 4.1.

As the MPP transmits input to the middle dendrite of the GC, and the LPP transmits input to the distal dendrite of the GC (Scharfman, 2011), these compartments are necessary for our granule cell model. We also need the soma as the metaplasticity mechanism in our model needs the somatic spike to produce LTP and LTD. We conducted a simulation without the proximal dendrite, and our observations showed that the firing

rate before and after HFS was zero which means the neuron was silent. We think, as the proximal and middle dendrites are close, and the density of the fast sodium (Na) ion in proximal dendrite is high, our model, without proximal compartments, would not generate enough spikes for LTP and LTD induction.

We also ran the simulation without the granule cell layer (GCLD). Although the model could reproduce LTP and LTD, we were unable to replicate the results from experimental studies. Although the GCLD is further from the middle and distal dendrites than the proximal, as the density of the Na channel in the GCLD is high, we did not observe a good match with experimental studies. Finally, we concluded that, at least for our plasticity model, all nine compartments are necessary.

### 6.2.2 The role of ion channels on synaptic plasticity

The granule cell model introduced by Santhakumar *et al.* (2005) contains nine ion channels: fast sodium (Na), fast delayed rectifier potassium ($fK_{DR}$), slow delayed rectifier potassium ($sK_{DR}$), A-type potassium ($K_A$), large conductance calcium and voltage-dependent potassium (BK), small conductance calcium-dependent potassium (SK) channels, and T-type (TCa), N-type (NCa), and L-type (LCa) calcium channels. These channel types are described by Hodgkin-Huxley-like equations (Aradi and Holmes, 1999).

The aim of this section is to evaluate the role of these ion channels on synaptic plasticity of the GC and investigate which of these ion channels are necessary for synaptic plasticity in our model. For simulations, we used the first part of experimental studies from section 4.1.

To assess the role of the fast Na channel on synaptic plasticity, we turned off this channel in all nine compartments. In our model the amount of observed LTP was small and almost no LTD was observed at all. This finding supports the investigations from Jedlicka *et al.* (2015) that blocking the sodium channels in the dendrites interrupts heterosynaptic LTD. As the fast sodium channel regulates the amplitude and width of the action potential (AP) (Aradi and Holmes, 1999), when this channel is blocked, there is no action potential from the soma to backpropagate to the lateral pathway which causes no LTD. Therefore, this ion channel is necessary for our plasticity model.

Then, to examine the role of the three potassium channels, fast delayed rectifier potassium ($fK_{DR}$), slow delayed rectifier potassium ($sK_{DR}$) and A-type potassium ($K_A$), on synaptic plasticity, we turned off the potassium channels in the all compartments. Results showed that both LTP and LTD were not stable due to the action potential refractoriness which depends on the potassium channels (Jedlicka *et al.*, 2015).

For the next simulation, we turned off the three calcium channels, T-type (TCa), N-type (NCa) and L-type LCa. Although we observed homosynaptic LTP in our model, the model was unable to produce stable heterosynaptic LTD and results did not match with experimental studies (Jedlicka *et al.*, 2015). We think this is due to the role of these ion channels on regulating the spike propagation into the dendrites of the GC neuron (Aradi and Holmes, 1999).

In the next simulation, we blocked the calcium-dependent potassium (SK) and (BK) channels. Without these ion channels, our model was able to replicate experimental studies. Although these two calcium-dependent potassium channels play an important role in generating the fast and medium AHPs (Aradi and Holmes, 1999), this specific feature of the GC does not affect our plasticity model. Therefore, our granule cell model does not include these channels.

## 6.3 Summary

In this chapter, we introduced equations to describe the relation between our metaplasticity rule and the sliding modification threshold from the BCM rule.

We then assessed the role of nine compartments of GC on synaptic plasticity and our result supported the hypothesis that in the nine compartmental model of GC introduced by Santhakumar *et al.* (2005) all nine compartments are necessary to produce homo- and hetero-synaptic LTP and LTD.

Our results also showed that this model needs only seven ion channels to reproduce synaptic plasticity which is in agreement with the other hypothesis that all nine ion channels from Aradi and Holmes (1999) are not necessary to produce homosynaptic LTP and concurrent heterosynaptic LTD. For the next chapter we combined the plasticity and metaplasticity rules to see if we could produce homosynaptic LTP and concurrent heterosynaptic LTD with the realistic compartmental model of the GC.

# Chapter 7

# Finding the model parameters

The aim of this chapter is to see if the GC model and the learning rules (plasticity and metaplasticity rules) from the previous chapter are able to reproduce the set of experimental data. In this study GC and plasticity models have some unknown parameters, therefore, we adjust the model parameters to find out whether it is possible for this model to replicate the experimental studies. Finding the correct parameter values is critical for the model because wrong values lead to inaccurate simulations. There are five parameters that we need to find for our plasticity and GC model. In order to find these parameters we use the experimental studies from section 4.1. In these experimental studies two HFS at two different time intervals were applied to the medial and lateral pathways. To find the applied parameter values we initially ran the simulation with the HFS applied only to the medial pathway.

We investigate the magnitude of LTP and LTD as a function of changing the values of a number of model parameters, i.e., $\tau_d$ , $\tau_p$, initial synaptic weights and frequency of medial and lateral noisy spontaneous activity. When we vary one parameter, all other values are fixed.

## 7.1 Finding the $\tau_d$ parameter

Table 7.1 shows the magnitude of LTP and LTD as a function of $\tau_d$, while we have kept the other parameters as constant values ($\tau_P$= 20 ms, synaptic weight=0.58 nS, lateral frequency= 7 Hz and medial frequency = 4.2 Hz).

We have chosen the interval [40 ms, 95 ms] for the alteration domain of $\tau_d$, because

Table 7.1: Percentage of LTP and LTD as a function of $\tau_d$.

| $\tau_d$ (ms) | LTP % | LTD % | Firing rate (Hz) |
|---|---|---|---|
| 40 | 104 | +21 | 2.2 |
| 45 | 92 | +10 | 2.1 |
| 50 | 80 | +1 | 1.7 |
| 55 | 71 | −5.3 | 1.62 |
| 60 | 70.6 | −11 | 1.55 |
| 65 | 61 | −14 | 1.4 |
| 70 | 59 | −17.6 | 1.3 |
| 75 | 55 | −20 | 1.2 |
| 80 | 55 | −23 | 1.1 |
| 85 | 53 | −25.3 | 1.1 |
| 90 | 50 | −26 | 1 |
| 95 | 47 | −27.3 | 0.99 |

in this interval the firing rate of the model GC is nonzero. When $\tau_d < 55$ ms, synaptic weights in the lateral pathway increases and LTD cannot be observed. Also in the experimental studies the value of $\tau_d$ is smaller than 100 ms. When the time window for a depression value is greater than 100 ms, the fluctuation of synaptic weight is very slow and homosynaptic LTP and heterosynaptic LTD occur without metaplasticity rule (we will explain this in the following section). Figure 7.1 shows the LTP curve as a function of $\tau_d$. When $\tau_d$ is between [40 ms, 55 ms], LTP magnitude sharply decreases, while between the values [55 ms, 95 ms] LTP has some small fluctuations. The LTD function is a monotonically function of $\tau_d$. In the interval between [55 ms, 95 ms], with increasing $\tau_d$, we observe more LTD. Therefore, we can conclude with rising $\tau_d$ mostly during interval [55 ms, 95 ms] we observe more LTD and less LTP.

## 7.2 Finding the $\tau_p$ parameter

To examine the effect of altering $\tau_p$ on the magnitude of LTP and LTD, we consider $\tau_p$ variations between [20 ms, 47 ms]. Table 7.2 shows the values of LTP, LTD and postsynaptic firing rate as a function of $\tau_p$, while we have kept the other parameters as constant values ($\tau_d$= 95 ms, synaptic weight= 0.58 nS, lateral frequency = 7 Hz and

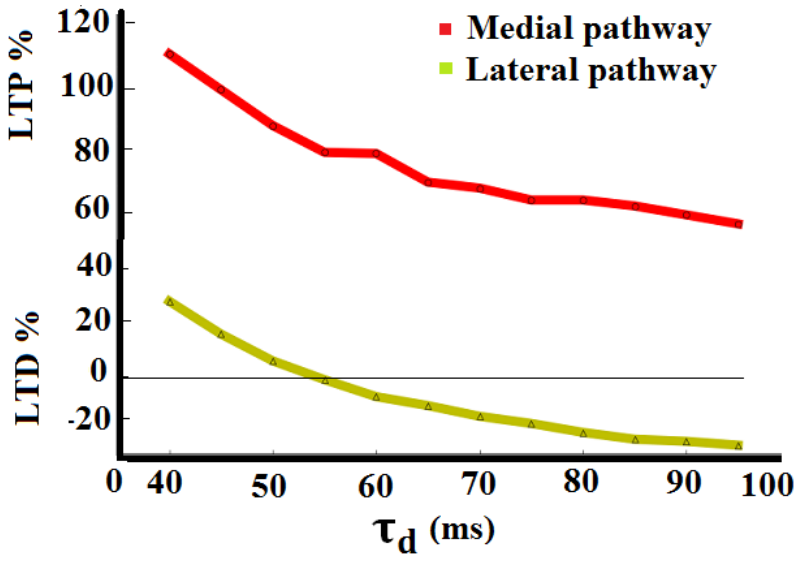


Figure 7.1: The red curve shows the percentage of LTP magnitude as a function of $\tau_d$ and the green curve shows the percentage of LTD magnitude as a function of $\tau_d$.

medial frequency = 4.2 Hz). For $\tau_p$ values equal or less than 18 ms, heterosynaptic LTD and homosynaptic LTP still can be observed even without metaplasticity rules. Therefore, to involve the metaplasticity rules in the synaptic plasticity $\tau_p$ values are considered bigger than 18 ms. For $\tau_p$ values bigger than 35 ms, synaptic weight increases in the lateral pathway and no LTD is observed in this pathway. However, in the medial pathway synaptic weight after HFS also increases and it diverges from the baseline. When $\tau_p$ value is in the interval [20 ms, 35 ms] gradually less LTD is observed (Figure 7.7). However, in this interval in the medial pathway the LTP function increases gradually and less LTD is observed.

## 7.3 Finding parameter for the initial synaptic weight

The other parameters that might have an effect on the LTP and LTD magnitudes are the medial and lateral path initial synaptic weights.

To examine the effects of initial synaptic weight on LTP and LTD, we varied initial synaptic weight nS so it falls between [0.54 nS, 0.67 nS] and other parameters are fixed as ($\tau_d$= 95 ms, $\tau_p$= 25 ms, lateral frequency= 7 Hz and medial frequency =4.2 Hz), see Table 7.3. Using our model we found when synaptic weight is less than 0.54 nS, the firing rate before HFS is zero, and when initial synaptic weight is more than 0.67 nS,

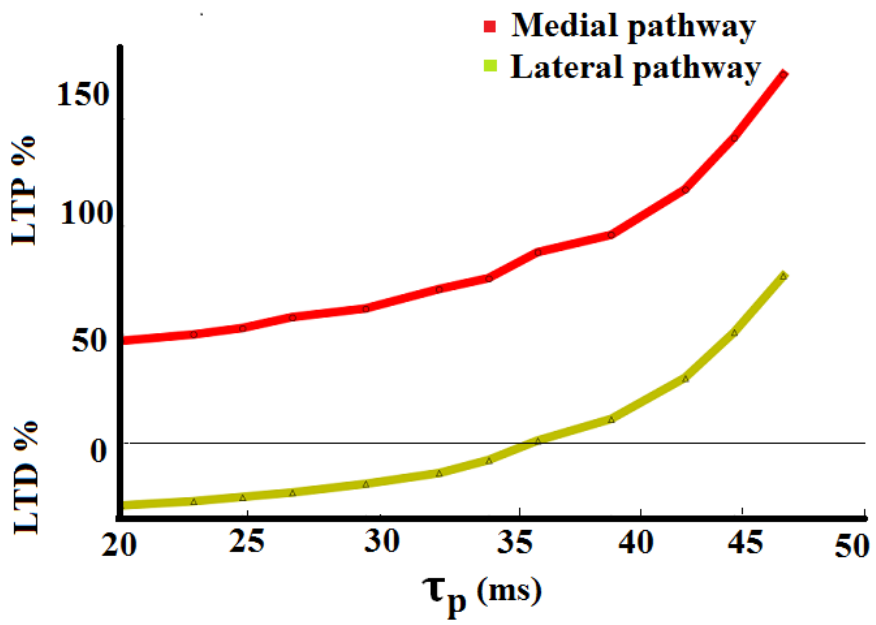


Figure 7.2: The red curve shows the percentage of LTP magnitude as a function of $\tau_p$ and the green curve shows the percentage of LTD magnitude as a function of $\tau_p$.

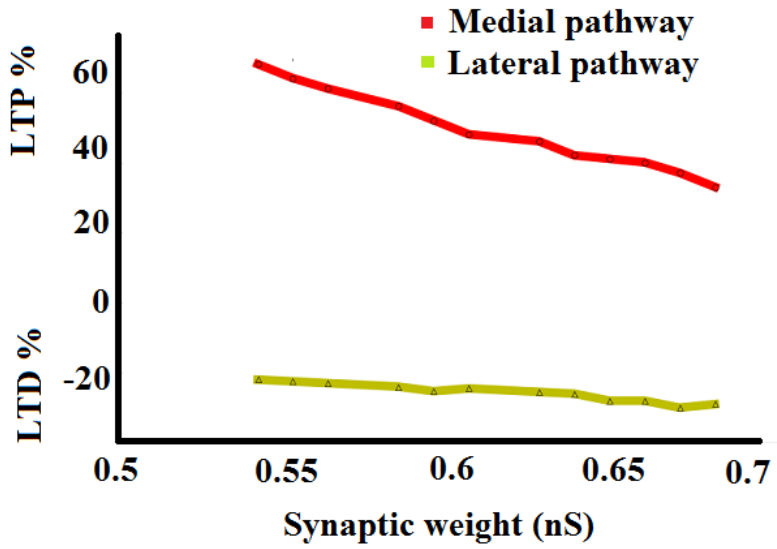


Figure 7.3: The red curve shows the percentage of LTP magnitude as a function of synaptic weights and the green curve shows the percentage of LTD magnitude as a function of synaptic weights.

Table 7.2: Percentage of LTP and LTD as a function of $\tau_p$.

| $\tau_p$ (ms) | LTP % | LTD % | Firing rate (Hz) |
|---|---|---|---|
| 47 | 170 | +77 | 3.3 |
| 45 | 141 | +51 | 2.9 |
| 43 | 117 | +30 | 2.6 |
| 40 | 96 | +11 | 2.2 |
| 38 | 88 | +1 | 1.9 |
| 35 | 76 | −8 | 1.8 |
| 33 | 71 | −14 | 1.6 |
| 30 | 62 | −19 | 1.5 |
| 27 | 58 | −23 | 1.3 |
| 25 | 53 | −25 | 1.1 |
| 23 | 50 | −27 | 1 |
| 20 | 47 | −29 | 0.9 |

LTD is not stable. The magnitude of LTP as a function of synaptic weight is shown in Figure 7.3. As synaptic weight is increasing, the magnitude of LTP decreases sharply during the whole interval, therefore LTP is a monotonically decreasing function of synaptic weight. However, when synaptic weights are growing, LTD tends to increase with a slight slope. As a result, with growing initial synaptic weights, we observe less LTP and more LTD.

## 7.4 Finding parameter for frequency of lateral activity

We then examined the effect of spontaneous lateral frequency on LTP and LTD magnitudes, while maintaining the other parameters at the constant values as ($\tau_d$= 95 ms, $\tau_p$= 25 ms, synaptic weight=0.65 nS and medial frequency =4.2 Hz).

As can be seen from Table 7.4, we have simulated LTP and LTD while the average frequency of spontaneous activity in the lateral pathway is between [4.7 Hz, 21.2 Hz]. However, experimental studies by Deshmukh *et al.* (2010) shows that the frequency of spontaneous activity is less than 10 Hz. Figure 7.4 shows the alteration of magnitude

Table 7.3: Percentage of LTP and LTD as a function of initial synaptic weight.

| $\omega(0)$ (nS) | LTP % | LTD % | Firing rate (Hz) |
|---|---|---|---|
| 0.54 | 68 | −22 | 1.5 |
| 0.55 | 64 | −22.5 | 1 |
| 0.56 | 61 | −23 | 1.2 |
| 0.58 | 56 | −24 | 1.1 |
| 0.59 | 52 | −25.3 | 1.2 |
| 0.60 | 48 | −24.5 | 1.2 |
| 0.62 | 46 | −25.5 | 1.2 |
| 0.63 | 42 | −26 | 1.3 |
| 0.64 | 41 | −28 | 1.4 |
| 0.65 | 40 | −28 | 1.4 |
| 0.66 | 37 | −30 | 1.5 |
| 0.67 | 33 | −29 | 1.6 |

of LTP when spontaneous lateral frequency is changing. LTP as a function of lateral frequency is a linear function. When lateral activity is between [4.7 Hz, 11.7 Hz], LTP is mostly decreasing with a slight slope, while in the interval [11.7 Hz, 21.2 Hz], the fluctuation of the LTP magnitude is very low. The LTD magnitude as a function of spontaneous lateral frequency is a monotonically decreasing function. From interval [4.7 Hz, 11.7 Hz], the LTD magnitude decreases sharply and we observe more LTD. From interval [11.7 Hz, 21.2 Hz], the LTD magnitude decreases with a slight slope.

## 7.5 Finding parameter for frequency of medial activity

Table 7.5 shows the magnitude of LTP and LTD as a function of frequency of medial spontaneous activity during interval [3 Hz, 7 Hz], while the other parameters are kept at the constant values as ($\tau_d$= 95 ms, $\tau_p$= 25 ms, synaptic weight=0.65 nS and lateral frequency = 6.5 Hz).

As can be seen in Figure 7.5, LTP is a nonlinear and monotonically decreasing function of medial spontaneous frequency. Unlike LTP, when the frequency of medial

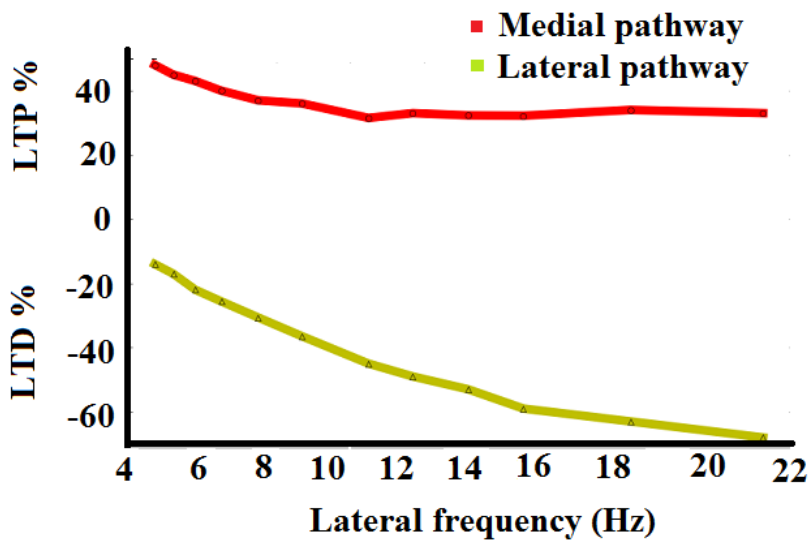


Figure 7.4: The red curve shows the percentage of LTP magnitude as a function of frequency of lateral spontaneous activity and the green curve shows the percentage of LTD magnitude as a function of frequency of lateral spontaneous activity.

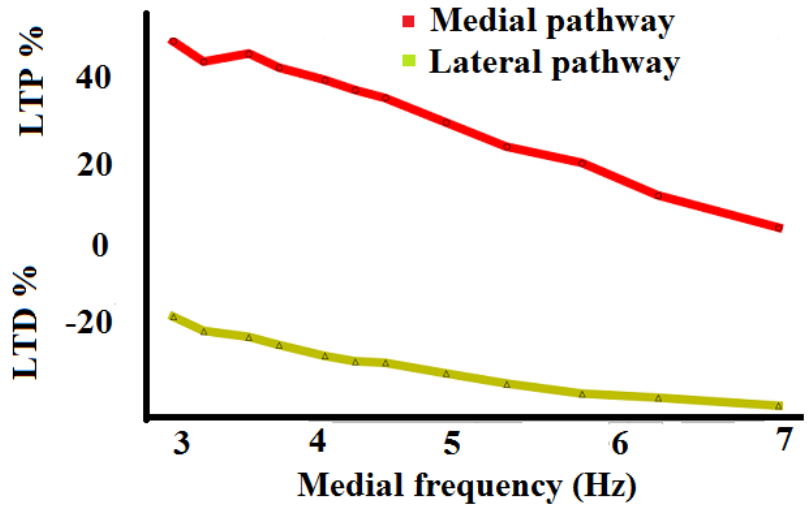


Figure 7.5: The red curve shows the percentage of LTP magnitude as a function of frequency of medial spontaneous activity and the green curve shows the percentage of LTD magnitude as a function of frequency of medial spontaneous activity.

Table 7.4: Percentage of LTP and LTD as a function of lateral spontaneous frequency.

| lat freq (Hz) | LTP % | LTD % | Firing rate (Hz) |
|---|---|---|---|
| 21.2 | 33 | −67 | 1.6 |
| 17.6 | 34 | −63 | 1.7 |
| 14.7 | 32.2 | −59 | 1.72 |
| 13.2 | 32 | −53 | 1.71 |
| 11.7 | 32.3 | −49 | 1.66 |
| 10.5 | 31.5 | −45 | 1.6 |
| 8.7 | 36 | −36.5 | 1.4 |
| 7.5 | 37 | −30.6 | 1.46 |
| 6.5 | 40 | −25.6 | 1.4 |
| 5.8 | 43 | −22 | 1.24 |
| 5.2 | 45 | −17 | 1.18 |
| 4.7 | 48 | −14 | 1.13 |

activity increases, LTD is decreasing linearly with the low slope until it probably reaches an asymptotic value.

After analysing all tables and graphs we concluded with our model (plasticity, metaplasticity and GC model) parameter values from Table 7.6 are replicating the homosynaptic LTP and concurrent heterosynaptic LTD quite well. These parameters also produce good results compared with the range of experimental data.

## 7.6 Relation of $\tau_d$ values smaller than 100 ms and the metaplasticity rules.

As we explained in the last section, the value of parameter of $\tau_d$ in the experimental studies is less than 100 ms. In this subsection we were interested to know what happens for the plasticity and metaplasticity phenomena when $\tau_d$ is bigger than 100 ms (Lin *et al.*, 2006).

For that reason, we tested the synaptic plasticity with the same plasticity and metaplasticity rules as equations 5.12, while the values of $\tau_d$ are bigger than 100 ms and other parameters are taken from Table 7.6. Table 7.7 shows the magnitude of LTP

Table 7.5: Percentage of LTP and LTD as a function of medial spontaneous frequency.

| med freq (Hz) | LTP % | LTD % | Firing rate (Hz) |
|---|---|---|---|
| 7 | 7 | −37 | 2.3 |
| 6.2 | 15 | −35 | 2.1 |
| 5.7 | 23 | −34 | 1.9 |
| 5.2 | 27 | −31.5 | 1.7 |
| 4.8 | 33 | −29 | 1.67 |
| 4.4 | 39 | −26.4 | 1.4 |
| 4.2 | 41 | −26 | 1.4 |
| 4 | 43.5 | −24.7 | 1.3 |
| 3.7 | 46.5 | −22 | 1.2 |
| 3.5 | 50 | −20 | 1. |
| 3.2 | 48 | −18.5 | 1.1 |
| 3 | 53 | −15 | 0.86 |

Table 7.6: Parameter values for optimal match with the experimental data.

| $D(0)$ | $P(0)$ | $\tau_D$ | $\tau_P$ | initial weight | Medial freq | Lateral freq | $\alpha$ | $\tau$ |
|---|---|---|---|---|---|---|---|---|
| 0.001 | 0.004 | 95 ms | 25 ms | 0.65 nS | 2.9 Hz | 6.8 Hz | 0.2500 | 60 s |

and concurrent LTD with the $\tau_d$ values bigger than 100 ms. The fluctuations of the LTP and LTD magnitude when the $\tau_d$ are in the interval [120 ms, 500 ms] is shown in Figure 7.6. The LTP fluctuations are very low for all values during this interval. The fluctuations of LTD magnitude, especially during the interval [150 ms, 500 ms], are also very low. We also tested the synaptic plasticity when the $\tau_d$ values are bigger than 100 ms with no metaplasticity rules meaning P = $P_0$ and D = $D_0$. Surprisingly, we discover that even without metaplasticty rules when $\tau_d$ values are bigger than 100 ms LTP and concurrent LTD can be observed. Therefore, we reached this important conclusion that when the time window for $\tau_d$ is quite large, metaplasticity is not needed to account for heterosynaptic plasticity.

Table 7.7: Percentage of LTP and LTD as a function of $\tau_d$ for values bigger than 100 ms.

| $\tau_d$ (ms) | LTP % | LTD % | Firing rate (Hz) |
|---|---|---|---|
| 120 | 28 | −33 | 1 |
| 150 | 29.6 | −37.5 | 0.88 |
| 200 | 27 | −40 | 0.65 |
| 250 | 30 | −47 | 0.38 |
| 300 | 27.5 | −43.5 | 0.48 |
| 350 | 28.5 | −45.5 | 0.44 |
| 400 | 29 | −45 | 0.44 |
| 450 | 31.5 | −46 | 0.38 |
| 500 | 32 | −45 | 0.34 |

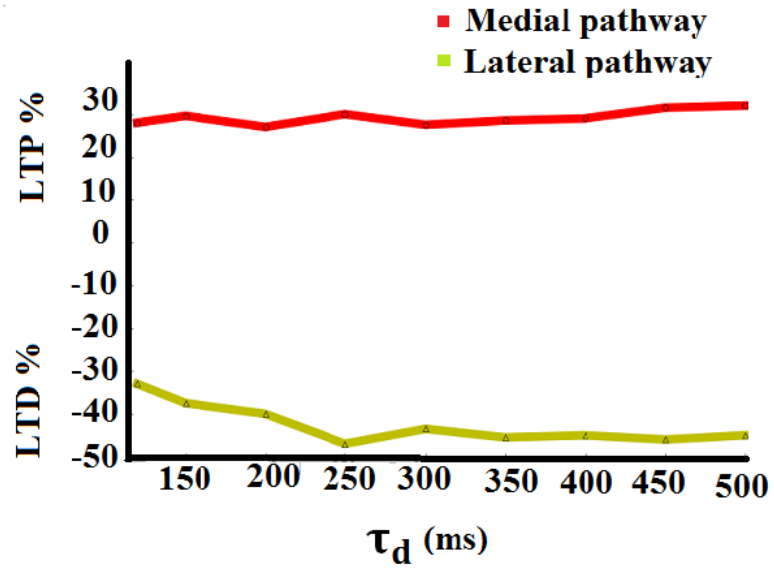


Figure 7.6: The magnitude of LTP in the medial pathway and concurrent LTD in the lateral pathway, when $\tau_d$ values are bigger than 100 ms with the parameters from Table 7.6 and metaplasticity rules from equations (5.12)

## 7.7 Relation of $\tau_p$ values greater than 18 ms and mataplasticity

We also explained that the value of parameter of $\tau_p$ in the experimental studies is 25 ms. In this section we are trying to find out the reason of that. Therefore, we tested the synaptic plasticity with the same plasticity and metaplasticity rules as equations

(5.12), while the values of $\tau_p$ are smaller than 20 ms and other parameters are taken from Table 7.6. Table 7.8 shows the magnitude of LTP and concurrent LTD with the $\tau_p$ values smaller than 20 ms. The fluctuations of the LTP and LTD magnitude when the $\tau_p$ are in the interval [2 ms, 18 ms] is shown in Figure 7.7. As can be seen the fluctuations of LTP are increasing very slowly during the intervals [6, 18]. And the fluctuations of LTD magnitude, especially during the interval [4 ms, 18 ms], are decreasing very slowly. We also tested the synaptic plasticity when the $\tau_p$ values are smaller than 18 ms with no metaplasticity rules means P = $P_0$ and D = $D_0$. We also find out that even without metaplasticity rules when $\tau_p$ values are smaller than 18 ms, LTP and concurrent LTD can be observed. Therefore, we concluded that, when the time window for $\tau_p$ is quite small, metaplasticity is not needed to account for the heterosynaptic plasticity.

Table 7.8: Percentage of LTP and LTD as a function of $\tau_p$ for values smaller than 18 ms.

| $\tau_p$ (ms) | LTP % | LTD % | Firing rate (Hz) |
|---|---|---|---|
| 18 | 29.5 | −30 | 1.1 |
| 16 | 30 | −33 | 1 |
| 14 | 28 | −31 | 0.93 |
| 12 | 26.5 | −33.5 | 0.93 |
| 10 | 25 | −31 | 1 |
| 8 | 24 | −32 | 0.78 |
| 6 | 20 | −30 | 0.65 |
| 4 | 13.5 | −24 | 0.53 |
| 2 | 6.5 | −17 | 0.39 |

## 7.8 Necessity of metaplasticity

In this subsection we examine whether the metaplasticity rules described in equations (5.12) and (3.58) are necessary for inducing LTP and concurrent LTD in our granule cell model. For this purpose we use the experimental studies for the first protocol from section (4.1). And for the STDP rules in equations (3.51) and (3.52), we put P = $P_0$ and D = $D_0$ as constant values. As can be seen from Figure 7.8 when P and D both

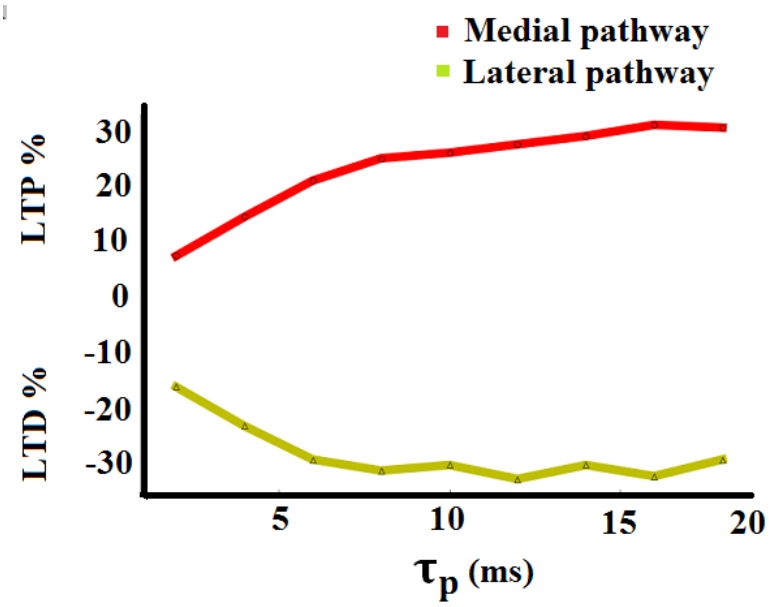


Figure 7.7: The magnitude of LTP in the medial pathway and concurrent LTD in the lateral pathway, when $\tau_p$ values are smaller than 18 ms with the parameters from Table 7.6 and metaplasticity rules from equation 5.12.

were constant values, we did not observe any LTP and concurrent LTD. Therefore, we concluded that in our model metaplasticity should be involved in STDP rules to observe LTP and concurrent LTD.

## 7.9 Summary

In this chapter we found parameter values for our model plasticity and GC. We also found that in order to take into account the metaplasticity rule in our plasticity model the value of $\tau_d$ should be less than 100 ms and also the value of $\tau_p$ should be bigger than 18. We also found if potentiation and depression values from the plasticity rule were constant i.e., $P = P_0$ and $D{=}D_0$, the granule cell model does not produce LTP and LTD. In the next chapter we show that our plasticity granule cell model replicates some experimental data.

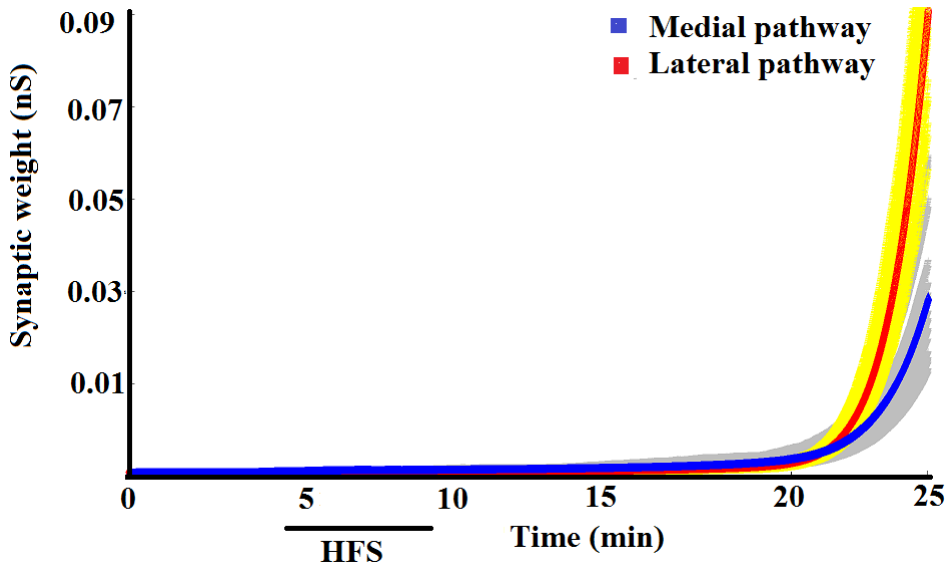


Figure 7.8: The average of medial synaptic weight (blue curve) and the average of lateral synaptic weights (red curve) when P and D are constant values.

# Chapter 8

# The first protocol

In this chapter we will test our hypotheses that computational modelling of plasticity (STDP rules) and metaplasticity with the reduced morphology multi-compartmental model of the GC combined with the noisy spontaneous activity yield homosynaptic LTP and concurrent heterosynaptic LTD. For this reason we use the experimental studies from Section 4.1. Firstly we simulated when HFS applies only to the medial pathway. For this simulation we use the parameters from Table 7.6. After applying the medial HFS, as a result of STDP combined with the BCM-like metaplasticity rule, homosynaptic LTP and concurrent heterosynaptic LTD occurred in the dentate granule cell (Figure 8.1). When simulation starts, it takes some time until both synaptic weights (yellow and grey traces) and the average synaptic weights (red and blue traces) become stable and stay at the baseline. This stability continues until starting the first burst of medial HFS. This shows there is almost no change in the average medial and lateral synaptic weight before medial HFS; therefore, we consider this level to be the 100% baseline level. When medial HFS starts the average of medial synaptic weights increases (blue trace) and the average of lateral synaptic weight decreases from baseline (red trace). To calculate the LTP and LTD size we measured the magnitude of medial and lateral synaptic weight as a difference from the 100% baseline level one minute before the first burst of HFS and one minute before the end of simulation. Therefore, numbers over 100% baseline show the percentage of LTP magnitude and less than 100% show the percentage of LTD magnitude. Our model produced LTP in the medial pathway at approximately 37% from the baseline and LTD in the lateral pathway at approximately $-27\%$ from the baseline. In comparison in the experimental studies (37

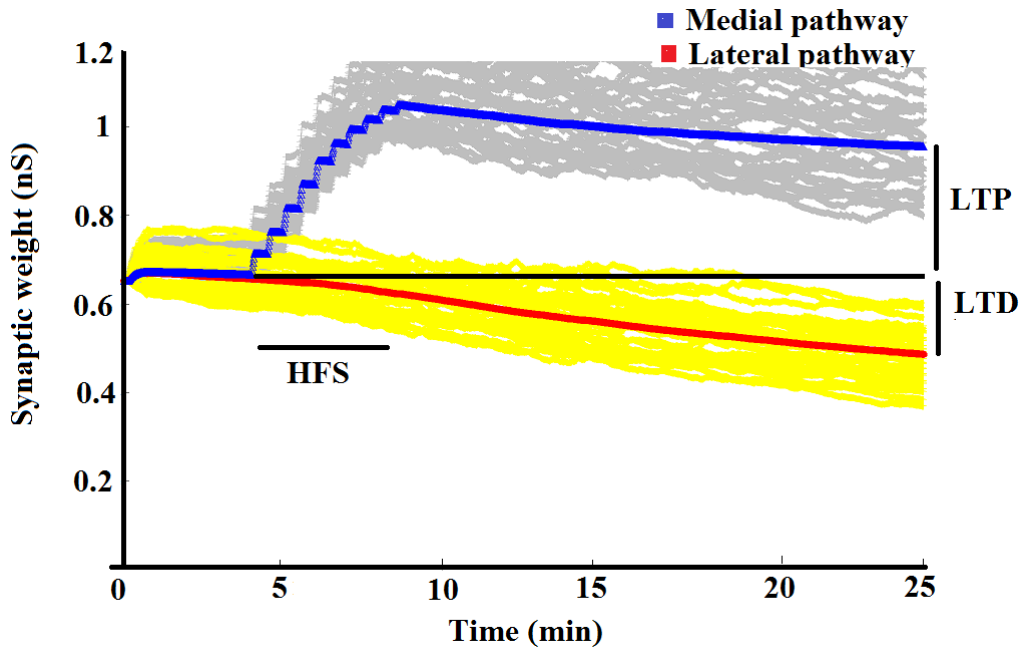


Figure 8.1: Evolution of synaptic weight expressed in terms of postsynaptic conductance over time. The blue trace corresponds to the average weight of all 150 medial synapses, while the red trace represents the average weight of all 150 lateral synapses. Grey traces represent individual medial synapses and yellow traces represent individual lateral synapses. Simulation is started with the same initial weight value for all synapses that is adjusted so that the granule cell model fires action potentials. Before medial HFS, both traces are stable on average, until starting the medial HFS (black horizontal line). During HFS, synaptic weights increase in the medial pathway and decrease in the lateral pathway. The percentage of LTP and LTD is calculated as difference between the average weight at 25 minutes from the baseline of the blue curve (for the medial pathway) and from the red curve (for the lateral pathway). In this run, we observe +37% LTP in the medial pathway and −27% LTD in the lateral pathway.

± 5% ) LTP in the medial pathway and (30 ± 5%) LTD in the lateral pathway was observed. As can be seen our results are quite a good match with the experimental studies.

## 8.1 Detecting pre- and postsynaptic events

In our synaptic plasticity model, we need to detect pre- and postsynaptic events to calculate the nearest-neighbours spike interactions in the STDP rule. In our compartmental model of granule cell, the presynaptic events are the presynaptic spikes, which are generated at the place of each synapse and lead to the generation of the excitatory postsynaptic potential (EPSPs) at the corresponding site of the dendrite. From there EPSPs propagate along dendrites to the soma because of the action of ion channels in the membrane and because of the passive electric properties of the dendritic model. Now we explain how to compute the postsynaptic event. Once the simulation starts and input activities are delivered to the granule cell, the somatic membrane potential depolarises, which increases the voltage above the initial resting potential. If the summation of input activities (EPSPs) is strong enough to depolarise the somatic membrane potential to pass the firing threshold, the granule cell produces a postsynaptic action potential (postsynaptic spike). Postsynaptic action potential backpropagates back to the dendrites (Mehta, 2004). The dendritic threshold for detection of a back-propagated action potential (bAP) is $-37$ mV (Krueppel *et al.*, 2011). This voltage is critical for induction of synaptic plasticity (Lisman and Spruston, 2005). In our model we have only one threshold for both LTP and LTD. The sum of synaptic EPSPs and bAP, which has crossed the dendritic threshold of $-37$ mV, is referred to as the postsynaptic event (Jedlicka *et al.*, 2015).

Figure 8.2 A shows the membrane voltage with one postsynaptic spike occurring in the soma (black), the middle part (blue) and distal part (red) of the dendrite before HFS. The initial resting potential is $-75$ mV, however, with delivering the ongoing spontaneous activity to the granule cell, the new steady-state membrane potential of around $-55$ mV is maintained. When spatio-temporal summation of EPSPs evoked by spontaneous activity depolarises the somatic membrane potential, the voltage increases to 30 mV. Back-propagation of action potential to the middle and distal part of the

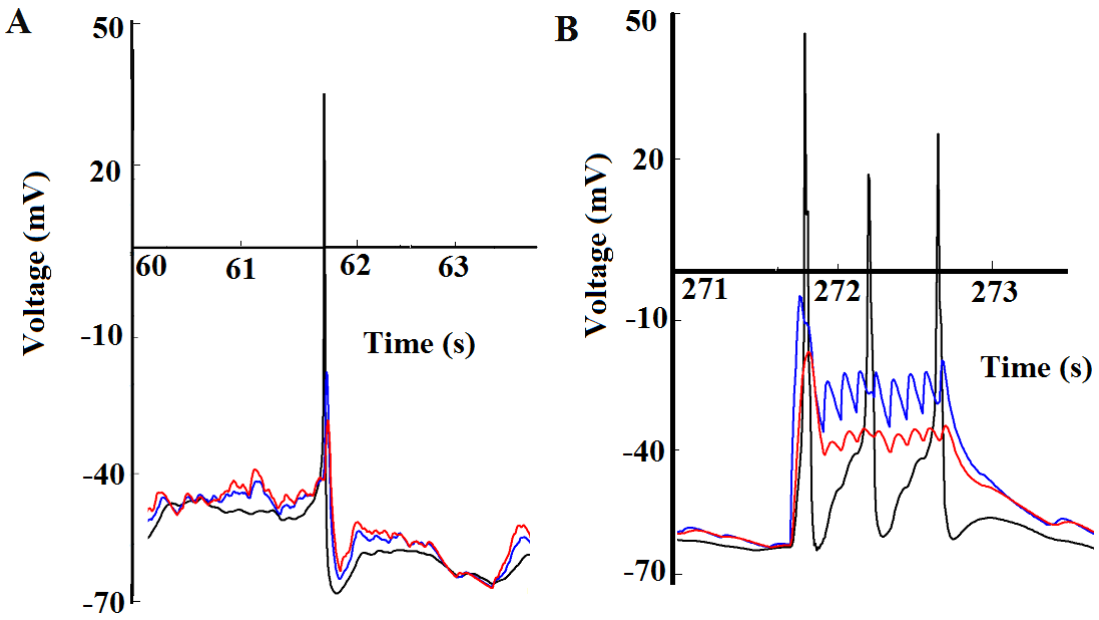


Figure 8.2: (A) Somatic membrane potential (black) and backpropagation of action potential to the distal (red) and middle (blue) parts of granule cell dendrites before HFS. New steady-state potential maintained by the ongoing presynaptic activity is −55 mV. The maximal after-hyperpolarization is −65 mV. (B) Somatic membrane potential (black) and backpropagation of action potential plus lateral and medial EPSPs to the distal (red) and middle (blue) parts of granule cell dendrites during one train of HFS.

granule cell depolarises the membrane potential in the dendrites and raises the voltage in the synapses of the lateral and medial pathway to −23 mV and −33 mV respectively, which is above the dendritic threshold of −37 mV. Therefore, in both the lateral and medial synapses a postsynaptic event is detected, which in this case is a result of spontaneous input activity. After the postsynaptic spike, the membrane potential becomes more negative than the steady-state potential. This after-hyperpolarisation (AHP) is around −65 mV compared to the pre-HFS steady-state potential of −55 mV. We also are able to record the postsynaptic events during the HFS and show how presynaptic and postsynaptic events interact with each other to calculate the nearest-neighbours STDP rules. Figure 8.2 B illustrates the increase of the EPSP of the granule cell during the first train of HFS delivered to the medial pathway. One train of HFS consists of ten input spikes at frequency 400 Hz. The summation of EPSPs evoked by the train of HFS as well as spontaneous activity, if any during this time, depolarises the somatic membrane potential and increases the voltage to −55 mV (black trace). Backpropagation of action potential combined with EPSPs in

the middle and distal parts of the dendrites is shown with the blue and red traces respectively. We call them postsynaptic events. As can be seen from Figure 8.2 B, all medial postsynaptic events could pass the dendritic threshold of $-37$ mV. This shows one train of presynaptic medial HFS can evoke ten post-events in the medial pathway (blue traces). Therefore, according to the nearest-neighbour interaction of STDP rules all 10 medial post events are paired with the preceding 10 pulses from the train of presynaptic (HFS) and spontaneous activity causing homosynaptic LTP to occur in the medial pathway. However, in the lateral pathway only five post-events (red traces) surpass the dendritic threshold while the others fail. In addition, presynaptic events are just spikes from the noisy spontaneous activity. Therefore, according to the STDP rules, the five lateral post-events are paired with spontaneous presynaptic spikes to induce LTP, hence the result is rather LTD than LTP. Another interesting phenomenon that we noticed in Figure 8.2 B was the number of HFS-induced postsynaptic spikes and the size difference of these spikes. Only 3 output spikes are evoked by 10 presynaptic pulses of each HFS train in the soma. Moreover, in this schematic picture, the first spike is the biggest one. We think the refractoriness property of the membrane mechanisms during each spike is the main reason the subsequent spikes have a smaller amplitude than the first one. Refractoriness describes the property of a membrane, which dictates that immediately after the first action potential it is more difficult to generate a second spike (Gerstner, 2000). After the first spike, the membrane potential decreases below the previous potential of about $-55$ mV and becomes more negative. As we explained previously, at this point the membrane potential is in the after-hyperpolarisation state of $-65$ mV, therefore more stimulation is needed to increase the membrane potential and surpass the threshold for the next spike. Therefore, the second postsynaptic spike has a smaller amplitude than the first one. Moreover, the reduction in amplitude from the second to third spike is much smaller than the reduction in amplitude from the first to second because of the increasing synaptic weight (STDP rule) that occurs after the first spike. According to Jedlicka *et al.* (2015), sodium channels in the soma determine the refractoriness property of the granule cell membrane. To examine the effect of this channel on refractoriness property, we blocked the sodium channel in the soma and observed that the duration of refractoriness time increased.

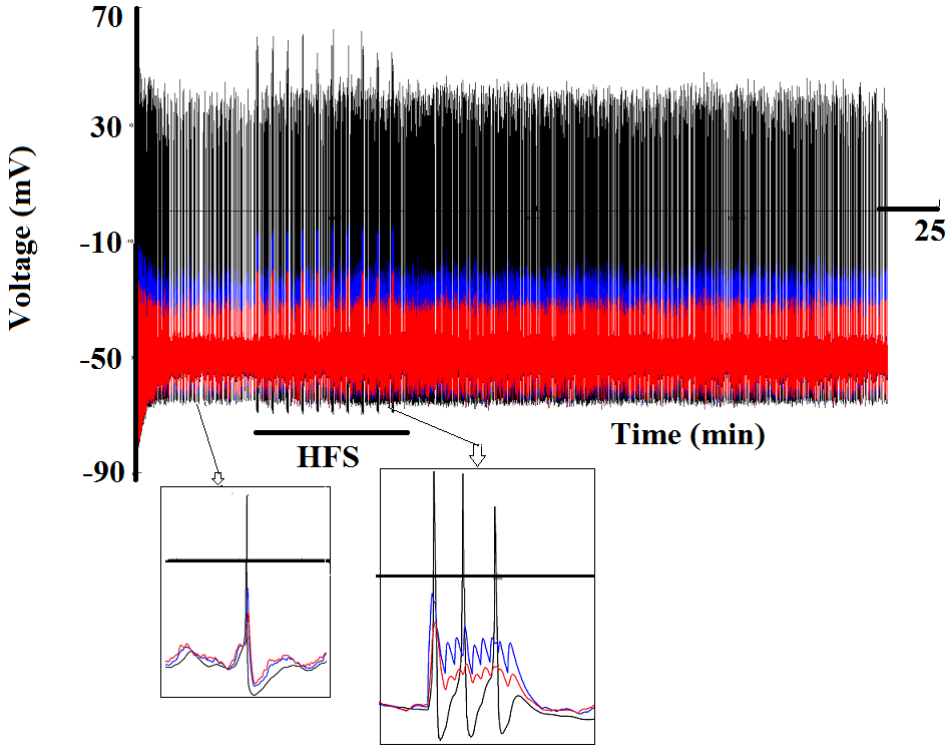


Figure 8.3: Membrane potential of the cell body, lateral and medial pathways with black, red and blue respectively. There are a few spikes before HFS because of the spontaneous activity. During HFS, membrane potential is increasing in the soma and backpropagation of action potentials raises the membrane potential in the lateral and medial pathway parts of dendritic tree. After HFS membrane potential declines in soma, lateral and medial pathways.

## 8.2 Postsynaptic voltage in the soma, lateral and medial pathways

Figure 8.3 shows the membrane potential in the soma (black trace) and the back propagation of spikes plus EPSPs in the dendrites with synapses from medial (blue) and lateral (red) pathways during 25 minutes of simulation. Before HFS, the summation of noisy spontaneous inputs (EPSPs) depolarises the membrane potential and increases the voltage, thus occasional postsynaptic spikes occur (after the initial stabilisation period). During the HFS delivery to the medial pathway, the summation of EPSPs resulting from HFS plus spontaneous activity adds up, which increases the membrane potential and causes more postsynaptic spikes. Therefore, the average postsynaptic voltage increases in the soma and the other pathways. After HFS, because the medial

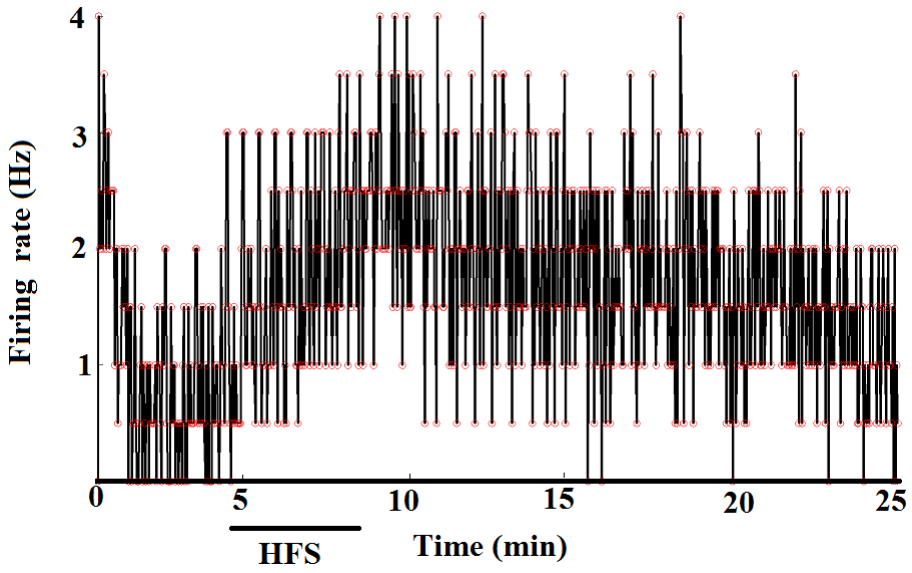


Figure 8.4: Instantaneous firing rate of the granule cell model. Before HFS firing rate is non zero because of the spontaneous activity. During HFS instantaneous firing rate is rising to 3 Hz. After HFS firing rate is decreasing until it goes to the steady state again.

synaptic weights increase more than lateral synapses depress, the average voltage is still high compared with before HFS. As the simulation continues, the metaplasticity effects of the BCM rules decrease the average voltage in the soma and the other pathways, and a steady-state is established.

## 8.3 Instantaneous firing rate

It can be seen in Figure 8.4 that before delivering the medial HFS, the average firing rate is not zero. This means as a result of medial and lateral noisy spontaneous activity, the granule cell is not silent. HFS is delivered to the medial pathway 4 minutes after starting the simulation, which increases the average voltage, and finally increases the average and instantaneous firing rate. After HFS, as a result of the STDP rule, synaptic weights increase in 150 synapses. Although in the lateral pathway synaptic weights decrease, LTP size is bigger than LTD, therefore synaptic drive increases as a whole. Therefore, the average firing rate is still quite high, of around 1.5 Hz. However, after some time, as a result of the metaplasticity rule, the average firing rate decreases back to pre-HFS value.

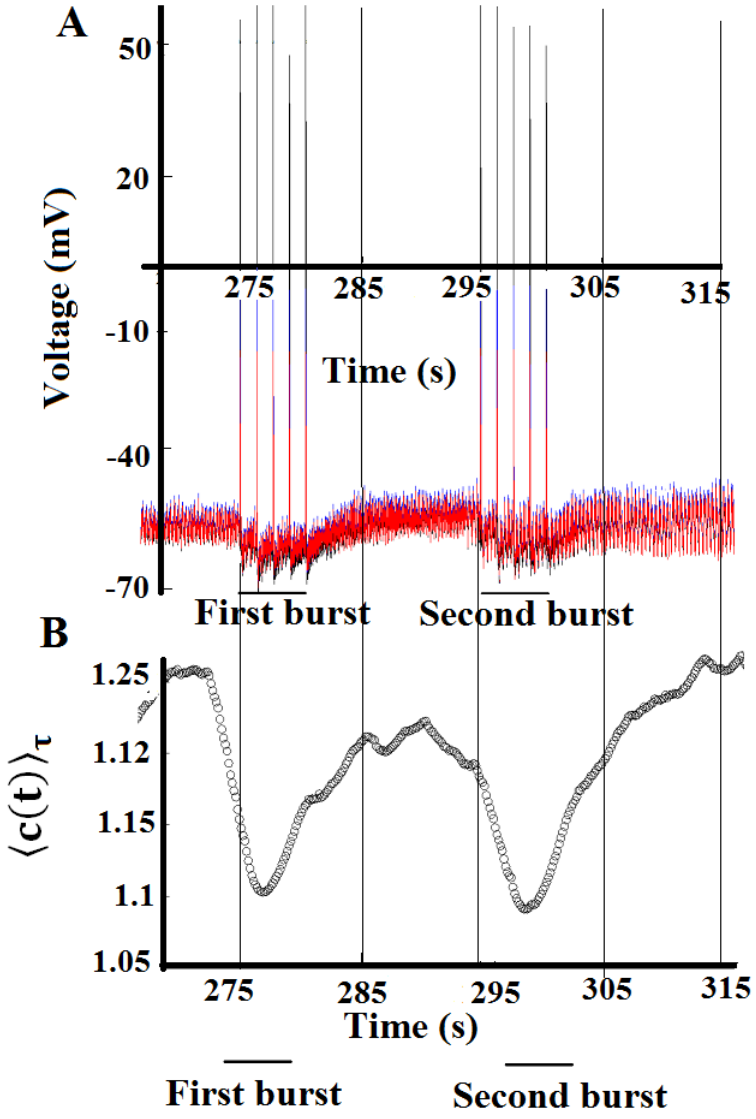


Figure 8.5: (A) Membrane potential just before HFS (when there is just spontaneous activity) and during the first and second bursts of HFS (in total there are 10 bursts). (B) Average of postsynaptic activity before HFS and during the first and second burst of HFS, with the exact timing as in A.

## 8.4 Computing the average of postsynaptic activity

Figure 8.5A shows the membrane potential voltage when the first and the second burst of HFS are applied to the medial pathway. The first burst starts at time 275 s. One burst consists of 5 trains with the interburst interval of 1 second (each train consists of 10 pulses at 400 Hz) and the second burst starts at time 295 s. According to Figure 8.5A and B, when the membrane potential is mostly in the after-hyperpolarisation

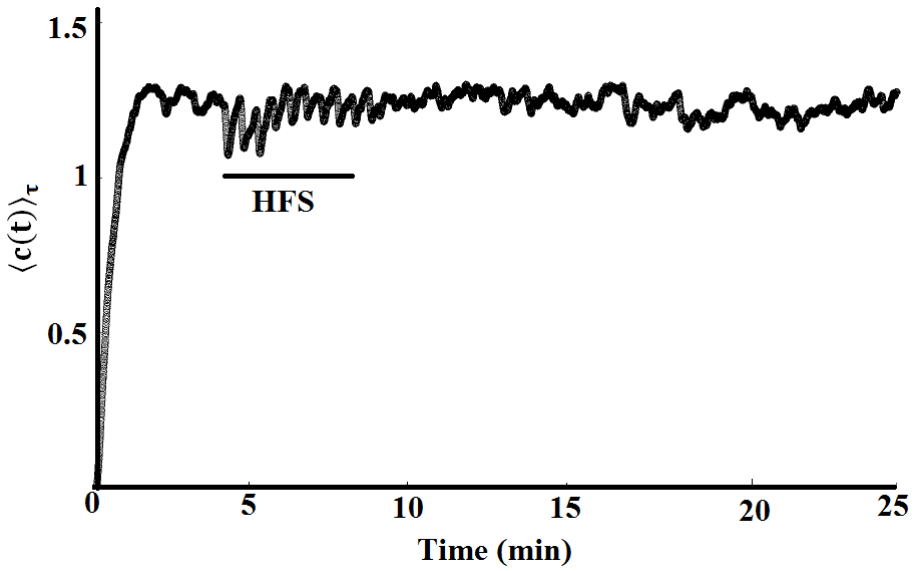


Figure 8.6: Average of postsynaptic potential during the whole simulation. During the bursts of HFS, because of the after-hyperpolarisation of membrane potential, the average of postsynaptic voltage decreases, and between two bursts the average of postsynaptic activity increases (as there is no tetanus)

status, the floating average of postsynaptic activity decreases. As we explained in the method section, when the voltage of membrane potential is between the initial values and after hyperpolarization values, the average of postsynaptic activity is in the lowest point. Now we interpret the fluctuations in average postsynaptic activity. As the simulation starts, average postsynaptic activity increases suddenly as the granule cell receives spontaneous activity. However, as the simulation continues, fluctuations in the average postsynaptic activity reduce until delivering the first burst of HFS (Figure 8.6). As can be seen from (Figure 8.5A and B) when this first burst of HFS is delivered to the medial pathway, the average of postsynaptic activity decreases because of the after-hyperpolarisation feature of granule cell firing. During the time of 30 seconds between the two bursts of HFS, the average of postsynaptic activity again increases to the pre-HFS value because there is no tetanus. However, the reduction that occurs during the second burst of HFS is smaller than the reduction that occurs during the first HFS because synaptic weights increased during this time as per the STDP rule. This scenario continues until all bursts are delivered. After HFS, because of the metaplasticity rule, the average of postsynaptic activity gradually reaches a steady state.

## 8.5 Interpretation of the fluctuations of depression factor

As we mentioned in the methods section, the metaplasticity part of our model is based on the running average of postsynaptic activity expressed by equation (5.14). Amplitudes of LTP and LTD for each synapse are dynamically adjusted based on this average. Let us keep $D(t)$ = constant. Figure 8.7 shows the time course of potentiation and depression factors, $P(t)$ and $D(t)$, during the whole simulation. As far as the simulation starts the potentiation factor decreases to 0.0025 and until coming the medial HFS, the fluctuations of the potentiation factor is very small. However as described previously after delivering the first burst of medial HFS , the average of postsynaptic activity decreases (Figure 8.6). Therefore, according to equation (5.12), potentiation factor (grey trace) increases. As we showed in Figure 8.5A, there is a 30-second gap between each burst of HFS, therefore during this interval, the average of postsynaptic activity increases, which yields a decrease of the potentiation factor. Then, when the next burst of HFS is delivered, potentiation factor increases again and this scenario continues until the end of the HFS. Because of the previously described increase in the medial synaptic weights subsequent to the HFS, the potentiation factor increases slightly past baseline. Then, after some time because of the metaplasticity effect, the fluctuations of potentiation factor again diminish until it reaches its steady state.

## 8.6 Homosynaptic LTP and concurrent heterosynaptic LTD

Finally, let us combine the nearest-neighbour STDP and metaplasticity BCM rules in explanation of homosynaptic LTP and concurrent heterosynaptic LTD. Before the medial HFS, the average of synaptic weights in both lateral and medial pathways is quite stable. As the first burst of HFS is delivered to the medial pathway, the membrane potential depolarises and the average of voltage increases in this pathway. Therefore, summation of EPSP events and bAPs produce the strong postsynaptic activity that can pair causally with the medial presynaptic activity to increase the medial weight

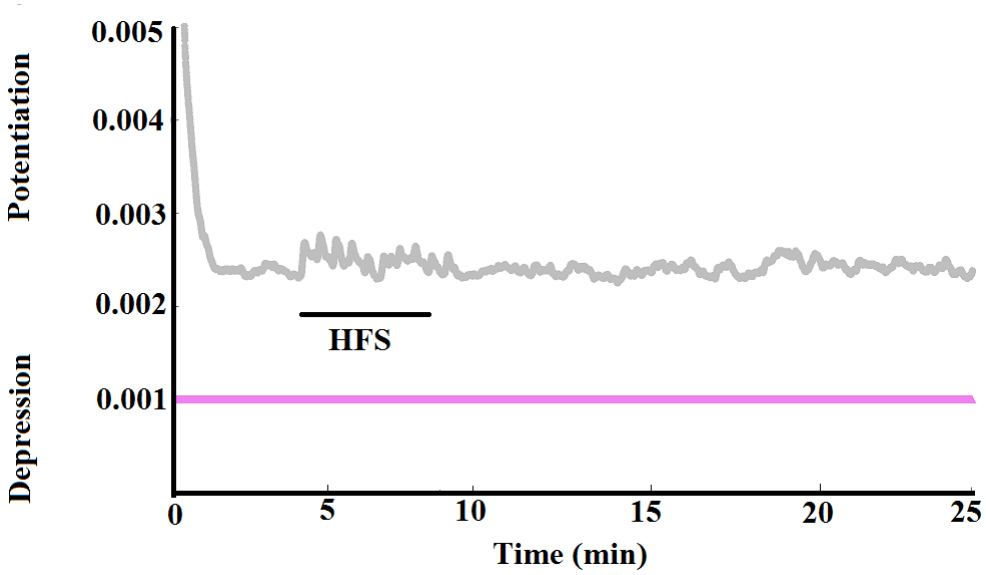


Figure 8.7: Dynamics of LTP amplitude is proportional to the average of postsynaptic potential. During the HFS bursts, because of the after-hyperpolarisation of the membrane potential, the average of postsynaptic voltage decreases which increases the amplitude of P(t).

(STDP rule). However, during the 30-second gap between the first and second burst of HFS synaptic, medial synaptic weight does not change. When the next burst is delivered, synaptic weight again increases and this sequence of events continues until the end of HFS. This synaptic potentiation phenomenon is called homosynaptic LTP (Figure 8.4). Similar to the medial pathway, modification simultaneously occurs in the lateral pathway. When the first burst of HFS is delivered to the medial pathway, the membrane potential depolarises, which increases the average of voltage in the lateral pathway, but not so much as in the medial synapses because the lateral pathway makes synapses at the distal end of dendritic tree. Therefore, although the summation of lateral EPSP events and bAPs produce the postsynaptic activity that sometimes passes the dendritic threshold, as there is only noisy spontaneous activity in the lateral pathway, synaptic weight increases slightly in this pathway. This plasticity phenomenon is called heterosynaptic LTD. After HFS, because of the homeostatic nature of the metaplasticity rules, synaptic weights reach a new steady state.

## 8.7 Depotentiation of LTP and concurrent dedepression of LTD

In this section we simulate the second part of the experimental studies of Section 4.1 with parameters taken from Table 7.6, when the second HFS is applied to the lateral pathway 16 minutes after the first medial HFS. The first HFS is applied to the medial pathways, while spontaneous activity is on throughout for the medial and lateral pathway. When the first HFS is applied to the medial pathway, according to the plasticity and metaplasticity rules, synaptic weights increase in the medial pathway and LTP occurs. Concurrent LTD occurs in the untetanized lateral pathway. When the second HFS is applied to the lateral pathway, synaptic weights increase in this pathway. It can be seen from Figure 8.8 that after the fifth burst of events within the first lateral HFS stimulation, the average of lateral synaptic weights passes the baseline. But after applying the entire HFS, average lateral synaptic weight decreases and no longer stays above the baseline. Therefore, although synaptic weight increases in the lateral pathway and dedepression occurred in this pathway, LTP failed to occur in the lateral pathway and we still observe $-8\%$ lateral LTD. In our model the reversal of much of the LTD in the lateral pathway happens after a transient potentiation of this pathway that was not observed in the experimental data, in which only the reversal of much of the LTD was observed. We think this is because lateral synapses are more distal to the soma than medial synapses, thus the given HFS pattern is not enough to cause potentiation in the already depressed pathway. Figure 8.8 illustrates that synaptic weights are depressed in the medial pathway and we observe a partial depotentiation. However, this amount is not enough to fall below the baseline, thus heterosynaptic LTD failed to occur. Therefore, in our simulation we still observe 15% LTP in the medial pathway. Since our metaplasticity rule has a homeostatic nature, the corresponding depotentiation in the medial pathway is also weak. Comparing our result with the experimental data shows our outcomes are in agreement, as both did not produce LTD in the medial pathway or LTP in the lateral pathway.

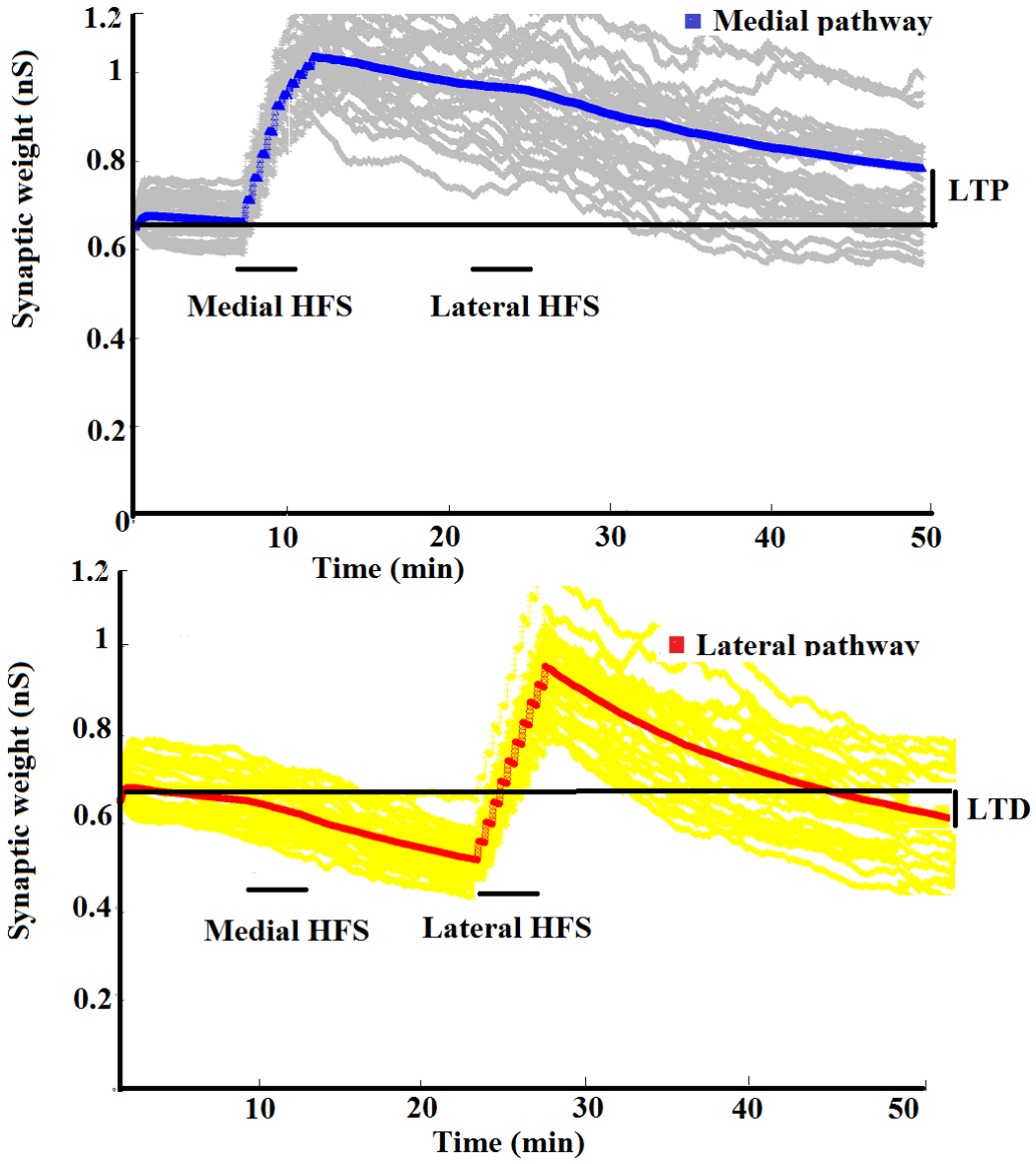


Figure 8.8: Blue curve is the average of medial synaptic weights and grey curves correspond to individual medial synaptic weights. Red curve is the average of lateral synaptic weights and the yellow curves are individual lateral synaptic weights. Medial synaptic weights increase during the medial HFS while lateral synaptic weights decrease. When the second HFS is applied to the lateral pathway, although synaptic weights initially potentiate in the lateral pathway, on average synaptic weight could not stay above the baseline. In the medial pathway, synaptic weights decrease but still could not reach under the baseline to produce LTD.

## 8.8 Summary

In this chapter we demonstrated that our plasticity model could reproduce the homosynaptic LTP and concurrent heterosynaptic LTD observed in the experimental data described in section 4.1.1. To better understand the output of the result we interpreted the voltage, average of postsynaptic activity, potentiation and depression factor and at the end we explained how synaptic plasticity occurs in the medial and lateral pathway. According to these findings our results support the hypothesis that our model can replicate homosynaptic LTP in the tetanized pathway and concurrent heterosynaptic LTD in the neighbouring non-tetanized pathway.

# Chapter 9

# The second protocol

In the second protocol to test whether or not the presence of noisy spontaneous activity is crucial for heterosynaptic LTD induction, we investigate the first part of experimental studies from Section 4.2 when an HFS is only applied to the medial pathway.

In our simulation in order to replicate the procaine inhibition of spontaneous activity in experimental data, we switch lateral spontaneous activity off during medial HFS. However, after HFS we switch the lateral activity on with different level of frequency as before HFS. In experimental studies, when procaine is injected to the lateral pathway, it takes about 60 minutes to wash out all procaine. We believe that during this period procaine might have a lasting effect on the level of spontaneous activity and decreases the frequency of lateral activity. That means after applying procaine it takes some time for the lateral activity to recover from the procaine inhibition and get back to the same frequency as before HFS. We assume this period is longer than the procaine washout period. Therefore, we introduce a new parameter called lateral frequency after HFS (LAH); to characterise the frequency of lateral activity after HFS, while other parameters are the same as Table 7.6.

Table 9.1 shows the magnitude of medial LTP and lateral LTD as a function of lateral spontaneous frequency after HFS (LAH); the frequency of the lateral activity before HFS (during baseline) is 6.8 Hz. When LAH is more than 4 Hz, the size of LTD in the lateral pathway is quite high and when the frequency of LAH reduces, the size of LTD reduces as well. Figure 9.1 shows the amplitude of LTP and LTD as a function of LAH. The fluctuation of LTP as a function of LAH is very low but mostly when the frequency of LAH is increasing, the size of LTP decreases and vice versa. On the other

Table 9.1: Percentage of LTP and LTD as a function of frequency of lateral activity after HFS

| LAH (Hz) | LTP % | LTD % | Firing rate (Hz) |
|---|---|---|---|
| 6.5 | 54 | −22.2 | 1.4 |
| 6.2 | 52 | −20 | 1.2 |
| 5.8 | 55.5 | −18.6 | 1.34 |
| 5.5 | 54.5 | −15 | 1.1 |
| 5 | 58.3 | −12 | 1 |
| 4.7 | 60 | −11 | 1.3 |
| 4.5 | 58.5 | −9 | 1.3 |
| 4 | 58.5 | −8 | 1 |
| 3.7 | 59.5 | −7 | 1.1 |
| 3.5 | 60 | −6 | 0.9 |

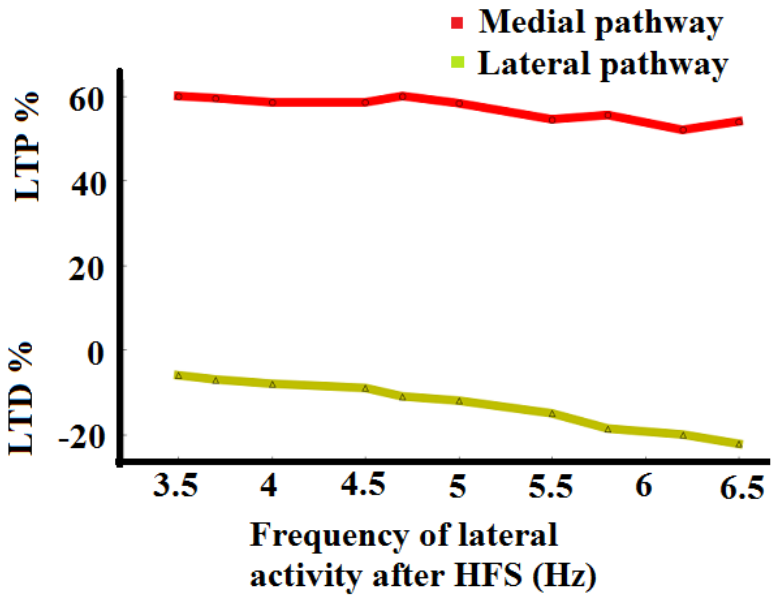


Figure 9.1: The red line shows the amplitude of LTP as a function of lateral frequency after HFS (LAH) and green line shows the amplitude of LTD as a function of lateral activity after HFS (LAH).

hand, LTD as a function of average of lateral activity after HFS is a strictly decreasing function. Therefore, as we decrease the frequency of spontaneous activity after HFS we get almost more LTD. We can explain it as a BCM rule as well: when there is no input or input frequency is very low, the sliding modification threshold shifts to the low value, which reduces the size of LTD. As can be seen from Table 9.1, when the frequency of the lateral activity after HFS (LAH) is 3.5 Hz we observe 60% LTP and

−6% LTD compared to baseline. However, in the experimental data, the LTP was 37 ± 5% and LTD was −10 ± 6% after applying procaine. From this investigation we concluded that to suppress LTD, the frequency of lateral activity after HFS should be less than 4 Hz to explain the procaine inhibition of heterosynaptic LTD with our model.

## 9.1 Average postsynaptic activity

The scaled running average of postsynaptic activity is shown in Figure 9.2. When the simulation starts and both pathways receive spontaneous activity, the average postsynaptic activity increases to 1.22 units. As simulation continues, average postsynaptic activity is stable. When we apply the first burst of HFS, the average postsynaptic activity drops dramatically from 1.22 to 0.35. As we explained from the first protocol, during the after-hyperpolarisation of the first burst of HFS the average voltage decreases. Moreover, in this case also the lateral activity is off during the medial HFS and lateral pathway does not receive any input. Therefore, average postsynaptic activity drops sharply. However, after HFS, because synaptic weights are increased in the medial pathway plus the lateral activity switched on again, average postsynaptic activity increases. As the simulation continues the average of postsynaptic activity goes to the steady state because of the metaplasticity rule.

## 9.2 Homosynaptic LTP and concurrent heterosynaptic LTD

Finally, according to equations (3.51), (3.52), and (5.12), the synaptic weights increase in the medial pathway (STDP rule). After HFS, because of the metaplasticity rule described in equation (5.12), the synaptic weights reach steady state; whereas in the lateral pathway no LTD occurs during HFS. We switch the lateral activity off, therefore there is no lateral activity in this pathway thus no synaptic weight change. However, after HFS because we switch the lateral activity on again (albeit with the lower frequency because of the proposed long-term effect of procaine), the average lateral synaptic weight has almost no change or only a very small reduction.

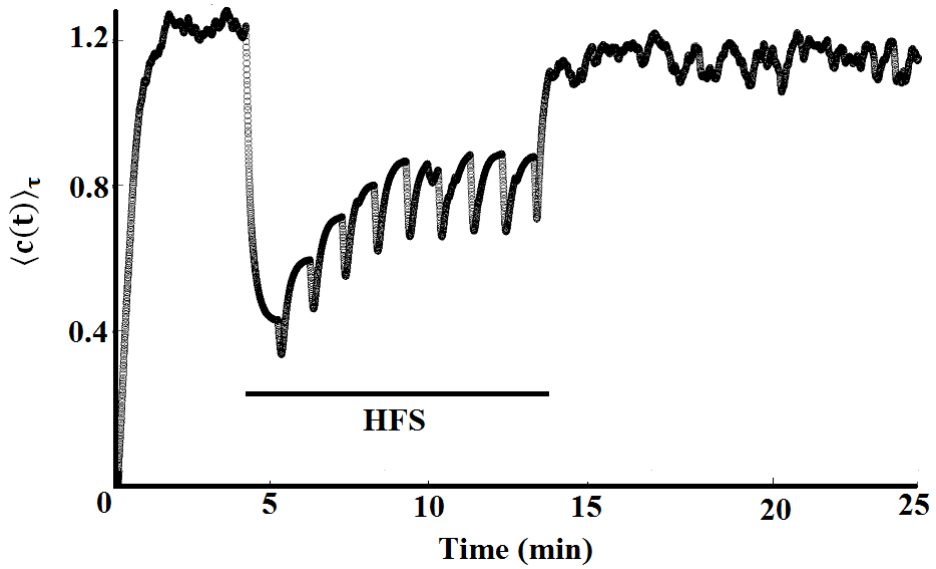


Figure 9.2: Scaled running average of postsynaptic activity before HFS is around 1.3. During HFS the average of postsynaptic activity is very low with some oscillations because of HFS bursts and switching off the lateral activity. After HFS it is rising again because of LTP and switching the lateral activity on.

## 9.3 Summary

In the second protocol we modeled the first part of experimental studies from Section 4.2. In this protocol we explained how our plasticity and metaplasticity model accompanied with compartmental model of GC is able to reproduce the procaine inhibition of the heterosynaptic LTD. We also concluded that reducing the frequency of spontaneous activity reduces the level of heterosynaptic LTD and for having almost no LTD, the frequency of lateral activity after HFS should be less than 4 Hz. This finding agrees with one of our hypotheses saying that the level of noisy spontaneous activity before HFS determines the magnitude of heterosynaptic LTD.

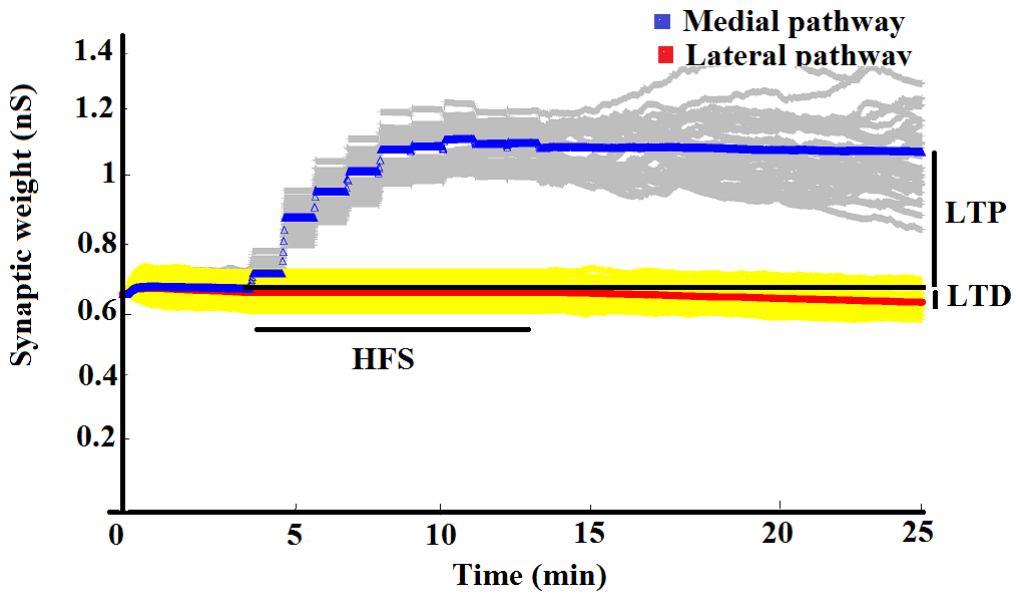


Figure 9.3: The blue curve is the average of medial synaptic weights and the grey curves are synaptic weights from 150 medial synapses. Red curve is the average of lateral synaptic weights and yellow curves are lateral synaptic weights. As the HFS starts at the medial pathway, synaptic weights increase in this pathway. However, almost no LTD happens in the lateral pathway as we switch the lateral activity off during HFS.

# Chapter 10

# Third protocol

In this chapter we simulate experimental studies from Section 4.3 . The goal of this investigation is to see how well our model could reproduce the synaptic plasticity and metaplasticity in this study. As for the experimental studies this protocol contains two groups procaine and control. In the control group we want to test whether our model could reproduce the metaplasticity impact of the first medial HFS on synaptic plasticity of the MPP and LPP resulting from the second medial HFS. In the procaine group we test whether our model could reproduce the metaplasticity impact of the first medial HFS and blocked LPP (during the first HFS) on the synaptic plasticity of the MPP and LPP resulting from the second medial HFS. For both groups we used the parameters from Table 7.6.

## 10.1 Homosynaptic LTP and concurrent heterosynaptic LTD in the control group

In the control group, results for medial and lateral synaptic weights are shown in two separate figures. A few milliseconds after starting simulation both medial and lateral synaptic weights and the average of synaptic weights in the MPP and LPP become stable. As can be seen from Figure 10.1 A and B and according to the STDP rules and equations (3.51), (3.52) and (5.12), when the first HFS is applied to the MPP the average of synaptic weights increases in this pathway and before applying the second HFS, 45% LTP is observed. However, in the LPP the average of synaptic weight decreases and we observe $-27\%$ LTD. When the second HFS following the first

one is applied to the MPP, the average synaptic weight mildly increases further in this pathway and we can observe a total of 54% LTP from the first baseline. This means we only get an additional 9% LTP from the second HFS. Therefore, according to Morrison (2012) synaptic plasticity from the first HFS causes homosynaptic metaplasticity in the medial pathway from the second HFS and we could not observe the same change in LTP as the first one. In the lateral pathway we observe −39% LTD from the first HFS, and in this pathway we also observed only −12% more LTD because of the second HFS. Therefore, in this pathway heterosynaptic metaplasticity occurred and we could not observe the same change in LTD as the first one.

## 10.2 Homosynaptic LTP and concurrent heterosynaptic LTD in the procaine group

Two separate graphs show the medial and lateral synaptic weights in the procaine group. Before HFS, the average of both medial and lateral synaptic weights are stable . As can be seen from Figure 10.2 A and B, when the first HFS is applied to the MPP the average of synaptic weights increases and 48% LTP observes. However, in the lateral pathway because we switch the spontaneous activity off during the first medial HFS and then switch it on with the lower frequency than before HFS (3.5 Hz), we only observe −6% LTD. With applying the second medial HFS, the average synaptic weight increases and we can observe a total of 56% LTP from the first baseline in the medial pathway. This means we get only an additional 8% LTP from the second HFS. However, in the LPP we observe −10% LTD from the second HFS, and in this pathway we also observed only an additional −4% LTD from the second HFS. Therefore, the plasticity effect of the first HFS causes metaplasticity in both pathways and we could not observe the same level of LTP and LTD as the first one.

## 10.3 Summary

The third protocol corresponded to the experimental studies from Section 4.3. In the control group, we examined the metaplasticity effect of the first medial HFS on synaptic plasticity induced during the second medial HFS. In this group noisy spontaneous

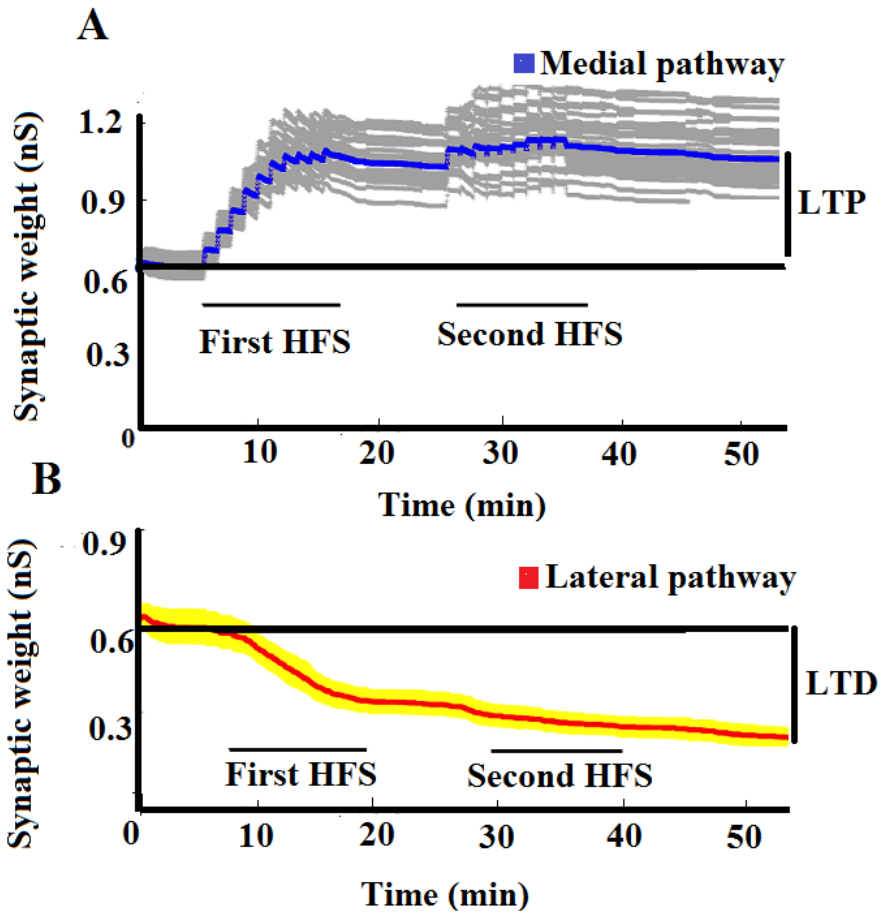


Figure 10.1: Results for two medial HFS with continued spontaneous activity on (control group). (A) Blue curve is the average of medial synaptic weights and grey curves are the individual medial synaptic weights from 150 synapses. During the first HFS, the average of synaptic weights increases up to 45% in the medial pathway, and after applying the second HFS the synaptic weight increases slightly and 9% more of LTP is observed. (B) Red curve shows the average of lateral synaptic weights and yellow curves show the individual lateral weights from 150 synapses. After the first HFS, average synaptic weight depresses in the lateral pathway by about $-27\%$. After the second HFS, average synaptic weight decreases by an additional $-12\%$.

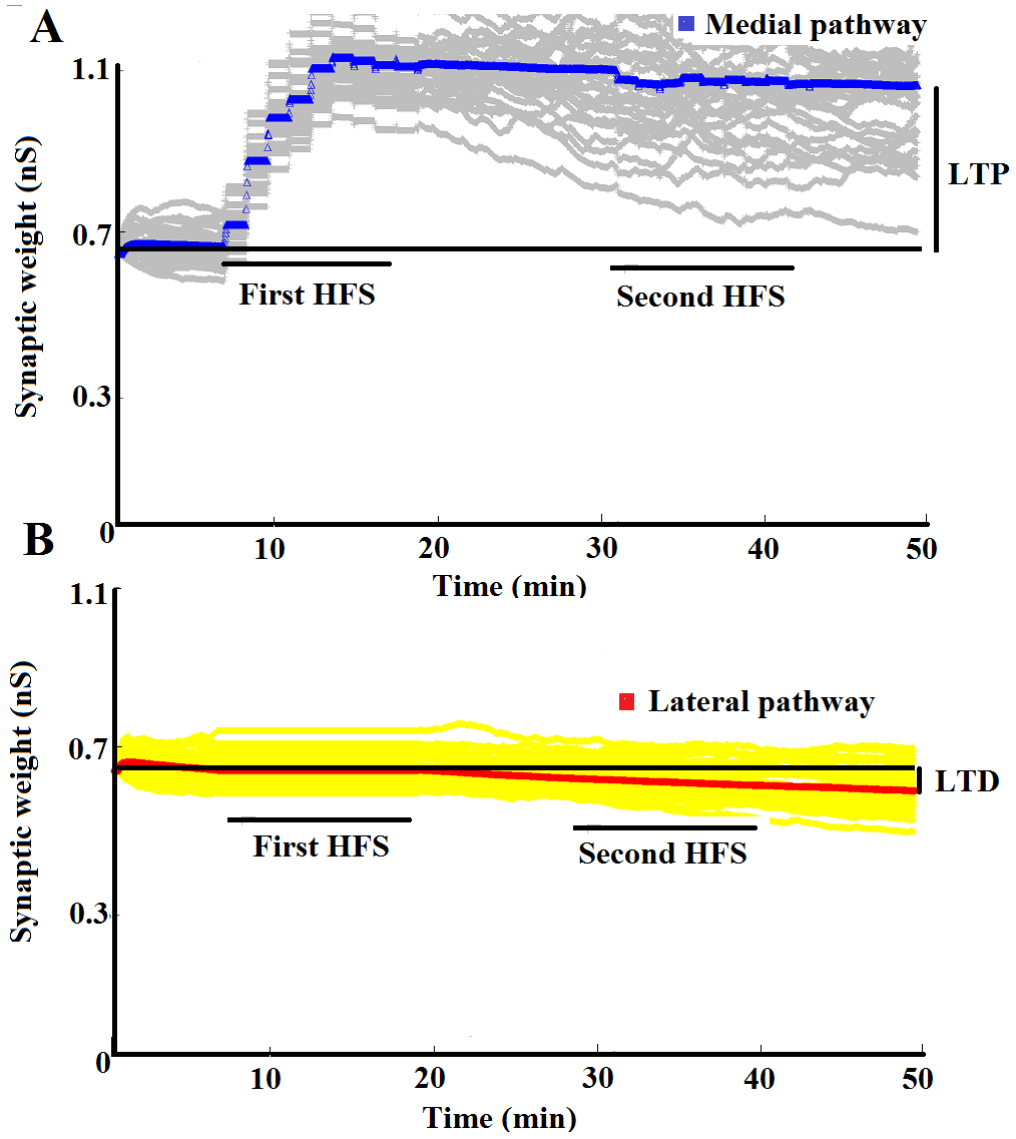


Figure 10.2: Results for two medial HFS and later spontaneous activity off during the first HFS (procaine group). (A) Blue curve is the average of medial synaptic weights and grey curves are the individual medial synaptic weights from 150 synapses. During the first HFS, the average of synaptic weights increases in the medial pathway but little further increase in synaptic weights occurs during the second HFS. (B) Red curve shows the average of lateral synaptic weights and yellow curves show the individual lateral weights from 150 synapses. In the lateral pathway as lateral activity is off during the first HFS no LTD happens, while after the first HFS, as lateral activity switches on with the low frequency hardly any LTD occurs during and after the second HFS.

activity was on during the whole simulation in both pathways. In the procaine group, the metaplasticity impact of the first medial HFS on synaptic plasticity reproduced during the second HFS is examined, when spontaneous activity was off during the first medial HFS. From both protocols we concluded that the metaplasticity effects of the first HFS prevents occurring the same level of synaptic plasticity produced by the second HFS. These results support the hypothesis that the metaplasticity of the first HFS reduces the level of synaptic plasticity caused by the second stimulation.

# Chapter 11

# Fourth protocol

To test our hypothesis that whether or not our plasticity and metaplasticity model could reproduce synaptic plasticity arising from different patterns of HFS, we simulate experimental studies from Section 4.4 with parameters taken from Table 7.6.

## 11.1 Homosynaptic LTP and concurrent heterosynaptic LTD

As can be seen from Figure 11.1 A, in our model, 400 Hz DBS produces 35% LTP in the MPP and simultaneously −26% LTD in the LPP. For 400 Hz TBS, Figure 11.1 B shows 30% LTP in the MPP and −25% simultaneous LTD in LPP. It is interesting that when the number of pulses reduces the amplitude of LTP and LTD reduces as well. In the last pattern of HFS we reduce the frequency from 400 Hz TBS to 100 Hz TBS (Figure 4.7). Surprisingly, we observe 63% LTP and −36% LTD (Figure 11.1 C). Comparing our result with experimental data shows that for 400 Hz DBS in the model and experiments a robust LTP and concurrent LTD were observed. As can be seen from Figure 11.1 B for 400 Hz TBS our result is quite a good match with experiments. However, for 100 Hz TBS surprisingly, we observed the highest LTP and LTD while in experimental data this pattern of HFS produces very low LTP and LTD. We believe the reason this model was not able to reproduce the same result as experiments is because of the short duration of after-hyperpolarisation of 100 Hz TBS compared with the two other patterns of HFS. As can be seen from Figure 11.2A, in 100 TBS pattern of HFS, the time between the end of the first burst and the beginning of the second burst is

only 7 s. In contrast, in 400 DBS pattern of HFS the time difference between the two bursts is 30.3 s. Reduction of the time course between two bursts, reduces the time duration of after hyperpolarisation as well. As we explained in the method section, in our model the average of postsynaptic activity is calculated by equation (5.14). We also explained that in the hyperpolarisation status, voltage is in the lowest level. As far as the voltage reaches the hyperpolarisation status, the next burst comes and voltage has to increase again. Reducing the duration of after-hyperpolarisation increases the amplitude of LTP and concurrent LTD (Sah and Bekkers, 1996). Therefore, with 100 Hz TBS more LTP and LTD than the two other patterns of HFS was observed and this model could not show the same result as the experimental data.

## 11.2 Summary

In the fourth protocol we examined our plasticity and compartmental model with experimental studies from Section 4.4. In this protocol we investigated whether or not our plasticity and metaplasticity model is able to reproduce different patterns of HFS induced weight change. It turns out that our model can reproduce the data to some extent but not entirely. Namely, the model more or less matches the experimental data for 400 Hz DBS and 400 Hz TBS, but gives an incorrect result for 100 Hz TBS. We think the reason for this is not in the meta- and plasticity rules but in the behaviour of the GC model with respect to the dynamics of after-hyperpolarisation. Therefore we concluded that this results support our hypothesis saying these different patterns of HFS can affect the level of homo- and hetero-synaptic plasticity.

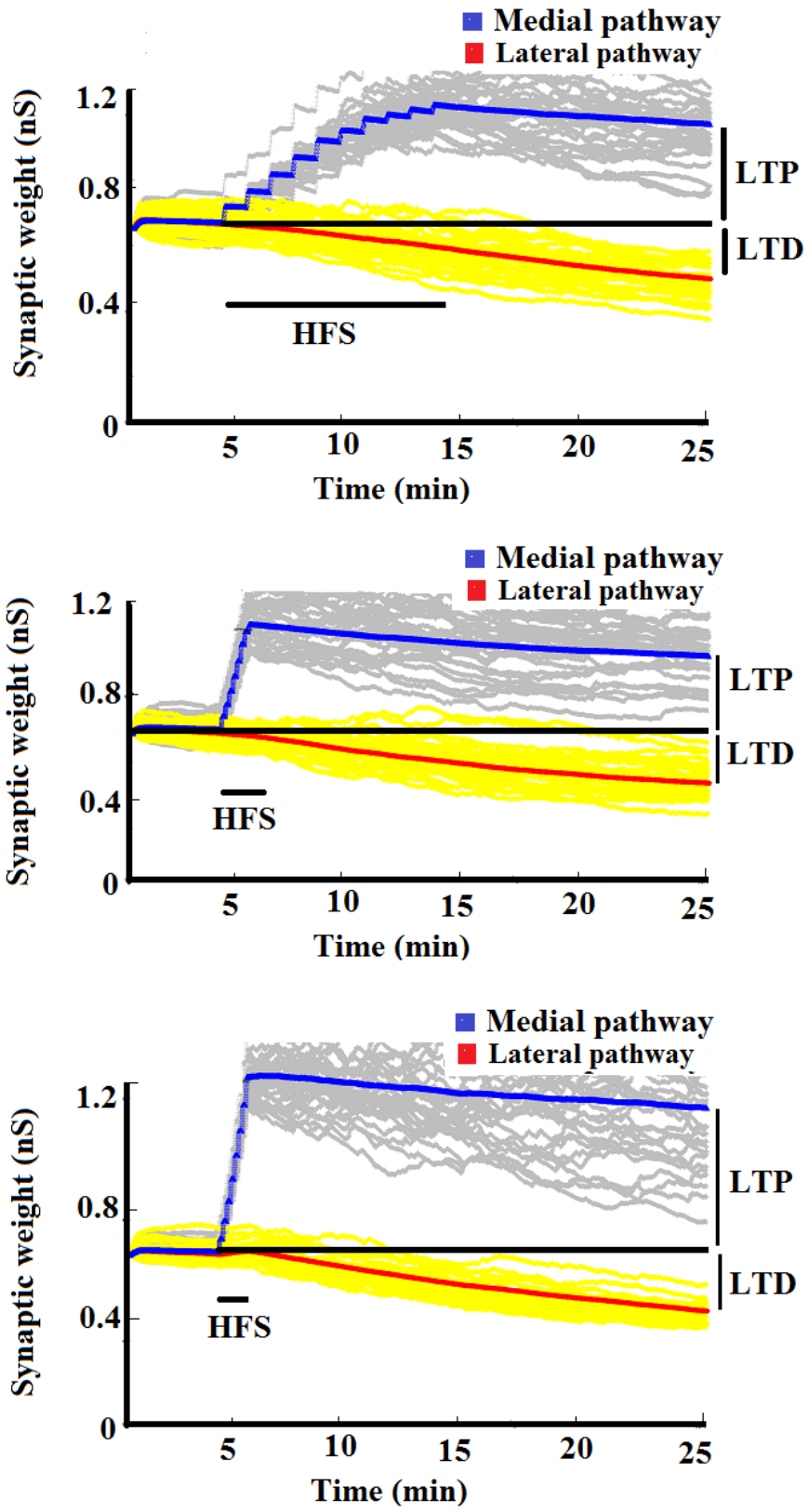


Figure 11.1: (A) 400 Hz delta burst stimulation (DBS) applied to the medial pathway generates 35% LTP and −26% LTD. (B) 400 Hz theta burst stimulation (TBS) generates 30% LTP and concurrent −25% LTD. (C) 100 Hz theta burst stimulation unlike experimental studies generates the highest LTP (63%) and LTD (−36%) .

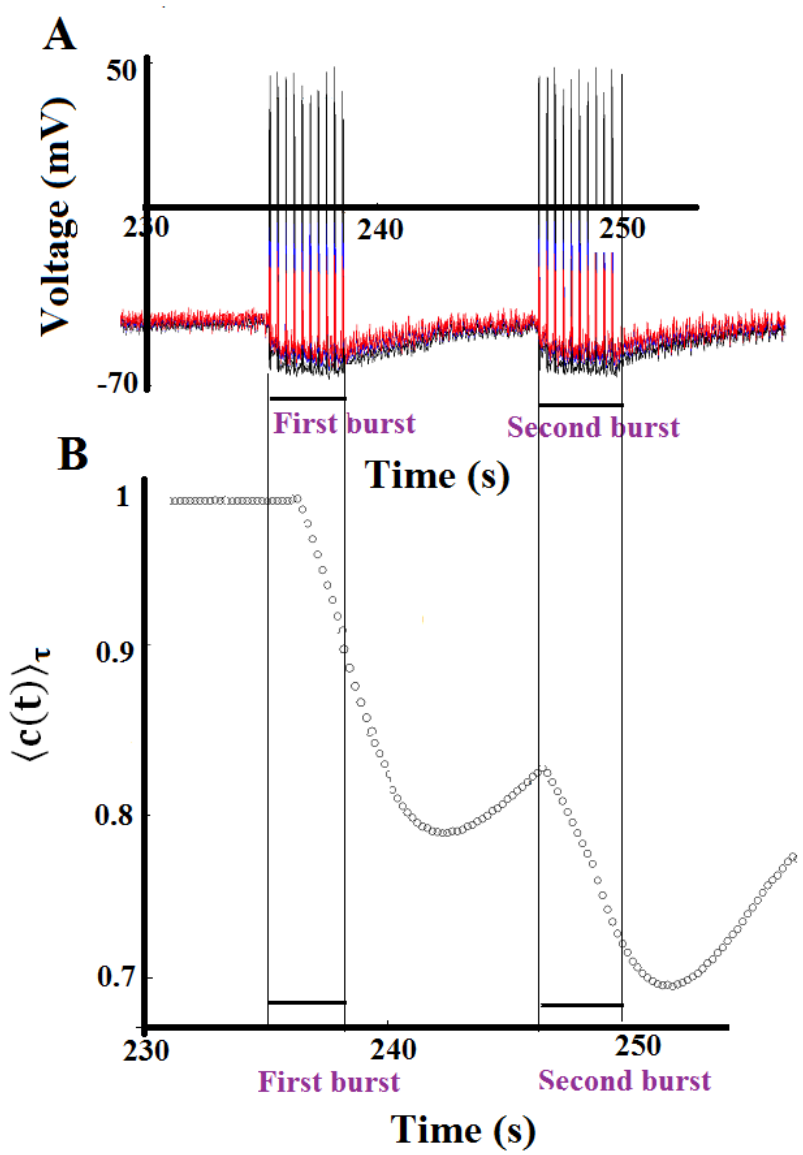


Figure 11.2: (A) Membrane potential of 100 Hz TBS during the first burst and the second burst of HFS. (B) Average postsynaptic activity of 100 Hz TBS during the first and the second burst of HFS, with the exact time as A.

# Chapter 12

# Discussion

The main achievement of this thesis was to show that our model could support the first hypothesis and reproduce homosynaptic LTP and concurrent heterosynaptic LTD in a single granule cell neuron across a range of experimental conditions. To achieve this goal we used computer simulation and employed the nine compartmental model of a granule cell with paired-based nearest neighbours STDP and metaplasticity models accompanied with noisy spontaneous activity. To test our plasticity model we used four different experimental studies from three different papers.

As mentioned in Chapter 3, sliding modification threshold $\theta_m$ from the BCM rule is equal to average of postsynaptic activity. To explain our plasticity model with this popular plasticity rule, we were inspired by Izhikevich and Desai (2003), who found the equations to describe the relationship between nearest-neighbor implementation of STDP and the BCM rule. We also found a relationship between our metaplasticity rule and sliding modification threshold from the BCM rule. Furthermore, using equation 6.4 we could show that the ratio of depression factor and potentiation factor from the Benuskova and Abraham (2007) rule is related to the square of $\langle c(t) \rangle$. Our results also supported the hypothesis that all nine compartments of the GC Santhakumar *et al.* (2005) model are necessary to replicate the synaptic plasticity in our model. The third hypothesis we tested was the necessity of nine ion channels from Aradi and Holmes (1999) to replicate synaptic plasticity. Our results showed that only seven ion channels are necessary to reproduce synaptic plasticity. As explained in Chapter 7 finding the right parameters was very critical for our model. One admirable point about the parameters we have found (see Table 7.6) is that for all simulations we were

able to use this set of parameters and could observe a good consistency with all the experimental studies whereas other simulations require the parameters to be changed for each experiment. The unique aspect of this work is that most plasticity models are examined in the CA1 circuits, however, our work was focused on the DG.

## 12.1 First Protocol

As we explained in the second chapter, real experimental studies in vivo show that homosynaptic LTP can be induced by applying high-frequency stimulation (HFS) to the tetanized pathway and simultaneously heterosynaptic LTD can occur in the neighbouring non-tetanized pathway (Abraham *et al.*, 2001). However, in our simulations from the first protocol we showed that during the first HFS as a result of STDP and metaplasticity rules accompanied with noisy spontaneous activity, the model could reproduce homosynaptic LTP in the MPP and concurrent heterosynaptic LTD in the non-tetanized LPP. This result can be interpreted as follows: when the first HFS is delivered to the medial pathway, the average voltage increases and summation of EPSP events with BAPs (back propagation action potential) produce the strong postsynaptic activity. When the postsynaptic activity follows the presynaptic activity as a result of STDP, synaptic weight increases in this pathway and homosynaptic LTP occurs. Modification also occurs in the lateral pathway; during the medial HFS the membrane potential depolarizes, which increases the average of voltage in the lateral pathway. As the lateral pathway makes synapses at the distal end of dendritic tree and this pathway contains only noisy spontaneous activity, the average voltage in this pathway increases less than for the medial pathway and causes less LTD. Our results also showed a good consistency with the experimental studies. When the second HFS was applied to the lateral pathway, LTP failed to occur in this pathway but we still observed lateral LTD. We believe LTP failed in this pathway due to the lateral pathway being located at the farthest part of the dendrites to the soma. Therefore the given HFS pattern is not enough to reproduce potentiation in the already depressed pathway. In the medial pathway heterosynaptic LTD also failed to occur but we still observed LTP in this pathway. We believe we did not observe LTD in the MPP is due to this pathway being non-tetanized and transition from LTP in the already potentiated pathway to

LTD needs more stimulation. We also observed a good match between our simulation results and experimental studies.

## 12.2 Second protocol

The fourth hypothesis we proposed was the level of noisy spontaneous activity after HFS determines the magnitude of heterosynaptic LTD. Our result from the second protocol when the lateral spontaneous activity was switched off during the first medial HFS showed that the presence of noisy spontaneous activity is critical for heterosynaptic LTD. We also introduced the parameter called LAH (lateral frequency after HFS). When LAH parameter was changing, the magnitude of LTD changed as well. This showed that the level of noisy spontaneous activity after HFS affects the magnitude of heterosynaptic LTD in the lateral pathway. Therefore, from our investigation we concluded that if we want to explain the procaine inhibition with our plasticity model, the frequency of lateral activity after HFS should be less than 4 Hz. The reason of this is because when there is no spontaneous activity, or the level of spontaneous activity is very low, the sliding modification threshold or $\langle c(t) \rangle$ shifts to a low value which reduces the size of LTD. Our simulation results are also in agreement with the experimental studies.

## 12.3 Third protocol

The fifth hypothesis we addressed was the metaplasticity of the first stimulation reduces the level of synaptic plasticity caused by the second stimulation. We examined our plasticity model with two procaine and control groups. Our result from the control group showed although synaptic weight increased in the medial pathway, the magnitude of LTP caused by the second HFS was not the same magnitude caused by the first HFS. Therefore, we concluded previous plasticity produced by the first HFS caused homosynaptic metaplasticity in the medial pathway during the second HFS. When the second HFS was applied to the medial pathway, synaptic weight was depressed in the neighbouring lateral pathway, but the same level of heterosynaptic LTD was not observed. Therefore, we concluded that synaptic plasticity from the first HFS caused

heterosynaptic metaplasticity in the lateral pathway during the second HFS.

In the procaine group, spontaneous activity was off during the first HFS, while continuing to be present during the second HFS. Similar to the control group, the level of synaptic weight increased in the medial pathway, however, the same amount of LTP as was not observed after the second HFS. Therefore, we concluded that synaptic plasticity from the first HFS caused homosynaptic metaplasticity in the medial pathway during the second HFS. In the lateral pathway as a result of synaptic plasticity produced from the first HFS, and the reduced level of spontaneous activity after the first HFS, the magnitude of LTD produced during the second HFS was less than the magnitude of LTD produced by the first HFS. Therefore, we observed heterosynaptic metaplasticity in the lateral pathways from the second HFS. Results from our simulation showed good consistency with the experimental studies.

## 12.4 Fourth protocol

In this protocol we examined our plasticity model with different patterns of HFS. When the number of pulses from 400 Hz DBS reduced to 400 Hz TBS, the amplitude of LTP and LTD reduced as well. Comparing our result with experimental data showed that for 400 Hz DBS in model and experiments, a robust LTP and concurrent LTD were observed. However, reducing the frequency from 400 Hz TBS to 100 Hz TBS surprisingly showed the highest LTP and LTD, while in the experimental data this pattern of HFS produced very low LTP and LTD. We think the reason our model could not reproduce the same result as experimental data is because the duration of after-hyperpolarisation in 100 Hz TBS is shorter than two other patterns of HFS. The time difference between the first burst and the second burst in 100 Hz DBS was four times shorter than the 400 Hz DBS pattern. This showed the membrane potential of the 100 Hz TBS required more time between burst than its provided. As the time course between the two bursts reduced, the time duration of after hyperpolarisation also reduced. As we mentioned in the method section, in our model the average of postsynaptic activity was calculated by the average of voltage. We also illustrated that in the hyperpolarization status the average of voltage was at the lowest level. As soon as the voltage reaches hyperpolarization status, the next burst comes and voltage

has to increase again. Reducing the duration of after-hyperpolarisation increased the amplitude of LTP and concurrent LTD (Sah and Bekkers, 1996). Therefore, with 100 Hz TBS more LTP and LTD than the two other patterns of HFS was observed and this model could not show the same result as the experimental data. These results support the hypothesis that different patterns of HFS affect on the level of homo- and heterosynaptic plasticity.

We also are able to suggest some experimentally testable predictions from our model as follows:

1. Without the PD compartment, the GC neuron is silent. LTP and LTD also can not be replicated as in experimental studies without GCLD compartment.

2. Blocking the sodium channels in all nine compartments interrupts the heterosynaptic LTD and also reduces the amount of homosynaptic LTP.

3. Blocking the three potassium channels in the all compartments causes unstable LTP and LTD.

4. Blocking the three calcium channels in the all compartments also causes unstable LTD and no match with the experimental studies for LTP.

5. With blocking the calcium-dependent potassium channels, LTP and LTD still can be replicated the same as experimental studies.

6. To observe the synaptic plasticity, one of $P$ or $D$ factors from the plasticity model needed to be non-constant.

7. To add metaplasticity to the model, the value of $\tau_p$ (time constant for potentiation factor) should be bigger than 18 ms and the value of $\tau_d$ (time constant for depression factor) should be less than 130 ms.

8. If the frequency of lateral spontaneous activity after the medial HFS is less than 4 Hz, almost non heterosynaptic LTD is produced.

9. Metaplasticity from the first stimulation fails the same amount of synaptic plasticity produced by the second stimulation.

10. Different patterns of HFS produce different levels of homo- and hetero-synaptic plasticity.

## 12.5 Comparing our model with the other models and data

Although the Hebbian rule as a first plasticity model could explain a variety of experimental studies, this model is not able to explain heterosynaptic plasticity phenomena. However, our plasticity model could reproduce homosynaptic LTP in the one pathway and heterosynaptic LTD in the neighbouring pathway.

The BCM rule as a fundamental theory of synaptic plasticity explains many experimental studies quite well and the sliding modification threshold $\theta_m$ from the BCM rule can explain our metaplasticity rule.

Investigations from Wei and Koulakov show that combining the STDP rule (with both LTP and LTD windows) with neural noise in the network of neurons extend the life-time of the long-term memory. However, the STDP rule with only the LTP window combined with neural noise cannot produce stable memory (Wei and Koulakov, 2014). In our model, just as in the Wei and Koulakov model, neural noise is generated randomly. As can be seen from equation (3.53), in the Wei and Koulakov model, all neurons of the network receive only one range of inputs but all of them receive noise. However, our model granule cell has two different ranges of inputs: spontaneous activity and HFS. In our model only spontaneous activity is noisy, while all patterns of HFS are regular without any noise. As we mentioned in Chapter 3, applying HFS accompanied with noisy spontaneous activity is needed for homosynaptic LTP in one pathway and heterosynaptic LTD in the non-tetanized neighbouring pathway (Abraham *et al.*, 2001). However, Wei and Koulakov did not specify on which synapses LTP occurs and on which of them LTD occurs. As we simulate a single neuron, more details about the intrinsic feature of the spikes, such as after-hyperpolarization status, are needed, therefore we believe our model plasticity with two different inputs such as (noisy spontaneous activity and applied regular HFS) is more realistic. In contrast, Wei and Koulakov simulate a network of neurons and therefore they do not need to be

specific.

In the Benuskova and Abraham (2007) metaplasticity rule, the potentiation factor $P$ and depression factor $D$ from plasticity rules are not constant, since they both depend on average postsynaptic activity, $\langle c(t) \rangle$. Our metaplasticity rule, as in the Benuskova and Abraham model, also depends on average postsynaptic activity. However, motivated by the Clopath *et al.* (2010) metaplasticity model, either potentiation or depression factor being dependent on average postsynaptic plasticity is enough to reproduce homosynaptic LTP in one pathway and heterosynaptic LTD in the neighbouring pathway. Furthermore, according to equation (3.57), the way Benuskova and Abraham (2007) calculated the pre- and post-synaptic spikes for the pair-based STDP model is based on all-or-nothing events. However, we believe it is more realistic to calculate the EPSP events based on the average of voltage rather than treating the spike as an all-or-nothing event.

In the Froemke metaplasticity rule, potentiation factor $A_+$ and depression factor $A_-$ are both constant; however, when both these factors were constant metaplasticity was not produced, therefore at least one of factors should be allowed to vary.

The way that Pfister and Gerstner (2006) calculate the pairing spikes for their STDP model is based on the triplet-based spike model which we believe be more accurate than to all-to-all interaction due to the agreement of the former experimental studies. However, in their metaplasticity model, potentiation $A_3^+$ and depression $A_3^-$ factors are also constant and not dependent on the postsynaptic spikes.

In the metaplasticity model recommended by Clopath *et al.* (2010), the potentiation factor is a fixed value and the depression factor is introduced as a function of average of postsynaptic activity. Therefore, as in our model, only one factor (here the depression factor) depends on the average of voltage. Although they specifically considered depression $A_-$ as a metaplasticity factor, as we mentioned above either potentiation or depression factors can be dependent on average activity. The way they calculated postsynaptic spikes is also similar to our model which is based on average voltage; they also believe that postsynaptic spikes should be represented by voltage rather than an all-or-nothing event.

The Zhenq and Schwabe 2014 model as in our model, has two inputs: the Poisson noisy inputs and synchronous spikes as a signal. In their model, noisy inputs are

correlated synchronously with the signals; however, because of our compartmental model, each synapse receives spikes at different times from the other synapses. This is a more realistic model of spontaneous activity. The dSTDP model that Zhenq and Schwabe have used is AP-STDP which is similar to our STDP model dependence on average voltage. The neuron model Zheng and Schwabe (2014) have chosen is a simple one-compartment model and they stated they can use this model for both a single neuron and a network of neurons. We think to calculate the synaptic plasticity of a network of neurons it is fine to use a simplified model but as explained in Chapter 3 to see the intrinsic property of a single neuron it is better to use a more realistic model with more ion channels and more compartments.

Jedlicka *et al.* (2015) investigated the effects of different patterns of HFS on homosynaptic LTP and heterosynaptic LTD in a single granule cell neuron. Their model inputs, as for our model, contain noisy spontaneous activity but the level of noise in their model is different. In their model both medial and lateral pathways have the same frequency of noisy spontaneous activity at 8 Hz. However, we believe it is more realistic if both pathways have a different frequency of spontaneous activity. Therefore, in our model the frequency of spontaneous activity in the medial pathway is 2.9 Hz and in lateral pathway is 6.8 Hz, is in agreement with experimental studies by Gloveli *et al.* (1997). Jedlicka *et al.* (2015) also employed the same neuron model as us with nine compartments. They used nine ion channels to reproduce synaptic plasticity but we showed our model only needs seven ion channels. The Jedlicka *et al.* (2015) metaplasticity model is based on Benuskova and Abraham (2007) which means both $P$ and $D$ factors depend on average postsynaptic activity. We extended their model and as explained above we believe there is no need for both $P$ and $D$ factors to be dependent on $\langle c(t) \rangle$. To calculate pre and postsynaptic spikes for the STDP model they used equation 3.57, which means they also treat spikes as all-or-nothing events; however, we believe that postsynaptic spikes should be counted as an average of voltage as this is likely to be a more realistic driver of plasticity events, since both LTP and LTD are driven by the voltage-dependent properties of the NMDA receptor.

## 12.6 Summary

In this chapter we expressed the main purpose and contribution of our study. We summarized our results from each protocol with a brief interpretation and explanation. At the end we compared and contrasted our model with other published works and distinguished some differences and similarities between our model and others.

# Chapter 13

# Conclusion and further works

As discussed in the third chapter, homosynaptic plasticity by itself increases the amount of synaptic weight greatly, while heterosynaptic plasticity does not allow synaptic weight to increase excessively and keeps overall input to a cell in balance. Therefore, to regulate synaptic weights, both homosynaptic and heterosynaptic plasticity need to be induced. We also mentioned in the fifth chapter that in the granule cell neuron synaptic plasticity occurs homo- and heterosynaptically. To examine whether the STDP and metaplasticity models introduced in this thesis could replicate synaptic plasticity in the single granule cell, we used computer simulation. Our work showed that by employing a nine-compartment model of a granule cell with pair-based nearest neighbour STDP and metaplasticity rules accompanied by noisy spontaneous activity, both homosynaptic LTP and heterosynaptic LTD could be replicated. It was also significant to realize that in our model the level of noisy spontaneous activity determines the level of heterosynaptic LTD in the granule cell. Our model also could explain the effect of metaplasticity from the first stimulation on synaptic plasticity during the second stimulation quite well. In this study we examined the effect of only seven parameters on synaptic plasticity and neglected other parameters that might affect this phenomenon. This limitation was due to the large amount of time it took to find the right value for each parameter. For the fourth protocol, our model could not reproduce the exact experimental result when 100 Hz TBS was applied to the granule cell. We believe this was due to our model calculating the effect of spikes as an average of voltage. In the 100 Hz TBS pattern, the time duration between the two bursts was quite short. Reducing the time between bursts reduces the time duration of after-hyperpolarization.

During hyperpolarisation, the voltage is at its lowest level. Reducing the duration of after-hyperpolarisation increases the amplitude of LTP and concurrent LTD (Sah and Bekkers, 1996). Therefore, with 100 Hz TBS more LTP and LTD was observed in the experiments but we could not reproduce this same result with our model.

Our granule cell model has two dendrites and because the real granule cell has many dendritic branches it is more realistic to simulate our plasticity model with more than two. As we mentioned in the method Chapter this model of granule cell does not have an axon, so it will be testable if an axon added to the model granule cell changes the results in any way (Aradi and Holmes, 1999). Therefore, in addition to postsynaptic action potential and EPSP events, back propagation of action potential from the axon will be included to the spikes as well. In this work we only considered excitatory synapses, but as the granule cell contains both excitatory and inhibitory synapses, in further works it would be worthwhile to involve the inhibitory synapses to the model also. This model only examined the dentate granule cell; in extension work it would be interesting to test it with other cells in the hippocampus such as CA1, CA2, CA3 pyramidal cells if in vivo LTP data are available. We have investigated our plasticity model with three specific experiments of freely moving or anesthetized rats; however, this model can be tested against other experiments with different animals such as mice which are commonly studied. Our STDP model is based on pair-based nearest neighbours, but this plasticity model could be examined with the triplet-based spike model (Pfister and Gerstner, 2006). The triplet-based spike model also considers the effect of the third spike on the overall of weight change and experimental studies from Wang *et al.* (2005) shows that synaptic potentiation and synaptic depression can be activated simultaneously by this type of spike interaction.

As we mentioned in the method Chapter, Zheng *et al.* (2014) included AP duration directly into the STDP window, and they called their new model dSTDP. As they emphasized AP is an important feature of the STDP model and has a significant role on synaptic plasticity, it would be worthwhile to examine our plasticity model with this new modification to the STDP. To simulate a single neuron, use of a more complex neuron model like our compartmental model with ion channels is recommended. For the network of neurons, usually simple neuron models can be used. However, Hayashi and Nonaka1 2011 used a compartmental model for a small network that contained

both feedforward and feedback inhibitory local circuits (Hayashi and Nonaka, 2011) but they did not add metaplasticity to their model. It would be interesting to test our metaplasticity rule with their small network. We believe our findings could facilitate further research on synaptic plasticity models and the mechanisms of learning and memory phenomena. Synaptic plasticity is a very extensive field and there remain many questions which need to be answered regarding the computational and plasticity properties of neurons in different areas of the brain.

# References


Abraham, W. and Goddard, G. V. (1983). Asymmetric relationships between homosynaptic long-term potentiation and heterosynaptic long-term depression.

Abraham, W. C. (2008). Metaplasticity: tuning synapses and networks for plasticity. *Nature Reviews Neuroscience*, *9*(5), 387–387.

Abraham, W. C., Christie, B. R., Logan, B., Lawlor, P., and Dragunow, M. (1994). Immediate early gene expression associated with the persistence of heterosynaptic long-term depression in the hippocampus. *Proceedings of the National Academy of Sciences*, *91*(21), 10049–10053.

Abraham, W. C. and Huggett, A. (1997). Repeated High?Frequency Stimulation in Rat Hippocampal Slices. *Hippocampus*, *7*, 137–145.

Abraham, W. C., Logan, B., Greenwood, J. M., and Dragunow, M. (2002). Induction and experience-dependent consolidation of stable long-term potentiation lasting months in the hippocampus. *The Journal of neuroscience*, *22*(21), 9626–9634.

Abraham, W. C., Logan, B., Wolff, A., and Benuskova, L. (2007). ?Heterosynaptic? LTD in the dentate gyrus of anesthetized rat requires homosynaptic activity. *Journal of neurophysiology*, *98*(2), 1048–1051.

Abraham, W. C., Mason-Parker, S. E., Bear, M. F., Webb, S., and Tate, W. P. (2001). Heterosynaptic metaplasticity in the hippocampus in vivo: a BCM-like modifiable threshold for LTP. *Proceedings of the National Academy of Sciences*, *98*(19), 10924–10929.

Acton, Q. (2012). *Advances in Peripheral Nervous System Research and Application: 2011 Edition: ScholarlyPaper*. ScholarlyEditions.

Andersen, P., Morris, R., Amaral, D., Bliss, T., and O'Keefe, J. (2006). *The hippocampus book*. Oxford University Press.

Aradi, I. and Holmes, W. R. (1999). Role of multiple calcium and calcium-dependent conductances in regulation of hippocampal dentate granule cell excitability. *Journal of computational neuroscience*, *6*(3), 215–235.

Barker, J. M., Boonstra, R., and Wojtowicz, J. M. (2011). From pattern to purpose: how comparative studies contribute to understanding the function of adult neurogenesis. *European Journal of Neuroscience*, *34*(6), 963–977.

Bastrikova, N., Gardner, G. A., Reece, J. M., Jeromin, A., and Dudek, S. M. (2008). Synapse elimination accompanies functional plasticity in hippocampal neurons. *Proceedings of the National Academy of Sciences*, *105*(8), 3123–3127.

Bear, M. F., Connors, B. W., and Paradiso, M. A. (2007). *Neuroscience*, Volume 2. Lippincott Williams & Wilkins.

Benuskova, L. and Abraham, W. C. (2007). STDP rule endowed with the BCM sliding threshold accounts for hippocampal heterosynaptic plasticity. *Journal of computational neuroscience*, *22*(2), 129–133.

Bienenstock, E. L., Cooper, L. N., and Munro, P. W. (1982). Theory for the development of neuron selectivity: orientation specificity and binocular interaction in visual cortex. *The Journal of Neuroscience*, *2*(1), 32–48.

Bliss, T. V. and Cooke, S. F. (2011). Long-term potentiation and long-term depression: a clinical perspective. *Clinics*, *66*, 3–17.

Bliss, T. V. and Lømo, T. (1973). Long-lasting potentiation of synaptic transmission in the dentate area of the anaesthetized rabbit following stimulation of the perforant path. *The Journal of physiology*, *232*(2), 331–356.

Blundon, J. A. and Zakharenko, S. S. (2008). Dissecting the components of long-term potentiation. *The Neuroscientist*, *14*(6), 598–608.

Bowden, J. B., Abraham, W. C., and Harris, K. M. (2012). Differential effects of strain, circadian cycle, and stimulation pattern on LTP and concurrent LTD in the dentate gyrus of freely moving rats. *Hippocampus*, *22*(6), 1363–1370.

Brodal, P. (2004). *The central nervous system: structure and function*. Oxford University Press.

Bush, D., Philippides, A., Husbands, P., and O'Shea, M. (2010). Reconciling the STDP and BCM models of synaptic plasticity in a spiking recurrent neural network. *Neural computation*, *22*(8), 2059–2085.

Caporale, N. and Dan, Y. (2008). Spike timing–dependent plasticity: a Hebbian learning rule. *Annu. Rev. Neurosci.*, *31*, 25–46.

Chistiakova, M., Bannon, N. M., Bazhenov, M., and Volgushev, M. (2014). Heterosynaptic Plasticity Multiple Mechanisms and Multiple Roles. *The Neuroscientist*, 1073858414529829.

Christie, B. R. and Abraham, W. C. (1994). Differential regulation of paired-pulse plasticity following LTP in the dentate gyrus. *Neuroreport*, *5*(4), 385–388.

Clopath, C., Büsing, L., Vasilaki, E., and Gerstner, W. (2010). Connectivity reflects coding: a model of voltage-based STDP with homeostasis. *Nature neuroscience*, *13*(3), 344–352.

Cohen, S. D. and Hindmarsh, A. C. (1994). CVODE user guide. Technical report, Technical Report UCRL-MA-118618, LLNL.

Collingridge, G. L., Peineau, S., Howland, J. G., and Wang, Y. T. (2010). Long-term depression in the CNS. *Nature Reviews Neuroscience*, *11*(7), 459–473.

Coon, D. and Mitterer, J. (2008). *Introduction to psychology: Gateways to mind and behavior*. Cengage Learning.

Cooper, L. N., Intrator, N., Blais, B. S., and Shouval, H. Z. (2004). *Theory of cortical plasticity*, Volume 150. World Scientific Singapore.

D?Angelo, E., Solinas, S., Garrido, J., Casellato, C., Pedrocchi, A., Mapelli, J., Gandolfi, D., and Prestori, F. (2013). Realistic modeling of neurons and networks: towards brain simulation. *Functional neurology*, *28*(3), 153.

Davis, K. L. *et al.* (2002). *Neuropsychopharmacology: the fifth generation of progress: an official publication of the American College of Neuropsychopharmacology.* Lippincott Williams & Wilkins.

Dempster, F. N. (1981). Memory span: Sources of individual and developmental differences. *Psychological Bulletin*, *89*(1), 63.

Deng, W., Aimone, J. B., and Gage, F. H. (2010). New neurons and new memories: how does adult hippocampal neurogenesis affect learning and memory? *Nature Reviews Neuroscience*, *11*(5), 339–350.

Deshmukh, S. S., Yoganarasimha, D., Voicu, H., and Knierim, J. J. (2010). Theta modulation in the medial and the lateral entorhinal cortices. *Journal of neurophysiology*, *104*(2), 994–1006.

Desmond, N. L. and Levy, W. B. (1984). Dendritic caliber and the 3/2 power relationship of dentate granule cells. *Journal of Comparative Neurology*, *227*(4), 589–596.

Dingledine, R., Borges, K., Bowie, D., and Traynelis, S. F. (1999). The glutamate receptor ion channels. *Pharmacological reviews*, *51*(1), 7–62.

Douglas, R. M. and Goddard, G. V. (1975). Long-term potentiation of the perforant path-granule cell synapse in the rat hippocampus. *Brain research*, *86*(2), 205–215.

Doyère, V., Srebro, B., and Laroche, S. (1997). Heterosynaptic LTD and depotentiation in the medial perforant path of the dentate gyrus in the freely moving rat. *Journal of neurophysiology*, *77*(2), 571–578.

Drew, L. J., Fusi, S., and Hen, R. (2013). Adult neurogenesis in the mammalian hippocampus: Why the dentate gyrus? *Learning & memory*, *20*(12), 710–729.

Ermentrout, G. B. and Terman, D. H. (2010). *Mathematical foundations of neuroscience*, Volume 35. Springer Science & Business Media.

Fellous, J.-M., Rudolph, M., Destexhe, A., and Sejnowski, T. J. (2003). Synaptic background noise controls the input/output characteristics of single cells in an in vitro model of in vivo activity. *Neuroscience*, *122*(3), 811–829.

Fioravante, D. and Regehr, W. G. (2011). Short-term forms of presynaptic plasticity. *Current opinion in neurobiology*, *21*(2), 269–274.

Foy, M. (2001). Long-term Depression (Hippocampus).

Froemke, R. C., Debanne, D., and Bi, G.-Q. (2010). Temporal modulation of spike-timing-dependent plasticity. *Spike-timing dependent plasticity*, 152.

Froemke, R. C., Letzkus, J. J., Kampa, B. M., Hang, G. B., and Stuart, G. J. (2010). Dendritic synapse location and neocortical spike-timing-dependent plasticity. *Spike-timing dependent plasticity*, 118.

Gerstner, W. (2000). Population dynamics of spiking neurons: fast transients, asynchronous states, and locking. *Neural computation*, *12*(1), 43–89.

Gerstner, W., Kempter, R., van Hemmen, J. L., and Wagner, H. (1996). A neuronal learning rule for sub-millisecond temporal coding. *Nature*, *383*(LCN-ARTICLE-1996-002), 76–78.

Gloveli, T., Schmitz, D., Empson, R. M., and Heinemann, U. (1997). Frequency-dependent information flow from the entorhinal cortex to the hippocampus. *Journal of neurophysiology*, *78*(6), 3444–3449.

Hall, J. E. (2010). *Guyton and Hall Textbook of Medical Physiology: Enhanced E-book*. Elsevier Health Sciences.

Hananeia, N. and Benuskova, L. (2016). Computational simulation of dentate gyrus granule cell?The role of metaplasticity. *Neurocomputing*, *175*, 300–309.

Hayashi, H. and Nonaka, Y. (2011). Cooperation and competition between lateral and medial perforant path synapses in the dentate gyrus. *Neural Networks*, *24*(3), 233–246.

Herz, A. V., Gollisch, T., Machens, C. K., and Jaeger, D. (2006). Modeling single-neuron dynamics and computations: a balance of detail and abstraction. *science*, *314*(5796), 80–85.

Hines, M. and Carnevale, N. T. (2001). NEURON: a tool for neuroscientists. *The Neuroscientist*, *7*(2), 123–135.

Hines, M. L. and Carnevale, N. T. (1997). The NEURON simulation environment. *Neural computation*, *9*(6), 1179–1209.

Huttenlocher, J. and Burke, D. (1976). Why does memory span increase with age? *Cognitive Psychology*, *8*(1), 1–31.

Izhikevich, E. M. (2004). Which model to use for cortical spiking neurons? *IEEE transactions on neural networks*, *15*(5), 1063–1070.

Izhikevich, E. M. and Desai, N. S. (2003). Relating stdp to bcm. *Neural computation*, *15*(7), 1511–1523.

Jedlicka, P. (2002). Synaptic plasticity, metaplasticity and BCM theory. *Bratislavské lekárske listy*, *103*(4/5), 137–143.

Jedlicka, P., Benuskova, L., and Abraham, W. C. (2015). A Voltage-Based STDP Rule Combined with Fast BCM-Like Metaplasticity Accounts for LTP and Concurrent ?Heterosynaptic? LTD in the Dentate Gyrus In Vivo. *PLoS Comput Biol*, *11*(11), e1004588.

Kail, R. and Salthouse, T. A. (1994). Processing speed as a mental capacity. *Acta psychologica*, *86*(2), 199–225.

Kernighan, B. and Pike, R. (1984). Appendix 2: Hoc manual. *The UNIX programming environment*, 329–333.

King, L. A. (2008). *Study Guide to Accampany the Science of Psychology: An Appreciative View*. McGraw-Hill Higher Education.

Krueppel, R., Remy, S., and Beck, H. (2011). Dendritic integration in hippocampal dentate granule cells. *Neuron*, *71*(3), 512–528.

Kullmann, D. M. and Lamsa, K. P. (2007). Long-term synaptic plasticity in hippocampal interneurons. *Nature Reviews Neuroscience*, *8*(9), 687–699.

Larson, J., Wong, D., and Lynch, G. (1986). Patterned stimulation at the theta frequency is optimal for the induction of hippocampal long-term potentiation. *Brain research*, *368*(2), 347–350.

Levy, W. and Steward, O. (1983). Temporal contiguity requirements for long-term associative potentiation/depression in the hippocampus. *Neuroscience*, *8*(4), 791–797.

Levy, W. B. and Steward, O. (1979). Synapses as associative memory elements in the hippocampal formation. *Brain research*, *175*(2), 233–245.

Lin, Y.-W., Yang, H.-W., Wang, H.-J., Gong, C.-L., Chiu, T.-H., and Min, M.-Y. (2006). Spike-timing-dependent plasticity at resting and conditioned lateral perforant path synapses on granule cells in the dentate gyrus: different roles of N-methyl-d-aspartate and group I metabotropic glutamate receptors. *European Journal of Neuroscience*, *23*(9), 2362–2374.

Lisman, J., Schulman, H., and Cline, H. (2002). The molecular basis of CaMKII function in synaptic and behavioural memory. *Nature Reviews Neuroscience*, *3*(3), 175–190.

Lisman, J. and Spruston, N. (2005). Postsynaptic depolarization requirements for LTP and LTD: a critique of spike timing-dependent plasticity. *Nature neuroscience*, *8*(7), 839–841.

Lüscher, C. and Malenka, R. C. (2012). NMDA receptor-dependent long-term potentiation and long-term depression (LTP/LTD). *Cold Spring Harbor perspectives in biology*, *4*(6), a005710.

Malenka, R. C. (1994). Synaptic plasticity in the hippocampus: LTP and LTD. *Cell*, *78*(4), 535–538.

Markram, H., Lübke, J., Frotscher, M., and Sakmann, B. (1997). Regulation of synaptic efficacy by coincidence of postsynaptic APs and EPSPs. *Science*, *275*(5297), 213–215.

Mehta, M. R. (2004). Cooperative LTP can map memory sequences on dendritic branches. *Trends in neurosciences*, *27*(2), 69–72.

Menon, V. (2012). *Resting state brain activity: Implications for systems neuroscience*. Frontiers E-books.

Miller, G. A. (1956). The magical number seven, plus or minus two: some limits on our capacity for processing information. *Psychological review*, *63*(2), 81.

Morrison, D. (2012). Metaplasticity: A new frontier in the neural representation of memory. *University of British Columbia's Undergraduate Journal of Psychology*, *1*.

Moujahid, A., d?Anjou, A., Torrealdea, F., and Torrealdea, F. (2011). Energy and information in Hodgkin-Huxley neurons. *Physical Review E*, *83*(3), 031912.

Nakashiba, T., Cushman, J. D., Pelkey, K. A., Renaudineau, S., Buhl, D. L., McHugh, T. J., Barrera, V. R., Chittajallu, R., Iwamoto, K. S., McBain, C. J., *et al.* (2012). Young dentate granule cells mediate pattern separation, whereas old granule cells facilitate pattern completion. *Cell*, *149*(1), 188–201.

Noback, C. R., Strominger, N. L., Demarest, R. J., and Ruggiero, D. A. (2005). *The human nervous system: structure and function*. Number 744. Springer.

Patten, A. R., Yau, S. Y., Fontaine, C. J., Meconi, A., Wortman, R. C., and Christie, B. R. (2015). The benefits of exercise on structural and functional plasticity in the rodent hippocampus of different disease models. *Brain Plasticity*, *1*(1), 97–127.

Paugam-Moisy, H. and Bohte, S. (2012). Computing with spiking neuron networks. In *Handbook of natural computing*, 335–376. Springer.

Pfister, J.-P. and Gerstner, W. (2006). Triplets of spikes in a model of spike timing-dependent plasticity. *Journal of Neuroscience*, *26*(38), 9673–9682.

Raymond, C. R. and Redman, S. J. (2006). Spatial segregation of neuronal calcium signals encodes different forms of LTP in rat hippocampus. *The Journal of physiology*, *570*(1), 97–111.

Saar, D., Grossman, Y., and Barkai, E. (1998). Reduced after-hyperpolarization in rat piriform cortex pyramidal neurons is associated with increased learning capability during operant conditioning. *European Journal of Neuroscience*, *10*(4), 1518–1523.

Sah, P. and Bekkers, J. M. (1996). Apical dendritic location of slow afterhyperpolarization current in hippocampal pyramidal neurons: implications for the integration of long-term potentiation. *The Journal of neuroscience*, *16*(15), 4537–4542.

Santhakumar, V., Aradi, I., and Soltesz, I. (2005). Role of mossy fiber sprouting and mossy cell loss in hyperexcitability: a network model of the dentate gyrus incorporating cell types and axonal topography. *Journal of neurophysiology*, *93*(1), 437–453.

Scharfman, H. E. (2011). *The Dentate Gyrus: A Comprehensive Guide to Structure, Function, and Clinical Implications: A Comprehensive Guide to Structure, Function, and Clinical Implications*, Volume 163. Elsevier.

Schwartz, B. L. (2010). *Memory: foundations and applications*. Sage.

Seel, N. M. (2012). Encyclopedia of the Sciences of Learning.

Sjöström, J. and Gerstner, W. (2011). Spike-timing dependent plasticity. *Frontiers in Synaptic Neuroscience*, 35–44.

Sjöström, P. J., Rancz, E. A., Roth, A., and Häusser, M. (2008). Dendritic excitability and synaptic plasticity. *Physiological reviews*, *88*(2), 769–840.

Snyder, J., Kee, N., and Wojtowicz, J. (2001). Effects of adult neurogenesis on synaptic plasticity in the rat dentate gyrus. *Journal of neurophysiology*, *85*(6), 2423–2431.

Sousa, D. A. (2011). *How the brain learns*. Corwin Press.

Stahl, S. M. (2013). *Stahl's essential psychopharmacology: neuroscientific basis and practical applications*. Cambridge university press.

Staubli, U. and Lynch, G. (1987). Stable hippocampal long-term potentiation elicited by ?theta?pattern stimulation. *Brain research*, *435*(1), 227–234.

Sterratt, D., Graham, B., Gillies, A., and Willshaw, D. (2011). *Principles of computational modelling in neuroscience*. Cambridge University Press.

Tejada, J. and Roque, A. C. (2014). Computational models of dentate gyrus with epilepsy-induced morphological alterations in granule cells. *Epilepsy & Behavior*.

Ulinski, P. S. (1999). Neural mechanisms underlying the analysis of moving visual stimuli. In *Models of Cortical Circuits*, 283–399. Springer.

Van Rossum, M. C., Bi, G. Q., and Turrigiano, G. G. (2000). Stable Hebbian learning from spike timing-dependent plasticity. *The Journal of Neuroscience*, *20*(23), 8812–8821.

Wang, H.-X., Gerkin, R. C., Nauen, D. W., and Bi, G.-Q. (2005). Coactivation and timing-dependent integration of synaptic potentiation and depression. *Nature neuroscience*, *8*(2), 187–193.

Watt, A. J. and Desai, N. S. (2010). Homeostatic plasticity and STDP: keeping a neuron?s cool in a fluctuating world. *Spike-timing dependent plasticity*, 240.

Wei, Y. and Koulakov, A. A. (2014). Long-term memory stabilized by noise-induced rehearsal. *Journal of Neuroscience*, *34*(47), 15804–15815.

Wible, C. G. (2013). Hippocampal Physiology, Structure and Function and the Neuroscience of Schizophrenia: A Unified Account of Declarative Memory Deficits, Working Memory Deficits and Schizophrenic Symptoms. *Behavioral Sciences*, *3*(2), 298–315.

Winson, J. and Dahl, D. (1986). Long-term potentiation in dentate gyrus: induction by asynchronous volleys in separate afferents. *Science*, *234*(4779), 985–988.

Yger, P. and Gilson, M. (2015). Models of metaplasticity: a review of concepts. *Frontiers in computational neuroscience*, *9*, 138.

Yuen, G. and Durand, D. (1991). Reconstruction of hippocampal granule cell electrophysiology by computer simulation. *Neuroscience*, *41*(2), 411–423.

Zheng, Y., Schwabe, L., and Plotkin, J. L. (2014). Location-Dependent Dendritic Computation in a Modeled Striatal Projection Neuron. In *International Conference on Artificial Neural Networks*, 741–748. Springer.

# Appendix A

# Rate functions

Activation and inactivation gates at compartment i are formulated as:

$$\frac{dz_i}{dt} = \alpha_{z_{i_i}} - (\alpha_{z_i} + \beta_{z_i})z_i \\ (z_i : m_i, h_i, n_{f,i}, n_{s,i}, k_i, l_i, a_i, b_i, c_i, d_i, e_i, r_i, q_i), \tag{A.1}$$

variable $z_i$ represents $m_i$ ,$h_i$ ,$n_{f,i}$ ,$n_{s,i}$ ,$k_i$ ,$l_i$ ,$a_i$ ,$b_i$ ,$c_i$ ,$d_i$ ,$e_i$ ,$r_i$ and $q_i$ ion-gating variables. Rate functions at compartment i determine the transition between open and closed states of the ion channels and they are presented as following equations (Aradi and Holmes, 1999). Implementation of the rate functions can be seen from the Appendix B.

$$\alpha_{m,i}(V) = -0.3(V_i - 25)/[\exp(\frac{V_i - 25}{-5}) - 1] \tag{A.2}$$

$$\beta_{m,i}(V) = 0.3(V_i - 53)/[\exp(\frac{V_i - 53}{5}) - 1] \tag{A.3}$$

$$\alpha_{h,i}(V) = 0.23/\exp(\frac{V_i - 3}{20}) \tag{A.4}$$

$$\beta_{h,i}(V) = 3.33/[\exp(\frac{V_i - 55.5}{-10}) + 1] \tag{A.5}$$

$$\alpha_{n_f,i}(V) = -0.07(V_i - 47)/[\exp(\frac{V_i - 47}{-6}) - 1] \tag{A.6}$$

$$\beta_{n_f,i}(V) = 0.264/\exp(\frac{V_i - 22}{40}) \tag{A.7}$$

$$\alpha_{n_s,i}(V) = -0.028(V_i - 35)/[\exp(\frac{V_i - 35}{-6}) - 1] \tag{A.8}$$

$$\beta_{n_s,i}(V) = 0.1056/\exp(\frac{V_i - 10}{40}) \tag{A.9}$$

$$\alpha_{k,i}(V) = -0.05(V_i + 25)/[\exp(\frac{V_i + 25}{-15}) - 1] \tag{A.10}$$

$$\beta_{k,i}(V) = 0.1(V_i + 15)/[\exp(\frac{V_i + 15}{8}) - 1] \tag{A.11}$$

$$\alpha_{l,i}(V) = 0.00015/\exp(\frac{V_i + 13}{15}) \tag{A.12}$$

$$\beta_{l,i}(V) = 0.06/[\exp(\frac{V_i + 68}{-12}) + 1] \tag{A.13}$$

$$\alpha_{a,i}(V) = 0.2(19.26 - V_i)/[\exp(\frac{19.26 - V_i}{10}) - 1] \tag{A.14}$$

$$\beta_{a,i}(V) = 0.009\exp(\frac{-V_i}{22.03}) \tag{A.15}$$

$$\alpha_{b,i}(V) = 10^{-6}\exp(\frac{-V_i}{16.26}) \tag{A.16}$$

$$\beta_{b,i}(V) = 1/[\exp(\frac{29.76 - V_i}{10}) + 1] \tag{A.17}$$

$$\alpha_{c,i}(V) = 0.19(19.88 - V_i)/[\exp(\frac{19.88 - V_i}{10}) - 1] \tag{A.18}$$

$$\beta_{c,i}(V) = 0.046\exp(\frac{-V_i}{20.76}) \tag{A.19}$$

$$\alpha_{d,i}(V) = 1.6 \times 10^{-4}\exp(\frac{-V_i}{48.4}) \tag{A.20}$$

$$\beta_{d,i}(V) = 1/[\exp(\frac{39 - V_i}{10}) + 1] \tag{A.21}$$

$$\alpha_{e,i}(V) = 15.69(81.5 - V_i)/\exp(\frac{81.5 - V_i}{10} - 1) \tag{A.22}$$

$$\beta_{e,i}(V) = 0.29\exp(\frac{-V_i}{10.86}) \tag{A.23}$$

In the equations A.2, A.3, A.6, A.8, A.10, A.11, A.14, A.18 and A.22, there is a possibility of facing 0/0 value. For skipping this problem, there is a function in our code (see, implementation of L'Hopital's rule from appendix B) is called "FUNCTION vtrap" which is implemented to use L'Hopital's rule with use of Taylor expansion to solve the problem.

# Appendix B

# Sample of simulation codes

This is not a complete code. It contains the main code, codes for rate functions, implementation of L'Hopital's rule, plasticity and metaplasticity rules. To access the rest of the codes please see: ModelDB database at (http://senselab.med.yale.edu/modeldb/, accession No. 51781).

```
v_init =-75// initial voltage
t_start = 0
t_stop = 1501000 //time stop
steps_per_ms = 1
dt = 0.2 // time step
STDP_START = 10000
//Parameters for potentiation and depression////
prepostPeriod = 60000
///Synaptic pathways inputs////
Nmpp = 150//Nmpp(Nlpp) is the number of synapses in the MPP (LPP)
Nlpp = 150
Nmpp_HFS = 150
Nlpp_HFS = 150
//////Somatic APs////////
ICLAMP_DUR = 1 //duration of postsynaptic current
clamp injections (ms)
ICLAMP_AMP = 30 //amplitude of posstsynaptic current clamp injections (nA)
```

```
///////LTP/LTD window parameters//
P0_BCMTHRESHOLD=0.004
D0_BCMTHRESHOLD=0.001
SCOUNT0_BCMTHRESHOLD = 1/5000
SCOUNTTAU_BCMTHRESHOLD=60000//averaging period for
postsynaptic spike count
ALPHA_BCMTHRESHOLD = .0025// scaling constant
PTAU = 25
DTAU=95
//////////synaptic parameters//////
TAU1 = 0.2  ms//rise time
TAU2 = 2.5 ms//decay time
REVERSAL = 0
G_OML=4.5*0.00029/Nlpp/2
G_MML=4.5*0.00029/Nmpp/2
printf( G_OML*1000, G_MML*1000)
G_OML*1000 //initial synaptic weight in the LPP
G_MML*1000 //initial synaptic weight in the MPP
////simulation and parameters for spontaneous activity///
OML_TRAIN-DELAY = 0
HFSstimMML_NUMBER=4
HFSstimMML_INTERVAL=2.5
HFS_DURATION = HFSstimMML_INTERVAL*HFSstimMML_NUMBER
printf(,HFSstimMML_INTERVAL, HFSstimMML_NUMBER, HFS_DURATION)
DULL=0 //initial silent interval to allow for stabilization of netstim intervals
TRAIN_START = DULL
TRAIN_NSPIKES = 20 //number of test stimuli
TRAIN_ISI = 12000 //test stimulation frequency:
1000/TRAIN_SI
TRAIN_ITI = OML_TRAIN_DELAY+HFS_DURATION+
(TRAIN_NSPIKES)*TRAIN_ISI //inter_train interval
TRAIN_NOISE = 0
```

```
HFSTRAIN_BI = 10000
///////medial HFS burst stimulation parameters///
HFSstimMML_START=-1e9
HFSstimMML_NUMBER= HFSstimMML_NUMBER
HFSstimMML_NTERVAL=HFSstimMML_INTERVAL
HFSstimMML_NOISE=0
metaHFSstimMML_START=-1e9
metaHFSstimMML_NUMBER=5 // (number of HFS trains)
metaHFSstimMML_INTERVAL=1000
metaHFSstimMML_NOISE=0
metametaHFSstimMML_START=TRAIN_START +TRAIN_NSPIKES*TRAIN_SI
metametaHFSstimMML_NUMBER=10 // (number of bursts of trains)
metametaHFSstimMML_INTERVAL=HFSTRAIN_IBI
metametaHFSstimMML_NOISE=0
///spontaneous activity for MPP and LPP//////
//spontaneous activity before and after HFS in the LPP
thetaOML_START=7
thetaOML_NUMBER=1e9
thetaOML_INTERVAL=160
thetaOML_NOISE=0.02 //noise
//////spontaneous activity before and after HFS in the MPP
thetaMML_START=7
thetaMML_NUMBER=1e9
thetaMML_INTERVAL=260
thetaMML_NOISE=0.02 //noise
//////spontaneous activity during HFS in the LPP
spontOML_START=134
spontOML_NUMBER=1e9
spontOML_INTERVAL=160
spontOML_NOISE=0.02 //noise
//////spontaneous activity during HFS in the MPP
spontMML_START=134
```

```
spontMML_NUMBER=1e9
spontMML_INTERVAL=320
spontMML_NOISE=0.02 //noise
/////Setting start and end times for HFS//////
START_PREBASELINE= TRAIN_START
printf( START_PREBASELINE)
objref START_BURST[metametaHFSstimMML_NUMBER],
END_BURST[metametaHFSstimMML_NUMBER]
 for i=0, metametaHFSstimMML_NUMBER-1 {
START_BURST[i]=new Vector()
END_URST[i]=new Vector()
START_BURST[i].append(TRAIN_NSPIKES*TRAIN_ISI+i*HFSTRAIN_IBI)
printf( i, START_BURST[i].x(0))
END_BURST[i].append(START_BURST[i].x(0)+metaHFSstimMML_NUMBER
*metaHFSstimMML_INTERVAL)
printf( i, END_BURST[i].x(0))
}
START_POSTBASELINE=TRAIN_NSPIKES*TRAIN_ISI
+(metametaHFSstimMML_NUMBER-1)*metametaHFSstimMML_INTERVAL
+metaHFSstimMML_NUMBER*metaHFSstimMML_INTERVAL
////Granule cell model compartment with ion channels////
ngcell = 1 //number of neuron
objref Gcell[ngcell]
begintemplate GranuleCell
ndend1=4
ndend2=4
public soma, gcdend1, gcdend2
public all, gcldend, pdend, mdend, ddend
create soma, gcdend1[ndend1], gcdend2[ndend2]
proc init() {
subsets()
gctemp()
```

```
}
objref all, gcldend, pdend, mdend, ddend
proc subsets(){ local i
objref all, gcldend, pdend, mdend, ddend
all = new SectionList()
 //inserting compartments to the dendrites
soma all.append()
for i=0, 3 gcdend1 [i] all.append()
for i=0, 3 gcdend2 [i] all.append()
    gcldend  = new SectionList()
gcdend1 [0] gcldend.append()
gcdend2 [0] gcldend.append()
    pdend  = new SectionList()
gcdend1 [1] pdend.append()
gcdend2 [1] pdend.append()
    mdend  = new SectionList()
gcdend1 [2] mdend.append()
gcdend2 [2] mdend.append()
    ddend  =new SectionList()
gcdend1 [3] ddend.append()
    gcdend2 [3] ddend.append()
}
proc gctemp() {
    soma {nseg=1 L=16.8 diam=16.8} // changed L and diam
gcdend1 [0] {nseg=1 L=50 diam=3}
for i = 1, 3 gcdend1 [i] {nseg=1 L=150 diam=3}
    gcdend2 [0] {nseg=1 L=50 diam=3}
    for i = 1, 3 gcdend2 [i] {nseg=1 L=150 diam=3}
     forsec all {
insert ccanl
catau_ccanl = 10
caiinf_ccanl = 5.e-6
```

```
Ra=210
}
    soma {insert ichan2  //inserting ion channels to soma
gnatbar_ichan2=0.12
gkfbar_ichan2=0.016
gksbar_ichan2=0.006
 insert borgka
gkabar_borgka=0.012
insert nca
gncabar_nca=0.002
insert lca
glcabar_lca=0.005
insert cat
gcatbar_cat=0.000037
gl_ichan2 = 0.00004
cm=1}
     forsec gcldend {insert ichan2
      // inserting ion channels to the GCLD
natbar_ichan2=0.018
        gkfbar_ichan2=0.004
    gksbar_chan2=0.006
    insert nca
    gncabar_ca=0.003
    insert lca
glcabar_lca=0.0075
    insert cat
gcatbar_at=0.000075
    gl_ichan2 = 0.00004
     cm=1}
forsec pdend {insert ichan2
     //inserting ion channels to the PD
gnatbar_ichan2=0.013
```

```
    gkfbar_ichan2=0.004
    gksbar_ichan2=0.006
insert nca
    gncabar_nca=0.001
    insert lca
glcabar_lca=0.0075
    insert cat
gcatbar_cat=0.0002
    insert cagk
    gkbar_cagk=0.001
    gl_ichan2 = 0.000063
    cm=1.6}
forsec mdend {insert ichan2
//inserting ion channels to the MD
gnatbar_ichan2=0.008
gkfbar_ichan2=0.001
gksbar_chan2=0.006
insert nca
gncabar_nca=0.001
insert lca
glcabar_lca=0.0005
insert cat
gcatbar_cat=0.0005
   gl_ichan2 = 0.000063
    cm=1.6}
     forsec ddend {insert ichan2
//inserting ion channels to the DD
gnatbar_ichan2=0.0
gkfbar_ichan2=0.001
gksbar_ichan2=0.008
insert nca
gncabar_ca=0.001
```

```
insert lca
glcabar_lca=0.0
insert cat
gcatbar_cat=0.001
gl_ichan2 = 0.000063
cm=1.6}
connect gcdend1[0](0), soma(1)
connect gcdend2[0](0), soma(1)
     for i=1,3 {
connect gcdend1[i](0), gcdend1[i-1](1)
}
for i=1,3 {
connect gcdend2[i](0), gcdend2[i-1](1)
}
      forsec all {enat = 45 ekf = -90 eks = -90  ek=-90
    elca=130 etca=130 esk=-90 el_ichan2 =-75
    cao_ccanl=2 }  //
    }
func is_art() { return 0 }
     endtemplate GranuleCell

/////////creating GC///////////
for i=0, ngcell-1 {
Gcell[i] = new GranuleCell(i)
}
///////Spike counting mechanism//////////////
objectvar apc//Action Potential Count mechanism
GranuleCell[0].soma apc = new APCount(0.5)
apc.thresh = -30
objref outspikes
outspikes = new Vector()
apc.record(outspikes) //collect spike times
```

```
// Creating objects and procedures
for inserting synaptic inputs
objref list_of_synapses, list_of_terminalOMLpresynapses,
list_of_terminalMMLpresynapses, list_of_terminalIMLpresynapses,
list_of_presynapses, list_of_spontpresynapses,
list_of_spontOMLpresynapses, list_of_spontMMLpresynapses,
list_of_prepresynapses, list_f_OMLsynapses, list_of_MMLsynapses,
list_of_IMLsynapses, list_of_thetaOMLpresynapses,
list_of_thetaMMLpresynapses, list_of_preprepresynapses
list_of_synapses = new List()
list_of_terminalOMLpresynapses = new List()
list_of_terminalMMLpresynapses = new List()
list_of_terminalIMLpresynapses = new List()
list_of_presynapses = new List()
list_of_prepresynapses = new List()
list_of_preprepresynapses = new List()
list_of_spontpresynapses = new List()
list_of_spontOMLpresynapses = new List()
list_of_spontMMLpresynapses = new List()
list_of_OMLsynapses = new List()
list_of_IMLsynapses = new List()
list_of_MMLsynapses = new List()
list_of_thetaOMLpresynapses = new List()
list_of_thetaMMLpresynapses = new List()
objref list_of_terminalnetcons,
list_of_OMLnetcons, list_of_MLnetcons,
list_of_IMLnetcons, list_of_prenetcons,
list_of_spontnetcons, list_of_spontOMLnetcons,
list_of_spontMMLnetcons, list_of_testOMLnetcons,
list_of_testMMLnetcons, list_of_testIMLnetcons,
list_of_HFSnetcons, list_of_HFSOMLnetcons,
```

```
list_of_HFSMMLnetcons, list_of_preprenetcons,
list_of_thetaOMLnetcons, list_of_thetaMMLnetcons,
list_of_netcons, list_of_prepreprenetcons
list_of_terminalnetcons = new List()
list_of_OMLnetcons = new List()
list_of_MMLnetcons = new List()
list_of_IMLnetcons = new List()
list_of_prenetcons = new List()
list_of_spontnetcons = new List()
list_of_spontOMLnetcons = new List()
list_of_spontMMLnetcons = new List()
list_of_thetaOMLnetcons = new List()
list_of_thetaMMLnetcons = new List()
list_of_testOMLnetcons = new List()
list_of_testMMLnetcons = new List()
list_of_testIMLnetcons = new List()
list_of_HFSnetcons = new List()
list_of_HFSOMLnetcons = new List()
list_of_FSMMLnetcons = new List()
list_of_preprenetcons = new List()
list_of_prepreprenetcons = new List()
list_of_netcons = new List()
create terminalpresynapse
//artificial final presynaptic compartment for stimulation
access terminalpresynapse
{diam=0.01 L=0.01}
create presynapse
access presynapse
{diam=0.01 L=0.01}
create prepresynapse
access prepresynapse
{diam=0.01 L=0.01}
```

```
create preprepresynapse  //   artificial pre_pre_presynaptic compartment  for burst
access preprepresynapse
{diam=0.01 L=0.01}
proc createTerminalOMLStim() {
access terminalpresynapse
$o1 = new NetStim($2)
$o1.start = $3 //ms
$o1.start = -1e9
//ms this is better - avoids epsps at t=0 ms
$o1.number = $4
$o1.interval = $5 //ms
$o1.noise =$6
list_of_terminalOMLpresynapses.append($o1)}
proc createTerminalMMLStim() {
access terminalpresynapse
$o1 = new NetStim($2)
$o1.start = $3 ms
$o1.start = -1e9 //ms this is better avoids epsps at t=0 ms
$o1.number = $4
$o1.interval = $5 //ms
$o1.noise = $6
list_of_terminalMMLpresynapses.append($o1)
proc createTerminalIMLStim() {
access terminalpresynapse
$o1 = new NetStim($2)
$o1.start = $3 //ms
$o1.start = -1e9 //ms this is better avoids epsps at t=0 ms
$o1.number = $4
$o1.interval = $5 //ms
$o1.noise = $6
list_of_terminalIMLpresynapses.append($o1)
}
```

```
proc createStim() {
access presynapse
    $o1 = new NetStim($2)
$o1.start = $3 //ms
    $o1.number = $4
$o1.interval = $5 //ms
$o1.noise = $6
list_of_presynapses.append($o1)
}
proc createSpontOMLStim() {
access presynapse
$o1 = new NetStim($2)
$o1.start = $3 //ms
$o1.number = $4
  $o1.interval = $5 //ms
$o1.noise = $6
$o1.seed($7)//to begin each simulation
 round with a different NetStim seed
list_of_spontOMLpresynapses.append(\$o1)
}
proc createSpontMMLStim() {
access presynapse
$o1 = new NetStim($2)
$o1.start = $3 //ms
$o1.number = $4
$o1.interval = $5 //ms
$o1.noise = $6
$o1.seed($7) //to begin each
simulation round with a different NetStim seed
list_of_spontMMLpresynapses.append(\$o1)
}
proc createThetaMMLStim() {
```

```
access presynapse
$o1 = new NetStim($2)
$o1.start = $3 //ms
$o1.number = $4
$o1.interval = $5 //ms
$o1.noise = $6
$o1.seed($7) //to begin each
simulation round with a different NetStim seed
list_of_thetaMMLpresynapses.append($o1)
}
proc createThetaOMLStim() {
access presynapse
$o1 = new NetStim($2)
$o1.start = $3 //ms
$o1.number = $4
$o1.interval = $5 //ms
$o1.noise = $6
$o1.seed($7) //to begin each
 simulation round with a different NetStim seed
list_of_thetaOMLpresynapses.append($o1)
}
proc createInput() {
$o1 = new Exp2SynSTDP_multNNb_globBCM_intscount_precentred(\$2)
     $o1.tau1 = TAU1  //ms
     $o1.tau2 = TAU2  //ms
     $o1.e = REVERSAL //mV
 $o1.ptau = PTAU
 $o1.dtau = DTAU
 $o1.start = STDP_START
     setpointer $o1.d, d_BCMthreshold
setpointer $o1.p, p_BCMthreshold
list_of_synapses.append($o1)
```

```
}
//initiating random number generator//////
ropen("/proc/uptime")
{
     rseed = fscan()
ropen()
}
   objref random
    random = new Random(rseed)
objref terminalstim, teststimOML, teststimMML, metateststimOML,
metateststimMML, HFSstimOML, HFSstimMML, metaHFSstimOML,
metaHFSstimMML, metametaHFSstimMML,
metametaHFSstimOML, spontOML,
spontMML, thetaOML, thetaMML
objref syncon
access prepresynapse
metateststimOML = new NetStim(0.5)
metateststimOML.start = metateststimOML_START //ms
metateststimOML.number = metateststimOML_NUMBER
metateststimOML.interval = metateststimOML_INTERVAL //ms
metateststimOML.noise = metateststimOML_NOISE
list_of_prepresynapses.append(metateststimOML) //list_of_prepresynapses(0)
access prepresynapse
metateststimMML = new NetStim(0.5)
metateststimMML.start = metateststimMML_START //ms
metateststimMML.number = metateststimMML_NUMBER
metateststimMML.interval = metateststimMML_INTERVAL //ms
metateststimMML.noise = metateststimMML_NOISE
list-of-prepresynapses.append(metateststimMML) //list-of-prepresynapses(1)
createStim(teststimOML, 0.5,teststimOML_START,teststimOML_NUMBER,
teststimOML_INTERVAL, teststimOML_NOISE)
//list_of_presynapses.o(0)
```

```
createStim(teststimMML, 0.5,teststimMML-START, teststimMML-NUMBER,
teststimMML_INTERVAL, teststimMML_NOISE)
//list_of_presynapses.o(1)
createStim(HFSstimOML, 0.5,
HFSstimOML_START, HFSstimOML-NUMBER,HFSstimOML-INTERVAL, HFSstimOML_NOISE)
//list_of_presynapses.o(2)
createStim(HFSstimMML, 0.5, HFSstimMML_START, HFSstimMML_NUMBER,
HFSstimMML_INTERVAL,HFSstimMML-NOISE)//list-of-presynapses.o(3)

///////////Bursts of HFS/////////////
access prepresynapse
metaHFSstimOML = new NetStim(0.5)
metaHFSstimOML.start = metaHFSstimOML_START //ms
metaHFSstimOML.number = metaHFSstimOML_NUMBER
metaHFSstimOML.interval = metaHFSstimOML_INTERVAL //ms
metaHFSstimOML.noise = metaHFSstimOML_NOISE
list_of_prepresynapses.append(metaHFSstimOML)//list_of_prepresynapses(2)
metaHFSstimMML = new NetStim(0.5)
metaHFSstimMML.start = metaHFSstimMML_START //ms
metaHFSstimMML.number = metaHFSstimMML_NUMBER
metaHFSstimMML.interval = metaHFSstimMML_INTERVAL //ms
metaHFSstimMML.noise = metaHFSstimMML_NOISE
list_of_prepresynapses.append(metaHFSstimMML) //list_of_prepresynapses(3)
access preprepresynapse
metametaHFSstimOML = new NetStim(0.5)
metametaHFSstimOML.start =
metametaHFSstimOML-START //ms
metametaHFSstimOML.number =
metametaHFSstimOML-NUMBER
metametaHFSstimOML.interval =
metametaHFSstimOML-INTERVAL //ms
metametaHFSstimOML.noise =
```

```
metametaHFSstimOML-NOISE
list_of_preprepresynapses.append(metametaHFSstimOML)//list_of_preprepresynapses(0)
metametaHFSstimMML = new NetStim(0.5)
metametaHFSstimMML.start = metametaHFSstimMML_START //ms
metametaHFSstimMML.number = metametaHFSstimMML_NUMBER
metametaHFSstimMML.interval = metametaHFSstimMML_NTERVAL //ms
metametaHFSstimMML.noise = metametaHFSstimMML_NOISE
list_of_preprepresynapses.append(metametaHFSstimMML)
//Postsynaptic stimulation(for current injections with IClamp)///
//// for AP generation//////////
objref stim_spike, metastim_pike
createStim(stim_pike,0.5,stim_spike_START,stim_spike_NUMBER,
stim_pike_NTERVAL,stim_pike_NOISE)//list_of_presynapses.o(4)
createStim(metastim_pike, 0.5,metastim_spike_START, metastim_spike_NUMBER,metastim_
metastim_pike_NOISE) //list-of-presynapses.o(5)
///NetCon for generating somatc postsynaptic APs///
objref spike
Gcell[0].soma {
spike = new stimIClamp(.5)
spike.dur = ICLAMP_DURATION
}
/////BCM spike(and d and p)
counter for metaplasticity//
objref bcm
Gcell[0].soma {
objref bcm
bcm = new BCMthreshold(.5)
p0_BCMthreshold=P0_BCMTHRESHOLD
d0_BCMthreshold=D0_BCMTHRESHOLD
scount0_BCMthreshold = SCOUNT0_BCMTHRESHOLD
scounttau_BCMthreshold = SCOUNTTAU_BCMTHRESHOLD
alpha_BCMthreshold = ALPHA_BCMTHRESHOLD
```

```
bcmslow_BCMthreshold = BCMSLOW_BCMTHRESHOLD
}
access presynapse
objref syncon-spike
syncon_spike = new NetCon
(stim_spike, spike, 0, 0, ICLAMP_AMP)
printf( syncon-spike.weight[0])
objref metasyncon_spike
metasyncon_spike = new NetCon(metastim_spike,stim_spike, 0, 0, 1)
//connections for HFS stimulation///
access prepresynapse
syncon = new NetCon(list_of_prepresynapses.o(2),
list_of_presynapses.o(2))//LPP-GC  HFS stimulator
syncon.weight=1.1
syncon.delay=0
syncon.threshold=0
list_of_preprenetcons.append(syncon)
syncon = new NetCon(list_of_prepresynapses.o(3),
list_of_presynapses.o(3))//MPP_GC  HFS stimulator
syncon.weight=1.1
syncon.delay=0
syncon.threshold=0
list_of_preprenetcons.append(syncon)
access preprepresynapse
syncon = new NetCon(list_of_preprepresynapses.o(0),list_of_prepresynapses.o(2))
//LPP-GC meta meta HFS stimulator
syncon.weight=1.1
syncon.delay=0
syncon.threshold=0
list_of_preprepreprenetcons.append(syncon)
syncon = new NetCon(list_of_preprepresynapses.o(1),list_of_prepresynapses.o(3))
//MPP_GC meta meta HFS stimulator
```

```
syncon.weight=1.1
syncon.delay=0
syncon.threshold=0
list_of_preprepreprenetcons.append(syncon)
objref syn
syncounter=0
MMLsyncounter=0
OMLsyncounter=0
////Terminal stimulation(terminalpresynapse_GC)////
///////Terminal LPP synapses///////
    access Gcell[0].gcdend1[3]
    nsyn = Nlpp/2
if (nsyn>nseg) {
k=int(nsyn/nseg)
for j=1, k {
  for i=0,nseg-1 {
node = (2*(i+1)-1)/(2*nseg)
createInput(syn, node)
syncounter+=1
OMLsyncounter+=1
createTerminalOMLStim(terminalstim, 0.5, 0,1, 0, 0)//list_of_terminalpresynapses
access Gcell[0].gcdend1[3]
syncon = new NetCon(list_of_terminalOMLpresynapses
o(syncounter-1),
list_of_synapses.o(syncounter-1),0,0,G_OML*Nlpp) //LPP_GC
list_of_OMLnetcons.append(syncon)
list_of_netcons.append(syncon)
}
}
for i=0,nsyn-(k*nseg)-1 {
node = (2*(i+1)-1)/(2*nseg)
createInput(syn, node)
```

```
syncounter+=1
OMLsyncounter+=1
createTerminalOMLStim(terminalstim,0.5, 0, 1, 0, 0)
access Gcell[0].gcdend1[3]
syncon = new NetCon
(list_of_terminalOMLpresynapses.o(syncounter-1),
list_of_synapses.o(syncounter-1),0, 0, G_OML*Nlpp) //LPP_GC
list_of_OMLnetcons.append(syncon)
list_of_Netcons.append(syncon)
}
} else {
for i=0,nsyn-1 {
node = (2*(i+1)-1)/(2*nseg)
createInput(syn, node)
syncounter+=1
OMLsyncounter+=1
createTerminalOMLStim(terminalstim,0.5, 0, 1, 0, 0)
access Gcell[0].gcdend1[3]
syncon = new NetCon
(list_of_terminalOMLpresynapses.o(syncounter-1),
list_of_synapses.o(syncounter-1), 0, 0, G_OML*Nlpp)//LPP_GC
list_of_OMLnetcons.append(syncon)
    list_of_netcons.append(syncon)
}
}
    access Gcell[0].gcdend2[3]
    nsyn = Nlpp/2
    if (nsyn>nseg) {
k=int(nsyn/nseg)
for j=1, k {
for i=0,nseg-1 {
node = (2*(i+1)-1)/(2*nseg)
```

```
createInput(syn, node)
syncounter+=1
   OMLsyncounter+=1
createTerminalOMLStim(terminalstim,0.5, 0, 1, 0,0)
 //list_of_terminalpresynapses
access Gcell[0].gcdend2[3]
syncon = new NetCon
(list_of_terminalOMLpresynapses.o(syncounter-1),
list_of_synapses.o(syncounter-1),0, 0, G-OML*Nlpp) //LPP_GC
list_of_OMLnetcons.append(syncon)
list_of_netcons.append(syncon)
}
}
for i=0,nsyn-(k*nseg)-1 {
node = (2*(i+1)-1)/(2*nseg)
createInput(syn, node)
syncounter+=1
OMLsyncounter+=1
createTerminalOMLStim(terminalstim,0.5, 0, 1,0, 0)
 //list_of_terminalpresynapses
access Gcell[0].gcdend2[3]
syncon = new NetCon(
list_of_terminalOMLpresynapses.o(syncounter-1),
list_of_synapses.o(syncounter-1),0, 0, G-OML*Nlpp) //LPP_GC
list_of_OMLnetcons.append(syncon)
list_of_netcons.append(syncon)
}
} else {
for i=0,nsyn-1 {
node = (2*(i+1)-1)/(2*nseg)
createInput(syn, node)
syncounter+=1
```

```
    OMLsyncounter+=1
createTerminalOMLStim(terminalstim,0.5, 0, 1, 0, 0)
 //list_of_terminalpresynapses
access Gcell[0].gcdend2[3]
syncon = new NetCon
(list_of_terminalOMLpresynapses.o(syncounter-1),
list_of_synapses.o(syncounter-1),0, 0, G_OML*Nlpp) //LPP_GC
    list_of_OMLnetcons.append(syncon)
list_of_netcons.append(syncon)
}
}
///terminal synapses for the medial pathway/////
MMLsyncounter=0
access Gcell[0].gcdend1[2]
nsyn = Nmpp/2
if (nsyn>nseg) {
k=int(nsyn/nseg)
for j=1, k {
for i=0,nseg-1 {
node = (2*(i+1)-1)/(2*nseg)
    createInput(syn, node)
    syncounter+=1
       MMLsyncounter+=1
createTerminalMMLStim(terminalstim,
 0.5, 0, 1,0, 0)
 //list-of-terminalpresynapses
access Gcell[0].gcdend1[2]
syncon = new NetCon
(list_of_terminalMMLpresynapses.o(MMLsyncounter-1),
list_of_synapses.o(syncounter-1), 0, 0,G_MML*Nmpp)//MPP_GC
    list_of_MMLnetcons.append(syncon)
list_of_netcons.append(syncon)
```

```
}
}
for i=0,nsyn-(k*nseg)-1 {
node = (2*(i+1)-1)/(2*nseg)
createInput(syn, node)
syncounter+=1
MMLsyncounter+=1
createTerminalMMLStim
(terminalstim, 0.5, 0,1, 0, 0)
//list-of-terminalpresynapses
access Gcell[0].gcdend1[2]
syncon = new NetCon
(list_of_terminalMMLpresynapses.
o(MMLsyncounter-1),
list_of_synapses.
o(syncounter-1), 0, 0, G_MML*Nmpp)//MPP_GC
    list_of_MMLnetcons.append(syncon)
list_of_netcons.append(syncon)
}
} else {
for i=0,nsyn-1 {
node = (2*(i+1)-1)/(2*nseg)
createInput(syn, node)
syncounter+=1
MMLsyncounter+=1
createTerminalMMLStim(terminalstim,0.5, 0, 1, 0, 0)
 //list_of_terminalpresynapses
access Gcell[0].gcdend1[2]
syncon = new NetCon
(list_of_terminalMMLpresynapses.
o(MMLsyncounter-1),
 list_of_synapses.o(syncounter-1),0, 0, G_MML*Nmpp)//MPP_GC
```

```
list_of_MMLnetcons.append(syncon)
list_of_netcons.append(syncon)
}
}
     access Gcell[0].gcdend2[2]
     nsyn = Nmpp/2
     if (nsyn>nseg) {
k=int(nsyn/nseg)
     for j=1, k {
for i=0,nseg-1 {
node = (2*(i+1)-1)/(2*nseg)
createInput(syn, node)
syncounter+=1
MMLsyncounter+=1
createTerminalMMLStim(terminalstim,0.5, 0,1, 0, 0)
 //list_of_terminalpresynapses
access Gcell[0].gcdend2[2]
syncon = new NetCon
(list_of_terminalMMLpresynapses.o(MMLsyncounter-1),
 list_of_synapses.o(syncounter-1),0, 0, G_MML*Nmpp) //MPP_GC
list_of_MMLnetcons.append(syncon)
list_of_netcons.append(syncon)
}
}
for i=0,nsyn-(k*nseg)-1 {
node = (2*(i+1)-1)/(2*nseg)
createInput(syn, node)
syncounter+=1
MMLsyncounter+=1
    createTerminalMMLStim(terminalstim, 0.5, 0,1, 0, 0)
    //list_of_terminalpresynapses
access Gcell[0].gcdend2[2]
```

```
syncon = new NetCon
(list_of_terminalMMLpresynapses.o(MMLsyncounter-1),
list_of_synapses.o(syncounter-1),0, 0, G_MML*Nmpp) //MPP_GC
list_of_MMLnetcons.append(syncon)
list_of_netcons.append(syncon)
}
} else {
for i=0,nsyn-1 {
    node = (2*(i+1)-1)/(2*nseg)
createInput(syn, node)
syncounter+=1
MMLsyncounter+=1
createTerminalMMLStim
(terminalstim, 0.5, 0, 1,0, 0) //list_of_terminalpresynapses
access Gcell[0].gcdend2[2]
syncon = new NetCon
(list_of_terminalMMLpresynapses.o(MMLsyncounter-1),
 list_of_synapses.o(syncounter-1),0, 0, G_MML*Nmpp) //MPP_GC
    list_of_MMLnetcons.append(syncon)
list_of_netcons.append(syncon)
}
}
////////// HFS stimulation ////////
////HFS stimulation medial pathway //////
nsyn = Nmpp
for i = 0, nsyn-1 {
syncon = new NetCon
(list_of_presynapses.o(3),
    list_of_terminalMMLpresynapses.o(i), 0, 0,1.1) //MPP_GC HFS stimulator;
list_of_HFSMMLnetcons.append(syncon)
}
//////// Spontaneous stimulation//////////
```

```
//initiating random number generator
ropen("/proc/uptime")
{
  rseed = fscan()
ropen()
}
objref random
    random = new Random(rseed)
////Spontaneous stimulation in the LPP during HFS//
nsyn = Nlpp
for i = 0, nsyn-1 {
      createSpontOMLStim(spontOML,0.5,spontOML_START,
      spontOML_NUMBER,spontOML_INTERVAL,spontOML_NOISE,
      random.uniform(0,rseed))
syncon = new NetCon
(list_of_spontOMLpresynapses.o(i),
list_of_terminalOMLpresynapses.o(i), 0,0, 1.1) //LPP_GC
spont. stimulator
list_of_spontOMLnetcons.append(syncon)
////Spontaneous stimulation in the MPP during HFS//
nsyn = Nmpp
for i = 0, nsyn-1 {
    createSpontMMLStim(spontMML,0.5, spontMML_START, spontMML_NUMBER,
    spontMML_INTERVAL,spontMML_NOISE,random.uniform(0,rseed))
syncon = new NetCon
(list_of_spontMMLpresynapses.o(i),
list_of_terminalMMLpresynapses.o(i), 0,0, 1.1)
//MPP_GC spont. stimulator
list_of_spontMMLnetcons.append(syncon)

////Spontaneous stimulation in the LPP before and after HFS///
nsyn = Nlpp
```

```
for i = 0, nsyn-1 {
    createThetaOMLStim(thetaOML, 0.5,thetaOML_START, thetaOML_NUMBER,thetaOML_INTER
    thetaOML_NOISE,random.uniform(0,rseed))
syncon = new NetCon
(list_of_thetaOMLpresynapses.o(i),
list_of_terminalOMLpresynapses.o(i),0, 0, 1.1)
//LPP_GC theta stimulator
list_of_thetaOMLnetcons.append(syncon)
}
/////Spontaneous stimulation in the MPP before and after HFS///
nsyn = Nmpp
for i = 0, nsyn-1 {
    createThetaMMLStim(thetaMML, 0.5,thetaMML_START,
     thetaMML_NUMBER,thetaMML_INTERVAL, thetaMML_NOISE,
random.uniform(0,rseed))
syncon = new NetCon
(list_of_thetaMMLpresynapses.o(i),
list_of_terminalMMLpresynapses.o(i), 0, 0, 1.1)
//MPP_GC theta stimulator
list_of_thetaMMLnetcons.append(syncon)
}
}
///////Recording and saving data//////
objref rect ,MPPweight[list_of_MMLnetcons.count],
LPPweight[list_of_OMLnetcons.count], meanMPPweight,
meanLPPweight, drec, prec, ALPHA_SCOUNTrec
objref somaV, rectime, MPPdendV, LPPdendV
objref HFSMMLnetcons_spikes
[list_of-HFSMMLnetcons.count],
objref spontMMLnetcons_spikes
[list_of_spontMMLnetcons.count],
objref thetaMMLnetcons_spikes
```

```
[list_of_thetaMMLnetcons.count],
objref  MMLnetcons-spikes
[list_of_MMLnetcons.count]
objref HFSOMLnetcons_spikes
[list_of_HFSOMLnetcons.count],
objref spontOMLnetcons_spikes
[list_of_OMLnetcons.count],
objref thetaOMLnetcons_spikes
[list_of_thetaOMLnetcons.count],
objref OMLnetcons_spikes
[list_of_OMLnetcons.count]
objref spontMPPweight
[list_of_spontMMLnetcons.count],
objref spontLPPweight
[list_of-spontOMLnetcons.count],
objref thetaMPPweight[
list_of_thetaMMLnetcons.count],
objref thetaLPPweight[list_of_thetaOMLnetcons.count]
rect = new Vector()
meanMPPweight = new Vector()
meanLPPweight = new Vector()
drec = new Vector()
prec = new Vector()
ALPHA_SCOUNTrec = new Vector()
somaV = new Vector()
MPPdendV = new Vector()
LPPdendV = new Vector()
rectime = new Vector()
for i=0,list_of_MMLnetcons.count-1 {
MPPweight[i] = new Vector()
}
for i=0,list_of_OMLnetcons.count-1 {
```

```
LPPweight[i] = new Vector()
}
////Vectors for saving weights
 to see whether spikes of spontaneous activity//
for i=0,list_of_spontMMLnetcons.count-1 {
spontMPPweight[i] = new Vector()
}
for i=0,list-of-thetaMMLnetcons.count-1 {
thetaMPPweight[i] = new Vector()
}
for i=0,list_of_spontOMLnetcons.count-1 {
spontLPPweight[i] = new Vector()
}
for i=0,list_of_thetaOMLnetcons.count-1 {
thetaLPPweight[i] = new Vector()
}
///creating vectors for
 recording presynaptic spikes////
for i=0,list_of_HFSMMLnetcons.count-1 {
HFSMMLnetcons_spikes[i] = new Vector()
}
for i=0,list_of_spontMMLnetcons.count-1 {
spontMMLnetcons_spikes[i] = new Vector()
}
for i=0,list_of_thetaMMLnetcons.count-1 {
thetaMMLnetcons_spikes[i] = new Vector()
}
for i=0, list_of_MMLnetcons.count-1 {
MMLnetcons_spikes[i] = new Vector()
}
for i=0,list_of_HFSOMLnetcons.count-1 {
HFSOMLnetcons_spikes[i] = new Vector()
```

```
}
for i=0,list_of_spontOMLnetcons.count-1 {
spontOMLnetcons_spikes[i] = new Vector()
}
for i=0,list_of_thetaOMLnetcons.count-1 {
thetaOMLnetcons_spikes[i] = new Vector()
}
for i=0, list_of_OMLnetcons.count-1 {
OMLnetcons_spikes[i] = new Vector()
}
proc record() {local i
   recstep = 1000*dt
  for i=0,list_of_MMLnetcons.count-1 {
  MPPweight[i].
  record(\&list_of_MMLnetcons.
     o(i).weight[1],recstep)
  }
  for i=0,list_of_OMLnetcons.count-1 {
  LPPweight[i].
  record(\&list_of_OMLnetcons.
     o(i).weight[1],recstep)
  }
  rectime.record(\&t)
  rect.record(\&t,recstep)
  ALPHA_SCOUNTrec.record(\&alpha_scount_BCMthreshold,recstep)
  drec.record(\&d_BCMthreshold,recstep)
   prec.record(\&p_BCMthreshold,recstep)
  somaV.record(\&Gcell[0].soma.v(.5))
   MPPdendV.record(\&Gcell[0].gcdend1[2].v(0.5))
  LPPdendV.record(\&Gcell[0].gcdend1[3].v(0.5))
  list_of_HFSMMLnetcons.o(0).record(HFSMMLnetcons_spikes[0])
  list_of_spontMMLnetcons.o(0).record(spontMMLnetcons_spikes[0])
```

```
  list_of_thetaMMLnetcons.o(0).record(thetaMMLnetcons_spikes[0])
  list_of_MMLnetcons.o(0).record(MMLnetcons_spikes[0])
  list_of_HFSOMLnetcons.o(0).record(HFSOMLnetcons_spikes[0])
   list_of_spontOMLnetcons.o(0).record(spontOMLnetcons_spikes[0])
  list_of_thetaOMLnetcons.o(0).record(thetaOMLnetcons_spikes[0])
  list-of-OMLnetcons.o(0).record(OMLnetcons_spikes[0])
  spontMPPweight[0].record(\&lis_of_spontMMLnetcons.o(0).
  weight[0],recstep)
  spontLPPweight[0].record(\&list_of_spontOMLnetcons.o(0)
  .weight[0],recstep)
  thetaMPPweight[0].record(\&list_of_thetaMMLnetcons.o(0)
  .weight[0],recstep)
  thetaLPPweight[0].record(\&list_of_thetaOMLnetcons.o(0)
  .weight[0],recstep)
}
proc weight_mean() {local i
   for i=0,list_of_MMLnetcons.count-1 {
  meanMPPweight = meanMPPweight.c.add(MPPweight[i])
  }
  meanMPPweight = meanMPPweight.
  c.mul(1/list_of_MMLnetcons.count)
  for i=0,list_of_OMLnetcons.count-1 {
  meanLPPweight = meanLPPweight.c.add(LPPweight[i])
  }
  meanLPPweight = meanLPPweight.
  c.mul(1/list_of_OMLnetcons.count)
}
 ////Procedure for calculation
 % of potentiation and depression//
   proc plasticity()
   {local i //counter, meanMPPpre,
   counter = 0
```

```
   meanMPPpre = 0
   meanMPPpost = 0
   meanLPPpre = 0
   meanLPPpost = 0
for i=0, rect.size()-1 {
if (rect.x(i)>=
(START-BURST[0].x(0)-prepostPeriod)
&& rect.x(i)<START-BURST[0].x(0)) {
meanMPPpre=meanMPPpre+meanMPPweight.x(i)
meanLPPpre=meanLPPpre+meanLPPweight.x(i)
counter=counter+1
} else {}
}
if (counter==0) {} else
{meanMPPpre = meanMPPpre/counter}
if (counter==0) {}
else {meanLPPpre = meanLPPpre/counter}
    counter = 0
    for i=0, rect.size()-1 {
if (rect.x(i)>=(tstop-prepostPeriod)
&& rect.x(i)<tstop) {
meanMPPpost=meanMPPpost+meanMPPweight.x(i)
meanLPPpost=meanLPPpost+meanLPPweight.x(i)
counter=counter+1
} else {}
}
if (counter==0) {} else
 {meanMPPpost = meanMPPpost/counter}
if (counter==0) {} else
 {meanLPPpost = meanLPPpost/counter}
 if (meanMPPpre==0) {} else
  {meanMPP_plasticity =
```

```
  100*meanMPPpost/meanMPPpre}
     if (meanLPPpre==0) {}
     else {meanLPP-plasticity =
100*meanLPPpost/meanLPPpre}
}
objref savMPPdata, savLPPdata
strdef MPPbasename, LPPbasename, extension,
MPPfilename, LPPfilename,
 MPPpathname, LPPpathname
extension = "dat"
MPPbasename = "MPP"
LPPbasename = "LPP"
proc save() {local i
    savMPPdata.wopen(MPPpathname)
savLPPdata.wopen(LPPpathname)
for i=0,rect.size()-1 {
     savMPPdata.printf(rect.x(i),
      meanMPPweight.x(i))
savLPPdata.printf( rect.x(i),
 meanLPPweight.x(i))
}
savMPPdata.close()
savLPPdata.close()
}
////Numeric integration method///////
secondorder=2
//Crank-Nicholson (Ion currents (ina, ik, etc)
are fixed up so that they are second
 order correct when plotted at t-dt/2)
///Setting time-dependent noise
of spontaneous MPP stimulation//
proc noise_thetaMML() {local i
```

```
access presynapse
  for i=0,list_of_thetaMMLpresynapses.
  count-1 {
   list-of_thetaMMLpresynapses.o(i).noise = $1
  }
}
proc noise_thetaOML() {local i
    access presynapse
  for i=0,list_of_thetaOMLpresynapses.
  count-1 {
    list_of_thetaMMLpresynapses.o(i).
    noise = $1
  }
}
proc weight_thetaMML() {local i
   for i=0,list_of_thetaMMLnetcons.count-1 {
  list_of_thetaMMLnetcons.o(i).weight = $1
  }
}
proc weight_thetaOML() {local i
  for i=0,list_of_thetaOMLnetcons.count-1 {
    list_of_thetaOMLnetcons.o(i).weight = $1
  }
}
proc weight_spontMML() {local i
   for i=0,list_of_spontMMLnetcons.count-1 {
  list_of_spontMMLnetcons.o(i).weight = \$1
  }
}
proc weight_spontOML() {local i
  for i=0,list_of_spontOMLnetcons.count-1 {
   list_of_spontOMLnetcons.o(i).weight = \$1
```

```
  }
}
proc stiminit() { // executed at start of simulation
   weight_thetaMML(0)
   weight_thetaOML(0)
  weight_spontMML(0)
  weight_spontOML(0)
 //Pre_HFS and post_HFS(= pre/post-baseline) LPP/MPP

  //spontaneous activity during_HFS_LPP//
 cvode.event(START_PREBASELINE, "weight_thetaMML(2)
  weight_thetaOML(2)")
   // to start baseline spontaneous. medial and lateral spontaneous//
   cvode.event(START_BURST[0].x(0),"weight_thetaMML(0)
  weight_thetaOML(0) weight_spontMML(2)
 weight_spontOML(2)")
   cvode.event(START_POSTBASELINE,"weight_thetaMML(2)
      weight_thetaOML(2) weight_spontMML(0)
       weight_spontOML(0)")
objref fih
fih = new FInitializeHandler("stiminit()")

//////////////////Plotting weight means/////////
objref gweight, galpha,
gsomaV, gdp, gspontweight,g1weight
/////for plots of presynaptic spikes////////
objref gprespikesMML, gprespikesOML, gspontweight
objref yHFSMML, yspontMML, ythetaMML, yMML
objref yHFSOML, yspontOML, ythetaOML, yOML
yHFSMML = new Vector()
yspontMML = new Vector()
ythetaMML = new Vector()
```

```
yMML = new Vector()
yHFSOML = new Vector()
yspontOML = new Vector()
ythetaOML = new Vector()
yOML = new Vector()
proc showrecords() {
gweight = new Graph(0)
  for (i=0; i<=list_of_MMLnetcons.
  count-1; i=i+5) {
  MPPweight[i].mark
  (gweight, rect, "+", 12, 9)
  }
  for (i=0;i<=list_of_OMLnetcons.count-1; i=i+5) {
       LPPweight[i].mark(gweight, rect, "+", 12, 8)
  }
     meanLPPweight.mark(gweight, rect, "o", 12, 2)
  meanMPPweight.mark(gweight,rect, "t", 12, 3)
  gweight.size(0,rect.max(),0,maximum)
  gweight.view(0, 0, rect.max(),
   maximum, 65, 105, 300.48, 200.32)
  gweight.label(.1, .9, "Weights: meanLPP(red) LPP(yellow)
  meanMPP(blue) MPP(gray)")
   galpha = new Graph(0)
    ALPHA_SCOUNTrec.mark(galpha, rect, "o", 12, 1)
  galpha.size(0,rect.max(),0,ALPHA_SCOUNTrec.max())
  galpha.view(0, 0, rect.max(), ALPHA_SCOUNTrec.max(),
  565, 105, 300.48, 200.32)
  galpha.label(.1, .9, "alpha_scount")
   gdp = new Graph(0)
   drec.mark(gdp, rect, "o", 12, 7)
   prec.mark(gdp, rect, "t", 12, 9)
   gdp.size(0,rect.max(),0,prec.max())
```

```
   gdp.view(0, 0, rect.max(),prec.max(),
   565, 405, 300.48, 200.32)
   gdp.label(.1, .9, "d(violet) p(gray)")
    gsomaV = new Graph(0)
     somaV.plot(gsomaV, rectime)
     MPPdendV.plot(gsomaV, rectime, 3,1)
     LPPdendV.plot(gsomaV, rectime, 2,1)
       gsomaV.size(0, rectime.max(), -100, somaV.max())
       gsomaV.view(0, 0, rectime.max(), somaV.max(),
       65, 405, 300.48, 200.32)
  gsomaV.label(.1, .9, "voltage (mV): soma (black)
   MPPdend (0.5,blue) LPPdend (0.5,red)")
///////plotting medial presynaptic spikes////////
yHFSMML.resize(HFSMMLnetcons_spikes[0].size())
yHFSMML.fill(0.5)
yspontMML.resize(spontMMLnetcons_spikes[0].size())
yspontMML.fill(1)
ythetaMML.resize(thetaMMLnetcons_spikes[0].size())
ythetaMML.fill(1.5)
yMML.resize(MMLnetcons_spikes[0].size())
  yMML.fill(2)
   gprespikesMML = new Graph(0)
   yHFSMML.mark(gprespikesMML,
    HFSMMLnetcons-spikes[0], "|", 12, 3)
  yspontMML.mark(gprespikesMML,
  spontMMLnetcons-spikes[0], "|", 12, 3)
  ythetaMML.mark(gprespikesMML,
   thetaMMLnetcons-spikes[0], "|",  12, 3)
  yMML.mark(gprespikesMML,
   MMLnetcons_spikes[0], "|", 12, 3)
  gprespikesMML.size(0,tstop,0,2)
  gprespikesMML.view(0, 0, tstop, 2,
```

```
   165, 205, 300.48, 200.32)
   gprespikesMML.label(.1, .9, "HFSMML(0.5)
    spontMML(1) thetaMML(1.5) MML(2)")
///////plotting lateral presynaptic spikes/////////
   yHFSOML.resize(HFSOMLnetcons_spikes[0].size())
    yHFSOML.fill(0.5)
    yspontOML.resize
    (spontOMLnetcons_spikes[0].size())
    yspontOML.fill(1)
    ythetaOML.resize
    (thetaOMLnetcons_spikes[0].size())
     ythetaOML.fill(1.5)
    yOML.resize(OMLnetcons_spikes[0].size())
     yOML.fill(2)
     gprespikesOML = new Graph(0)
  yHFSOML.mark(gprespikesOML,
   HFSOMLnetcons_spikes[0], "|", 12, 2)
    yspontOML.mark(gprespikesOML,
    spontOMLnetcons_spikes[0],"|", 12, 2)
    ythetaOML.mark(gprespikesOML,
    thetaOMLnetcons_spikes[0], "|", 12, 2)
  yOML.mark(gprespikesOML,
  OMLnetcons_spikes[0], "|",12, 2)
   gprespikesOML.size(0,tstop,0,2)
   gprespikesOML.view(0, 0, tstop, 2, 65,
    205, 300.48, 200.32)
    gprespikesOML.label(.1, .9, "HFSOML(0.5)
    spontOML(1) thetaOML(1.5) OML(2)")
 }
/////Determining and plotting instantaneous frequency///////
objref fhist
objref gfreq
```

```
proc instfrequency() {
N = apc.n//N spikes have been counted
meanf = 1000 * N /rectime.max()
//[Hz], mean firing rate
printf("Mean firing rate was  Hz", meanf)
binW = 2000 //bin width
if (binW >rectime.max())
{binW = rectime.max()}
binL = 0
if (outspikes.size()==0)
 {outspikes.append(1e9)}
fhist = outspikes.
histogram(binL, rectime.max(), binW)
fhist.div(binW/1000)  //[Hz]
gfreq = new Graph(0)
gfreq.label(.1, .9,instantaneous firing rate
(bin = 2000 ms))
fhist.plot(gfreq, binW)
fhist.mark(gfreq, binW, "o", 12, 2)
    gfreq.size(binL,
    rectime.max(), 0, fhist.max())
gfreq.view(0, 0, rectime.max(),
fhist.max(), 1265, 105, 300.48, 200.32)
}
/////////////Running simulation/////////
i=1
SIMULATIONS_NUMBER = 1
for i=1, SIMULATIONS_NUMBER {
sprint(MPPfilename, MPPbasename, i, extension)
sprint(LPPfilename, LPPbasename, i, extension)
sprint(MPPpathname, MPPfilename)
sprint(LPPpathname, LPPfilename)
```

```
savMPPdata = new File(MPPpathname)
savLPPdata = new File(LPPpathname)
record()
init()
run()
meanLPPweight.resize(rect.size())
meanMPPweight.resize(rect.size())
weight_mean()
save()
maximum = meanLPPweight.max
h = meanMPPweight.max
if(h>maximum) {maximum=h}
    showrecords()
instfrequency()
plasticity()//to compute % of weight change
}
*******************************************************
*******************************************************
//////// Codes for rate functions ///////////////

In our codes, to keep the voltage above the resting potential, we added -65 mv to t

PROCEDURE rates(v){  //Computes rate and other constants
        LOCAL  alpha, beta, sum
        q10 = 3^((celsius - 6.3)/10)
         //"m" sodium activation system
alpha = -0.3*vtrap((v+60-17),-5)
beta = 0.3*vtrap((v+60-45),5)
sum = alpha+beta
mtau = 1/sum      minf = alpha/sum
    //"h" sodium inactivation system
alpha = 0.23/exp((v+60+5)/20)
```

```
beta = 3.33/(1+exp((v+60-47.5)/-10))
sum = alpha+beta
htau = 1/sum
        hinf = alpha/sum
       //"ns" sKDR activation system
  alpha = -0.028*vtrap((v+65-35),-6)
beta = 0.1056/exp((v+65-10)/40)
    sum = alpha+beta
nstau = 1/sum
 //"nf" fKDR activation system = alpha/sum
  alpha = -0.07*vtrap((v+65-47),-6)
beta = 0.264/exp((v+65-22)/40)
sum = alpha+beta
nftau = 1/sum      nfinf = alpha/sum
}
PROCEDURE trates(v) {
// Computes rate and other constants
    // Call once from HOC to initialize inf
      LOCAL tinc
        TABLE minf, mexp, hinf,
        hexp, nfinf, nfexp, nsinf, nsexp,
         mtau, htau, nftau, nstau
DEPEND dt, celsius FROM -100 TO 100 WITH 200
       // not consistently executed
       from here if usetable_hh == 1
       tinc = -dt * q10
        mexp = 1 - exp(tinc/mtau)
        hexp = 1 - exp(tinc/htau)
nfexp = 1 - exp(tinc/nftau
nsexp = 1 - exp(tinc/nstau)
}
************************************************************
```

```
**********************************************************
////////This function implements L'Hopital's rule with use of
 Taylor expansion for exp(x/y)to avoid 0/0 condition/////////
 FUNCTION vtrap(x,y) {  //Traps for 0 in denominator of rate eqns.
        if (fabs(x/y) < 1e-6) {
               vtrap = y*(1 - x/y/2)
        }else{
                vtrap = x/(exp(x/y) - 1)
        }
}
UNITSON
*********************************************
*********************************************
////////////Adding STDP codes to the model //////
NET-RECEIVE(w (uS), wE (uS), tpre (ms), X) {
     INITIAL { wE = w  tpre = -1e9  X=0 }
// When a presynaptic spike occurs,
the mechanism receives an event with flag==0.
if (flag == 0) {
// presynaptic spike (after last post so depress)
 A = A + wE*factor
 B = B + wE*factor
 tpre = t
 counter=counter+1 // counting consecutive epsps
 presyntime[counter-1]=tpre
 // storing epsp time into an array
if (t>start) {
X = d * exp((tpost - t)/dtau)
wE = wE*(1-X)
}
if (wE>0) {} else {wE=0}
flagOLD = flag
```

```
}else if (flag == 2) { // postsynaptic spike
// The FOR_NETCONS loop iterates over all NetCons that
target this particular instance of the synaptic mechanism.
It changes each NetCon's X
so that it becomes a potentiation factor
depending on the latency between the
time of the most recent event (spike) that was
delivered by that NetCon and the
 time of the postsynaptic spike.
FOR_NETCONS(w1, wE1, tpres, X1)
{ // also can hide NET_RECEIVE args
   if (flagOLD==flag) {}
else {
// for each postsynaptic spike,
   / only 1 presynaptic spike is considered
if (t>start) {
FROM i=0 TO counter-1 {
     X1 = p*exp((presyntime[i] - t)/ptau)
wE1 = wE1*(1+X1)
FROM i=0 TO counter-1 {
  presyntime[i]=-1e9
   }
counter = 0 }
}
}
tpost = t
} else { // flag == 1 from INITIAL block
          WATCH (v > -37) 2
// This mechanism watches postsynaptic
membrane potential at the location
 of the synapse When a postsynaptic
spike occurs, the mechanism receives
```

```
 an event with flag == 2
}
}
**********************************
**********************************
////////////////// Metaplasticity codes//////////////////
//The mechanism should be inserted into soma to calculate
the value of alpha-scount and thereby of d and p for all
synaptic point processes which use d, p as POINTER variables.
At the hoc level d and p have to be set up as POINTER variables
to allow the synaptic point process to know the d and p value.
 setpointer syn.d, d_BCMthreshold
setpointer syn.p, p_BCMthreshold
ENDCOMMENT
NEURON {
POINT_PROCESS BCMthreshold
GLOBAL d0, p0, scount0, scounttau,
 alpha, alpha_scount,tstop
GLOBAL d, p, tspike
}
PARAMETER {
d0 // initial value for the depression factor
p0 // initial value for the potentiation factor
scounttau // averaging period for
postsynaptic spike count
alpha // scaling constant
scount0  // initial scount = 0
boltzman = 0 // initial boltzman = 0
    tstop
}
ASSIGNED {
v (mV)
```

```
flagOLD
scount
alpha_scount // scount scaled
by alpha sliding modification threshol
d// depression factor
(multiplicative to prevent < 0)
p // potentiation factor
boltzfactor
pf
output
tspike (ms)
}
INITIAL {
tspike = -100000
// flag is an implicit argument to NET-RECEIVE. It is an
integer, zero by default but a nonzero value can be
specified via the second argument to net-send().
net-send() is used to launch self-events. A self-event
comes back to the mechanism that launched it, no NetCon
required.
net-send(0, 1)
flagOLD = 1
scount = scount0
d = d0
p = p0
alpha_scount = alpha*scount
boltzfactor = exp( - 1.0 / scounttau)
if (boltzman == 0) {pf =
1.0 / (1 - boltzfactor)} else {pf = 1.0}
output = 0
}
BREAKPOINT {
```

```
scount = (scount * (pf - 1.0) +
(v + 75)*(v + 75)) / pf
   pf = pf * boltzfactor + 1.0
   alpha_scount = alpha *
    scount  // scount scaled by alpha
    if (alpha_scount > 0
     {p =  p0 * 0.75 / alpha_scount} else {p = p }
    d = d0
    output = 0
}
//The items in the argument list in the NET-RECEIVE
statement of a synaptic mechanism are actually the
elements of a weight vector. The first element, which is
called nc.weight[0], corresponds to the first item in the
NET-RECEIVE argument list--w--which remains constant during
a simulation. The second element is called nc.weight[1],
and it corresponds to wE. The value of this second
element does change as a consequence of STDP.
NET_RECEIVE(w) {
     INITIAL {w=0}
When a presynaptic spike occurs, the mechanism receives
 an event with flag == 0.
if (flag == 0) {
     output = 0 // no postsynaptic spike
} else if (flag == 2)
 { // postsynaptic spike
    tspike = t
  //just in case one needs time of the spike
output = 1
// postsynaptic spike
} else { // flag == 1 from INITIAL block
// WATCH (var > thresh) flag value is used in a
```

```
NET-RECEIVE block to specify a condition in the
postsynaptic cell that will generate a self-event with
latency 0 and a specified flag value. Generally, WATCH
is used to make NEURON monitor a variable for threshold
crossing, and generates a self event with the specified
flag value when the threshold is crossed.
If the postsynaptic cell is a biophysical model cell,
var is usually local membrane potential (or cai or
some other concentration); if the postsynaptic cell
is an artificial spiking cell, var is one of that
cell's state variables. But WATCH could in principle
be anything, such as the total number of spikes that
a cell has fired, or perhaps even t (time).
WATCH (v > 0) 2 //This mechanism watches
postsynaptic membrane potential at the
location of the mechanism when a postsynaptic spike occurs,
the mechanism  receives an event with flag == 2
}
}
```